Reconfigurable Antennas Based on Varactor-Loaded Stubs

by

Siti Nailah Mastura Zainarry

B. Eng. (Microelectronic Engineering),
University of Malaysia Perlis, Malaysia, 2009
M. Eng (Electronic Systems Design Engineering),
University of Science, Malaysia, 2010

Thesis submitted for the degree of

Doctor of Philosophy

in

School of Electrical & Electronic Engineering
Faculty of Engineering, Computer & Mathematical Sciences
The University of Adelaide

2019

Supervisors:

Prof. Christophe Fumeaux, School of Electrical & Electronic Engineering

Prof. Cheng-Chew Lim, School of Electrical & Electronic Engineering

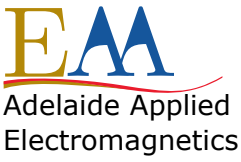

THE UNIVERSITY *of* ADELAIDE

Contents

Contents iii

Abstract vii

Originality Declaration ix

Acknowledgments xi

Thesis Conventions xiii

Abbreviation xv

Awards and Scholarships xvii

Publications xix

List of Figures xxi

List of Tables xxv

Chapter 1. Introduction and Motivation 1

1.1 Introduction 2

1.1.1 Reconfigurable antennas in microwave systems 2

1.1.2 Analysis of reconfigurability with stub-loaded varactors 4

1.2 Motivation and objectives 5

1.3 Thesis structure 7

1.4 Statement of original contributions 9

1.4.1 Stub-loaded varactor control for reconfigurable antenna designs 9

1.4.2 Stub-loaded varactor control for reconfigurable periodic structures 9

Chapter 2. Reconfiguration Mechanisms and Techniques 11

2.1 Introduction 12

2.1.1 Microstrip antennas 13
2.1.2 Reconfigurable antennas 14
2.2 Reconfiguration mechanisms 15
2.2.1 Radio-Frequency MicroElectroMechanical System (RF MEMS) switch 16
2.2.2 PIN diode 17
2.2.3 Varactor 18
2.3 Type of reconfigurable antennas 20
2.3.1 Frequency-reconfigurable antennas 20
2.3.2 Pattern-reconfigurable antennas 25
2.3.3 Polarisation-reconfigurable antennas 30
2.3.4 Compound-reconfigurable antennas 32
2.4 Conclusion 38

Chapter 3. A Frequency- and Pattern-Reconfigurable Two-Element Array Antenna 39

3.1 Introduction 40
3.2 Two elements array principle 42
3.3 Reconfigurable single-element configuration 43
3.3.1 Basic single-element structure 43
3.3.2 Resonance frequency detuning 44
3.4 Reconfigurable two-element array configuration 45
3.4.1 Relative phase of cavity mode 45
3.5 Mutual coupling optimisations 47
3.5.1 Direct coupling between elements 48
3.5.2 Coupling through the feeding network 48
3.6 Full-wave simulation of beam steering 51
3.7 Prototype and measurement results 53
3.7.1 Frequency reconfigurability 53
3.7.2 Pattern reconfigurability 55
3.8 Conclusion 60

Chapter 4. A Pattern-Reconfigurable Single-Element Microstrip Antenna **61**

4.1 Introduction . . . 62
4.2 Antenna design . . . 63
4.3 Operation principle . . . 65
4.4 Pattern reconfigurability . . . 67
4.5 Numerical optimisation . . . 68
4.6 Experimental results . . . 70
4.7 Conclusion . . . 74

Chapter 5. Concept of a Stub-Loaded Reconfigurable Reflectarray Unit Cell **75**

5.1 Introduction . . . 76
5.2 Principle of reflectarray . . . 78
5.3 Unit cell design . . . 80
5.4 Optimisation and parameter study . . . 82
5.4.1 Impedance analysis of the stub-loaded varactor . . . 83
5.4.2 Optimisation . . . 85
5.5 Scattering characteristic response . . . 86
5.6 Conclusion . . . 90

Chapter 6. A Reconfigurable Reflectarray Antenna Unit Cell **91**

6.1 Introduction . . . 92
6.2 Antenna structure and operation principle . . . 94
6.3 Infinite periodic structure analysis . . . 96
6.3.1 Normal incidence . . . 96
6.3.2 Oblique incidence . . . 101
6.4 Periodic analysis of a linear sub-array . . . 103
6.5 Design and simulation of offset-fed reconfigurable reflectarray antenna configuration . . . 106
6.5.1 Analysis of offset-fed configuration for the 2D reflectarray antenna 106
6.5.2 Feed model . . . 108

6.6 Validation of the reconfigurable reflectarray: numerical and experimental results . . . 109
6.6.1 Measurement with uniform phase . . . 111
6.6.2 Radiation pattern . . . 116
6.7 Conclusion . . . 118

Chapter 7. Summary and Future Work **119**
7.1 Thesis contributions . . . 120
7.2 Part1: Reconfigurable antennas . . . 120
7.2.1 Summary of original contributions . . . 120
7.2.2 Future work . . . 122
7.3 Part2: Reconfigurable periodic structure . . . 123
7.3.1 Summary of original contributions . . . 123
7.3.2 Future work . . . 125
7.4 Concluding statement . . . 125

Bibliography **127**

Biography **143**

Abstract

The term “reconfigurable” is typically used for devices which exhibit some flexibility of functionalities and agility in their operation characteristics, with the aim of achieving high performance in various conditions. In antenna technology, the reconfiguration can be fulfilled through several techniques that provide an ability to modify the electrical current on the antenna’s structure, primarily to accomplish a physically realised new response. The main key to the reconfigurable antenna application is their potential to avoid the use of multiple antennas for multi-functionality, thus facilitating miniaturisation of the antenna system configuration. In this context, several novel reconfigurable antennas with a wide performance range are proposed in this thesis. Varactor-loaded stubs are used as tuning mechanism for these microwave antenna designs with improved performance throughout this thesis. Two types of electromagnetic structures are studied in this work, namely reconfigurable antennas and reconfigurable periodic structures, with these two main topics building the two main major parts of this thesis.

In its first main part, the thesis proposes reconfigurable antenna designs with combined frequency and pattern reconfigurable characteristics. The main focus is first on the manipulation of near-resonant current distributions in a two-element array antenna as well as the optimisation of their feeding through T-junction power dividers. Each element has a controllable active component that allows the antenna to be tuned to different operating frequencies, while the concurrent adaption of the two elements is the basis of continuous beam scanning characteristics. Next, the thesis examines the exploitation of a single-element antenna structure based on the same operation principle. An optimisation procedure including a study of relevant design parameters is also presented. The core contribution for the two-element array and the single-element antenna is that they combine frequency-reconfigurability with effective beam scanning. The main difference between the two designs however is that they scan in the H-plane and the E-plane, respectively.

In the second main part, the thesis focuses on a reconfigurable reflectarray antenna design. Potential applications of this advanced antenna design include the development of high gain antennas with various controllable reflection beam directions throughout a wide range of operation frequencies. The proposed reflectarray antenna unit cell is

firstly proposed, together with an opimisation of the antenna characteristics in terms of reflection loss and phase range performance. It is further shown that the proposed antenna provides an excellent performance compared to the state-of-the-art. Performance measures include a near full phase tuning range of about 300° to 320° with a reflection loss of magnitude better than 3 dB within a fractional frequency range of operation of 18%. In contrast, most reflectarray antenna designs in the literature provide a limited phase range at a fixed operating frequency or within a narrower frequency tuning range. Experimental validation is provided with a 12-element linear reflectarray tested in two-dimensional settings, for which the experimental challenges are also discussed in detail. The capability of reflected beam scanning is verified and successfully demonstrated.

Originality Declaration

I certify that this work contains no material which has been accepted for the award of any other degree or diploma in my name, in any university or other tertiary institution and, to the best of my knowledge and belief, contains no material previously published or written by another person, except where due reference has been made in the text. In addition, I certify that no part of this work will, in the future, be used in a submission in my name, for any other degree or diploma in any university or other tertiary institution without the prior approval of the University of Adelaide and where applicable, any partner institution responsible for the joint-award of this degree.

I give consent to this copy of the thesis, when deposited in the University Library, being available for loan, photocopying, and dissemination through the library digital thesis collection, subject to the provisions of the Copyright Act 1968.

I also give permission for the digital version of my thesis to be made available on the web, via the Universitys digital research repository, the Library Search and also through web search engines, unless permission has been granted by the University to restrict access for a period of time.

Signed _____ Date _____

Acknowledgments

In the name of god, with his majesty for his unconditional blessing and his merciful nature, I have successfully completed this entire thesis. The composition in this thesis is not something that is easy to finish as well as not a part of an individual experience. It takes place in a social network includes several persons that I would like to thank sincerely for their support, skills and encouragements that leads me to the ending of this doctoral journey.

First and foremost, I would like to take the opportunity to express my sincere gratitude to my principal supervisor, **Prof. Christophe Fumeaux** for his kindness, constant support and willingness to accept me as a PhD candidate in back 2016 after some of the specific problems that I faced during my PhD journey at University of Adelaide. He introducing me to a new amazing world of antenna and propagation. He also excellently guided me with his theorical understanding and his great experiences in electromagnetic and microwave system. His encouragement, critical comments, constructive feedback, responsiveness and generous allowance/travel financial assistance have become my backbone factors in propelling my research forward. Dear Christophe, many thanks to you for being my best supervisor and mentor. You always take me in the right direction of my research where I personally do not believe I can afford to overcome.

Second, I am thankful to have **Prof. Cheng-Chew Lim** as my co-supervisor. He was the one who has taken me to a new path and would never let me touch the ground of failure because the great things take time to fulfill my dream. With his supervisions, I was able to gain my physical and mental strength as well as start building up my research skill and experiences.

Since I joined in the antenna world, I also work together with **Dr. Nghia Nguyen Trong** and **Dr. Shengjian Jammy Chen** as one research team. I am very grateful to them for their help in sharing their great experiences, ideas and suggestions in order to make my research going smoothly. I also wish to express my appreciation for **Dr. Wendy Suk Ling Lee** as my best friend and colleague, who have depth of caring heart to help me stay up and standing for me in helpless situations even until now. I'm so thankful for our friendship, for inspiring me to become a better person and for being the shoulder

that I can always depend on. She simply make everything brighter and I'm lucky to have her by my side.

Next, I do not want to miss the opportunity to thanks to my past and present members in the Applied Electromagnetic Group at University of Adelaide including **Dr Withawat Withayachumnankul, Dr. Ali Karami Horestani, Dr Zahra Shaterian, Dr. Cheng Zhao, Dr. Nicholas Lawrence, Dr. Amir Ebrahimi, Dr. Sree Pinapati, Andrew Udina, Xiaojing Lv, Xiaolong You, Jack Gao, Jin Huang, Ken Paramayudha and Ali Malakooti**. I have a great time with the group over the years and many thanks to their constant support and friendship.

Throughout my PhD candidature, I also have received valuable help from the **University of Adelaide** and the **School of Electrical and Electronic Engineering**, for providing me the Completion Scholarship and travel financial assistance that allowed me to completed my research study and attended international conferences. A special note of appreciation for the technical staff of the School of Electrical and Electronic Engineering Workshop, **Mr Alban OBrien, Mr Brandon Pullen** and **Mr Danny Di Giacomo** for their assistance on fabrication and material ordering. Also, I would like to thank the administrative staff team who have helped me in administrative work with effective cooperation.

In addition, I would like to express my depth gratitude to my father (**Zainarry**), mother (**Che Pauziah**) and my sbilings (**Najlaa, Najhan, Nabeel and Naqib**), who always pray for my success over the years. Their love and support giving me strength to stand and move forward throughout this journey. Thank you to my parents for what they did among their whole life and their sacrifices to make my life better and what I am today. Furthermore, I've come to show my appreciation to my best friends and also as hostel mates, **Kenshi Onishi** and **Andy Liniting** for being great friends that I can trust, for being my strength when I was down and for being my side in any situations. Thank you for being awesome and present in my life, all the time, all the way. Lastly, I am thankful to my AOSA hostel members which always cheers me up.

Siti Nailah Mastura Zainarry
August 2019
Adelaide, Australia

Thesis Conventions

The following conventions have been adopted in this Thesis:

Typesetting

This document was compiled using LaTeX2e. TeXnicCenter was used as text editor interfaced to LaTeX2e. Inkscape 0.92.1 was used to produce schematic diagrams and other drawings.

Spelling

Australian English spelling conventions have been used, as defined in the Macquarie English Dictionary (A. Delbridge (Ed.), Macquarie Library, North Ryde, NSW, Australia, 2001).

Referencing

The Harvard style is used for referencing and citation in this thesis.

System of Units

The units comply with the international system of units recommended in an Australian Standard: AS ISO 1000-1998 (Standards Australia Committee ME/71, Quantities, Units and Conversions 1998).

Abbreviation

AC	Alternating Current
DC	Direct Current
EBG	Electromagnetic Band Gap
f/D	Focal length to Diameter
FAE	Finite Array Environment
FFT	Fast Fourier Transform
LP	Linear Polarisation
LHCP	Left-Hand Circular Polarisation
MEMS	MicroMechanical System
RF	Radio Frequency
RHCP	Right-Hand Circular Polarisation
VLSI	Very Large Scale Integration

Awards and Scholarships

2018

- Completion Scholarship University of Adelaide
- Third Prize Best Paper Award, IEEE Radio and Antenna Days of The Indian Ocean

Publications

Journal Article

S.N.M. Zainarry, N. Nguyen-Trong, and C. Fumeaux, "A frequency-and pattern-reconfigurable two-element array antenna," *IEEE Antennas Wirel. Propag. Lett.*, vol. 17, no. 4, pp. 617–620, 2018.

Conferences

S.N.M. Zainarry, N. Nguyen-Trong, and C. Fumeaux, "Concept of a stub-loaded reconfigurable reflectarray unit cell," *In 2017 IEEE Asia Pacific Microwave Conference (APMC)*, pp. 302–305, 2017.

S.N.M. Zainarry, S.J. Chen, and C. Fumeaux, "A Pattern-Reconfigurable Single-Element Microstrip Antenna," *2018 IEEE Radio and Antenna Days of the Indian Ocean (RADIO)*, pp. 1–2, 2018.

List of Figures

1.1 A classification of electromagnetic spectrum 3
1.2 Circuit analysis of a concept of varactor-stub loading 5
1.3 Thesis outline 7

2.1 Antenna as a transition device 12
2.2 Static vs. reconfigurable antenna systems 15
2.3 Reconfiguration mechanisms 16
2.4 RF MEMS 17
2.5 PIN diode 18
2.6 Varactor 19
2.7 Variable junction capacitance of MA46H120 varactor 19
2.8 Example of RF MEMS frequency-reconfigurable antenna 22
2.9 Example of PIN diode frequency-reconfigurable antenna 23
2.10 Examples of varactor-controlled frequency-reconfigurable antenna . . . 24
2.11 Example of RF MEMS pattern-reconfigurable antenna 26
2.12 Examples of PIN diode pattern-reconfigurable antennas 28
2.13 Examples of varactor-controlled pattern-reconfigurable antennas 29
2.14 Example of RF MEMS polarisation-reconfigurable antenna 31
2.15 Example of PIN diode polarisation-reconfigurable antenna 32
2.16 Example of varactor-controlled polarisation-reconfigurable antenna . . . 33
2.17 Example of RF MEMS compound-reconfigurable antenna 35
2.18 Example of PIN diode compound-reconfigurable antenna 36
2.19 Example of varactor-controlled compound-reconfigurable antenna . . . 37

3.1 The reconfigurable two-element antenna configuration 42
3.2 Operation principle 43

3.3 Single-element configuration 44
3.4 Detuning of the patch from resonance frequency 46
3.5 Relative phase of the cavity mode 47
3.6 Parametric study of the patch width 49
3.7 Parametric study of feed line length 50
3.8 Reflection coefficient 51
3.9 Instantaneous electric-field distribution 52
3.10 Photograph of the fabricated prototype 53
3.11 Reflection coefficient for different combinations of bias voltages 54
3.12 Simulated reflection coefficient for different combinations of bias voltages 55
3.13 3-D plot of reflection coefficient 56
3.14 Realised gain patterns 57
3.15 Simulated realised gain patterns 58
3.16 Antenna realised gain and efficiency 59

4.1 A reconfigurable single-element microstrip antenna structure 64
4.2 The electric-field distribution of two modes 66
4.3 Simulated reflection coefficient for different number of vias 68
4.4 Parametric study of the additional length 69
4.5 The photograph of the fabricated antenna 71
4.6 Reflection coefficients with three different bias voltages 71
4.7 Normalised radiation patterns 72
4.8 Antenna gain and efficiency 73

5.1 Microstrip and parabolic antenna 76
5.2 Example of reflectarray antenna system 77
5.3 Reflectarray architecture 79
5.4 Operation principle 80
5.5 Unit cell straight-line stub-loaded configuration 81

5.6 Unit cell T-shaped stub-loaded configuration 82
5.7 Unit cell equivalent circuit 84
5.8 Resonance frequency as a function of the varactor capacitance values . . 85
5.9 Phase of the reflection coefficients 87
5.10 Magnitude of the reflection coefficients 87
5.11 Resonance frequency as a function of the varactor capacitance values . . 88
5.12 Progressive phase response 89
5.13 Instantaneous scattered field distribution 89

6.1 Unit cell configuration 95
6.2 The periodic boundary simulation 98
6.3 Diode losses 99
6.4 Phase of the reflection coefficients for normal incidence case 100
6.5 Magnitude of the reflection coefficients for normal incidence case 100
6.6 Reflection phase difference for normal incidence case 101
6.7 Phase of the reflection coefficients for oblique incidence case 102
6.8 Magnitude of the reflection coefficients for oblique incidence case 102
6.9 Reflection phase difference for oblique incidence case 103
6.10 Progressive phase response 104
6.11 Instantaneous scattered field distribution 105
6.12 Reconfigurable radiation pattern 105
6.13 Reflectarray antenna measurement system architecture 108
6.14 H-plane sectoral horn antenna structure 110
6.15 The horn antenna reflection coefficient 110
6.16 Prototype of the reflectarray antenna 111
6.17 Experimental setup 112
6.18 Simulated reflection phase along the tuning frequency band 114
6.19 Measured reflection phase along the tuning frequency band 114
6.20 Reflection phase through biasing of the varactors 115
6.21 Reflection phase at the frequency of 3.30 GHz 115

6.22 Field Distribution for a uniform varactors 116
6.23 Radiation pattern 117
6.24 Field Distribution for a progressive distribution of varactors 117
6.25 Radiation pattern with maximum beam steering 118

List of Tables

2.1 Varactor parameters 19

5.1 Varactor parameters 84

5.2 Final design parameters for the unit-cell geometry of Fig. 5.6. 86

6.1 Unit cell design parameters 99

Chapter 1

Introduction and Motivation

EVEN though the fundamentals of antenna theory and design have a history of more than 100 years, the emergence of a new era in antenna technology is currently underway due to the ubiquity of wireless connectivity. In parallel, progress is facilitated by the accelerated adoption of advanced materials and fabrication processes, as well as the commoditisation of powerful computational methods and accurate experimental technologies. This chapter provides a general overview of advanced systems based on reconfigurable antennas for major applications in microwave systems, which provides the rationale for the devices proposed in this thesis. This introduction is then followed by the motivation of the research work performed during this PhD candidature, and an outline of the constributions of this thesis. The thesis structure and a summary of the chapters are also presented in detail.

1.1 Introduction

The introduction of various novel wireless technologies and applications motivates new developments in advanced antenna systems. It also provides new perspectives and challenges which require dedicated analysis, optimisation and implementation. In this thesis, adaptive variations of antenna characteristics, including operating frequency, gain, impedance matching and radiation patterns are investigated in the framework of reconfigurable designs. An in-depth understanding of the fundamental parameter characteristics is important for researchers to implement reliable designs of antennas with predictable reconfiguration properties. Over past decades, numerous approaches have been implemented to achieve sophisticated properties of reconfigurable antennas by controlling the surface current distribution or modifying the electrical structure of the antenna without apparently changing the physical geometry (Johnson, 1992; Bernhard, 2007a; Balanis, 2015). The achieved dynamical adaptations of antenna characteristics provide performance advantages and a flexibiliy that can benefit advanced systems in various communications applications, where requirements in terms of compactness, bandwidth, patterns or polarisation cannot be attained with conventional static designs.

1.1.1 Reconfigurable antennas in microwave systems

With the advancement of new communications, identification and sensing technologies, reconfigurable antennas have emerged as promising solution to achieve high-performance designs in microwave systems. This has fostered an increasing level of research activities in this field over the past years. This is because the development of reconfigurable antennas provides potentially more effective designs with high flexibility in functionalities that would be difficult or even impossible to achieve in a static implementation. Reconfigurable antennas also could prove to become a necessary solution in industrial applications to extend functionalities beyond the limitations of conventional antenna systems (Pozar, 1998; Wincza and Gruszczynski, 2010). There have been numerous examples of reconfigurable microwave antennas reported in the literature (Panagamuwa *et al.*, 2006b; Erdil *et al.*, 2007; Liu and Langley, 2008; Rodrigo *et al.*, 2014a; Nguyen-Trong *et al.*, 2016b).

Generally, the microwave region is physically defined in the electromagnetic spectrum as covering the frequency range in between 500 MHz (1 m wavelength) to 300 GHz (1 mm wavelength) (Pozar, 1998). Figure 1.1 situates the microwave frequency region

in the electromagnetic spectrum together with the denominations commonly used to describe frequency bands. The microwave range possesses some of the most relevant features enabling efficient wireless communications and remote sensing systems. This motivates the development of small antennas to help miniaturisation of systems, especially for systems operating at lower frequencies. There are however physical limits to miniaturisation, and therefore, the concept of reconfigurable or agile antennas can provide a solution by clustering several functionalities into a single antenna, thus relaxing the space and weight problems associate with multiple antennas configurations.

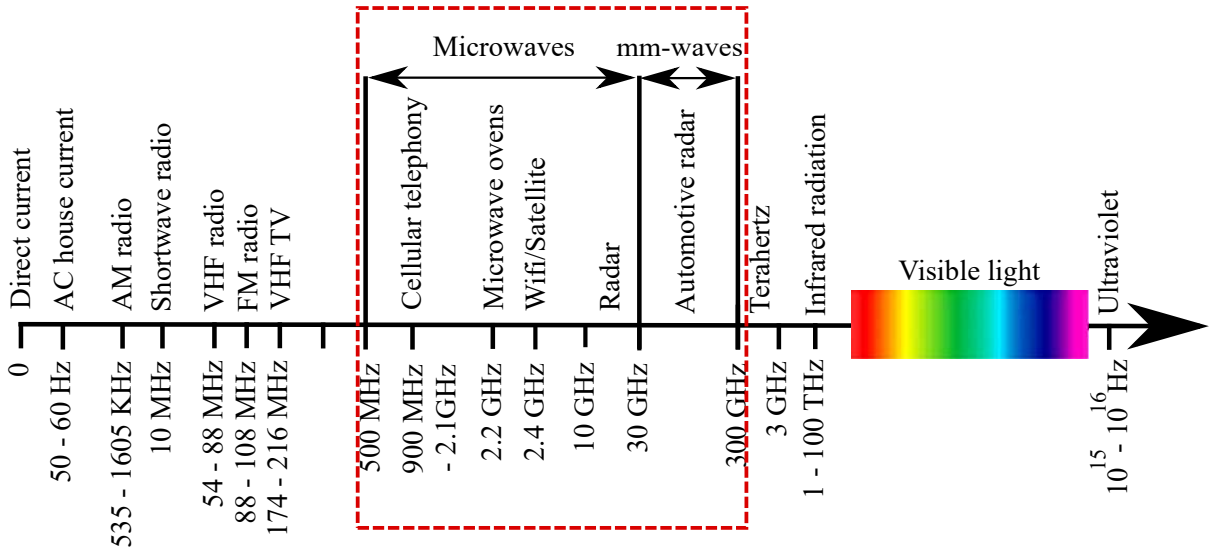

Designation	Band	Designation	Band
Direct current (DC)	0 Hz	Very High Frequency (VHF)	30 - 300 MHz
Very Low Frequency (VLF)	3 - 30 KHz	Ultra High Frequency (UHF)	300 - 3000 MHz
Low Frequency (LF)	30 - 300 KHz	Super High Frequency (SHF)	3 - 30 GHz
Medium Frequency (MF)	300 - 3000 KHz	Extreme High Frequency (EHF)	30 - 300 GHz
High Frequency (HF)	3 - 30 MHz	Microwave Frequencies	500 MHz - 300 GHz

Figure 1.1. A classification of electromagnetic spectrum. A classification of the electromagnetic spectrum showing various applications across the range of frequencies.

1.1.2 Analysis of reconfigurability with stub-loaded varactors

Reconfigurable antennas can be designed and realised in various ways as will be described in details in the literature review of Chapter 2. Generally, it is known that the operation of a reconfigurable antenna is associated with changes in the antenna's impedance matching that can degrade the performance of the system and affect the operational frequency and radiation pattern. In this context, the term of "impedance matching" can be defined as the process of adapting the antenna electrical load or internal impedance to a source of excitation. Since the antenna impedance is related to its current distribution, including importantly equivalent currents at radiating apertures, this section explains a general technique of impedance matching for reconfigurable antennas, with the aim of maximising the amount of the power transfer from the excitation source to the load. In the case of impedance mismatch at the antenna ports, the input power will be reflected back to the excitation source leading to the formation of a standing wave, on the feeding transmission line. The disadvantages of standing waves is that they cause additional power loss, as well as signal amplitude and phase variations leading to errors. For reconfigurable antennas, it is very challenging to achieve a good matching in the antenna impedance over the whole range of functionalities for a particular design. This thesis focuses on a concept of reconfigurable antenna impedance matching based on stub-loaded varactor control of the antenna resonance, achieved by varying the impedance at the radiating aperture.

Figure 1.2 shows the schematic of a stub-loaded varactor located at the edge of substrate-integrated antenna aperture. Specifically, the varactor is directly located at the edge of the open aperture and is connected with the loading stub. The other end of the stub is connected to a bias circuit network (consisting of a large resistor R_b and a choke inductor L_b) to drive the varactor while providing an open-circuit termination at radio-frequencies. In order to obtain a clear understanding of the analysis, the stub has a lenght L_{stub}, and its open-circuit termination leads to fringing fields at its end, which can be modelled as an additional length of the stub Δl. Taking into account the additional length, the impedance at the aperture then can be calculated according to the transmission line theory as stated in (Nguyen-Trong *et al.*, 2015c). The equivalent circuit of the varactor in between the antenna edge and the stub includes the varactor impedance Z_{var} taken from the varactor datasheet and three parasitic capacitances, which describe the capacitive interactions between the edges of the antenna, the stub and the ground plane. More specifically, the impedance Z_{var} of the varactor consists

of a variable junction capacitance $C(V)$ as well as parasitics including a series resistor R as well as series inductance L. The role of the variable junction capacitance is that it can be controlled to alter the distribution of currents on the antenna by changing the impedance of the aperture. In this context, the stub length L_{stub} provides additional design freedom to manipulate the aperture impedance, which may allow the antenna to operate at a different frequency without adjusting the antenna's physical geometry.

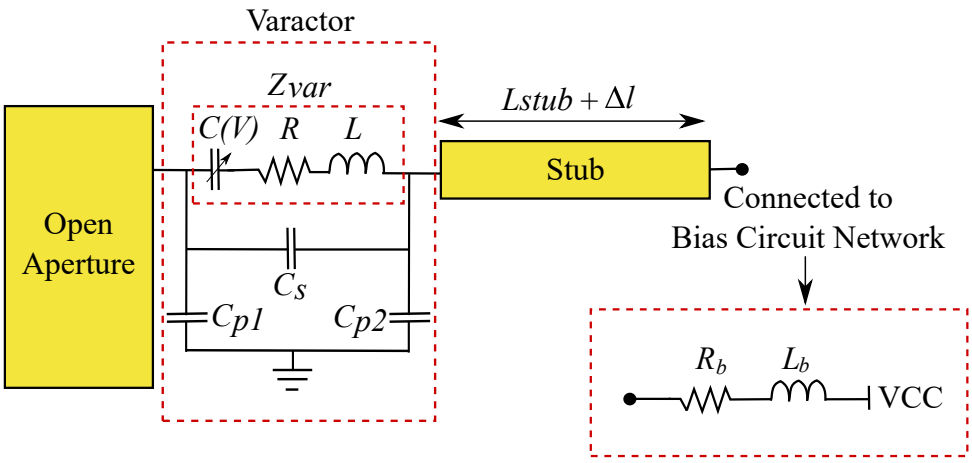

Figure 1.2. Circuit analysis of a concept of varactor-stub loading. Circuit analysis of a concept of varactor-stub loaded to an open aperture.

1.2 Motivation and objectives

The motivation for implementing reconfigurable properties in an antenna is to help solving the challenges associated with increasing requirements while reducing the number of necessary antennas. It may also provide additional functionalities that extend the performance of the antenna system, by helping control polarisation and radiation pattern of the device. This thesis introduces new designs of reconfigurable antennas with a focus on frequency and radiation pattern reconfigurations. The aims of this thesis are to contribute to solving the challenges of reconfigurable designs, with three main objectives addressed in details as follows.

1. **Lower antenna system complexity**

   Conventional antennas are designed for specific applications and operate at a particular frequency band, typically with a fixed radiation pattern. Consequently,

they lack the flexibility to accommodate new services. In contrast, reconfigurable antennas can introduce flexibility in the antenna functionality and improve the system performance without increasing the number of antennas. There are many challenges to solve when implementing reconfiguration, including preserving the antenna reflection coefficient, phase response and radiation properties. RF switches are the most popular tuning components used to achieve the antenna reconfiguration. In this thesis, the integration of varactor loaded with an open circuit stub is selected as the actuating mechanism in all contributions. The lower complexity associated with a single reconfigurable antenna also to reduce manufacturing costs and may lower the complexity compared to multiple antenna systems.

2. **Variation of the resonance frequency properties in a controlled manner**

   Access to a wide portion of the electromagnetic spectrum is necessary to achieve multiple functionalities efficiently and satisfy the increasingly high demand of modern communication systems. Conventional compact and planar antennas may not be able meet these requirements efficiently due to their operation at a fixed frequency. In contrast, reconfigurable antennas with similar profile may be able to fulfill wider specifications since their operating frequency can be modified dynamically within the allocated spectrum.

3. **Capability of steering a beam in desired directions**

   The configuration of array antennas can improve the performance of a system in term of desired radiation pattern and gain. However, the conventional array antenna usually involves a high level of complexity in the antenna geometry due to the feeding network management, and a high cost associated to phase shifters. Reconfigurable array antennas aim to have an easier network management and less complexity, while retaining some maneuverability. Most of the reconfigurable antenna designs in previous studies focussed on either reconfigurable radiation patterns at a fixed operating frequency or reconfigurable operating frequency with a fixed radiation pattern. In this thesis, the main objective of the antenna design is to overcome these limitations, and provide the ability to steer the beam in a desired direction within a particular tuning range of operating frequency.

1.3 Thesis structure

Figure 1.3 illustrates the structure of the thesis which is composed of 7 chapters divided into 4 groups. The first group includes Chapter 1 and 2 and gives an introductory overview and a literature review. The core groups 2 and 3 include the main chapters focusing on the research contribution of the thesis. The final group ends the thesis with a summary, outlook and bibliography. The groups are elaborated in more detail in the following.

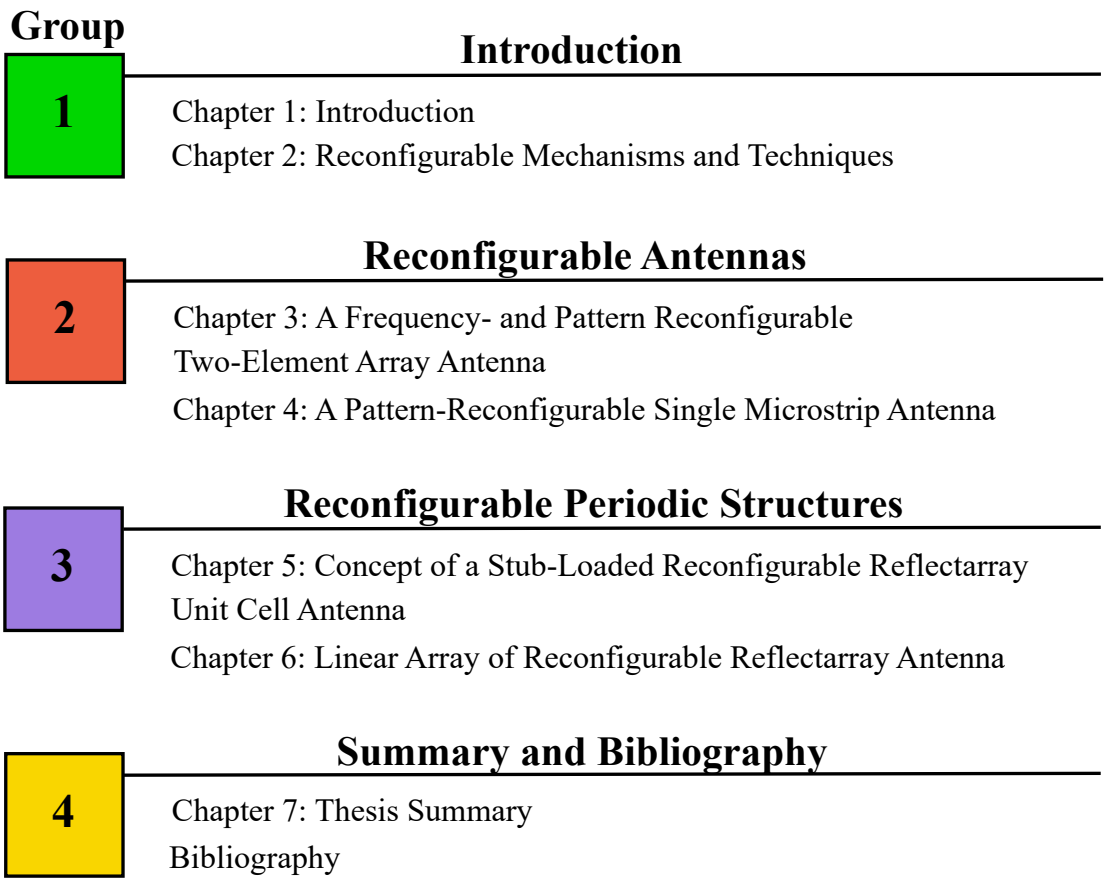

Figure 1.3. Thesis outline. The thesis is composed of 7 chapters including introduction and summary. The original contributions are distributed in Chapter 3 to Chapter 6. The thesis core can be divided into two major parts. The first part that includes Chapter 3 and 4 is mainly concerned with reconfigurable antenna designs. Meanwhile, the second part which includes Chapter 5 and 6 is dedicated to reconfigurable periodic stuctures. All chapters are virtually self-contained.

Group 1: Introduction. This present Chapter 1 provides a brief explanation of the context of reconfigurable antennas for microwave systems. It also introduces an analysis of reconfigurability with stub-loaded varactors as well as the motivation and objectives of this thesis. Chapter 2 describes in detail the possible mechanisms and techniques commonly used to achieve reconfiguration of antennas in term of frequency, radiation pattern, polarisation or compound properties. Both chapters also include selected examples of recently published works illustrating theoretical applications, potential and constraints of each reconfigurable antenna design approach.

Group 2: Reconfigurable antennas. This second group involves the analysis design, fabrication and measurement of reconfigurable microstrip antennas designs for beam scanning purpose, according to array antenna operating principles. Chapter 3 and 4 respectively introduce dual- and single-element microstrip antenna configurations with integrated stub-loaded varactors as a tuning mechanism to achieve a reconfiguration of operating frequency concurrently to a continuous scanning of the radiation patterns. The mutual coupling between the radiation elements is discussed in detail, as it can be exploited to compensate the imbalance between the radiation elements that affect to the beam scanning angle.

Group 3: Reconfigurable Periodic Structures. New concepts of reconfigurable reflectarray antennas based on stub-loaded varactors are presented in Chapter 5 and 6. These chapters explores the different unit cell configurations identified to provide good performance in reflection coefficient and phase response to fullfill the requirements of reflectarray antennas. Next, the design of a linear sub-array of the reflectarray antenna is demonstrated, analysed, fabricated and experimentally validated.

Group 4: Summary and Bibliography. Finally, Chapter 7 summarises the work contributions of this thesis and recommend possible work for future research in this area. It then followed by bibliography listing references that have been used to complement this thesis.

1.4 Statement of original contributions

In this thesis, original research contributions are presented in the two main core parts 2 and 3. The part 2 of the thesis explores the fundamentals of continuously beam steering reconfigurable antenna configurations. The third part is focussed on the fundamentals of reconfigurable periodic structures and their application. The detailed statements of original contributions are presented as follows.

1.4.1 Stub-loaded varactor control for reconfigurable antenna designs

- Chapter 3 focusses on the development of a reconfigurable two-element array antenna. This chapter firstly discusses the general approach which integrates varactors and stubs at the edge of a single element, thus leading to frequency reconfiguration. Then, in order to achieve beam scanning, two reconfigurable single elements with identical structure are coupled at a certain distance and excited by a common feed network. The operating principle of the array is then described in detail to explain and optimise the H-plane continuous scanning capability. The proposed antenna demonstrates multiple functionalities with frequency and pattern reconfigurability.
- Next, to simplify the array antenna design while taking inspiration from the same operating principle mentioned in Chapter 3, a pattern reconfigurable single-element antenna configuration is presented in Chapter 4. The chapter demonstrates two coupled cavities with partly independent resonance frequencies in the designed antenna structure. This functionality is achieved though a series of vias placed near the patch center. In this configuration where different phases are generated between the cavities, the reconfigurable radiation patterns take the form of E-plane scanning.

1.4.2 Stub-loaded varactor control for reconfigurable periodic structures

- In Chapter 5, a general design structure of reflectarray unit cell antenna is discussed. The reconfiguration of the unit cell relies on to the impedance transformation characteristics that are optimised over the length of the stub. To provide a

small unit cell structure, a T-shape stub configuration is proposed. In the framework of an infinite array environment simulation in Microwave Studio by CST ((2019)(CST), CST), a good performance of frequency tuning range with a phase response of nearly to 310° has been identified through simulations.

- Meanwhile, Chapter 6 explores the development of a reconfigurable reflectarray antenna configuration with folded stubs, which is amenable to practical realisation of beam steering. A fabricated linear array is demonstrated in two-dimensional settings. The chapter also discusses the two-dimensional measurement method for this linear array as experimental validation of the general concept.

Chapter 2

Reconfiguration Mechanisms and Techniques

THE relevance of reconfigurable antennas for future communications systems can no longer be denied as they get increasing attention in the research community and industry. This is motivated by the added flexibility and potentially increased link reliability in many applications compared to conventional antennas. This chapter presents a literature review of microstrip antennas that can be reconfigured in frequency, radiation pattern and/or polarisation. It describes in details various reconfiguration mechanisms that have been applied into reconfigurable antenna design approaches either through electrical, mechanical, optical or material changes. As this thesis is focused on an electrical tuning mechanism, a number of practical antenna examples for electrically actuated reconfiguration with advanced techniques are presented in the later sections.

2.1 Introduction

In advanced wireless communications and radar systems, antennas are components that are a key factor to enhance system performance since they provide the means of radiating and capturing electromagnetic waves. Figure 2.1 shows the operation principle of electromagnetic waves radiation in which the arrows are corresponding to the power flow. More specifically, the guided electromagnetic wave are launched by a RF source circuit and the antenna acts as the transition to enable radiation of the electromagnetic wave into free space. Usually, the shape and size of the antenna will determine how the wave can be radiated. There are numerous common types of antenna designs that are usually selected based on application-specific system requirements, either from mechanical or electrical considerations. Examples include aperture antennas, microstrip antennas, dipole/monopole antennas or loop antennas (Balanis, 2015).

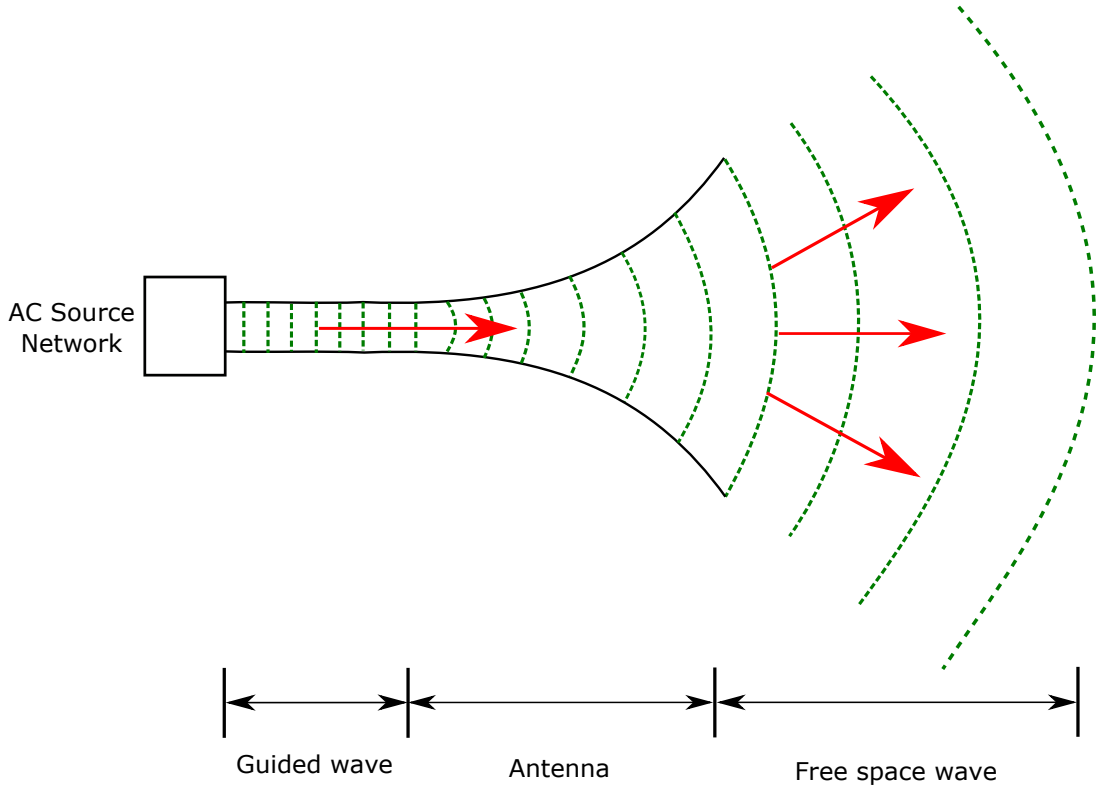

Figure 2.1. Antenna as a transition device. Antenna as a transition device between guided waves and free-space waves.

In this chapter, the microstrip antenna is selected for review, due to its simple planar configuration and advantages for application in most communications systems as explained in Section 2.1.1. In this case, the antenna implementations can range from simple single-element configurations to complex designs such as array antennas.

2.1.1 Microstrip antennas

As each type of antenna possesses constitutive advantages for a specific application, microstrip antennas have received particular attention since they are based on printed circuit technology. Therefore, they have a low profile, low cost, light weight, high reliability and they can be integrated conveniently with other planar circuits. In past theoretical studies, the fundamentals of microstrip antenna designs have established the dependency of the desired resonance frequency on the effective relative permittivity, height of the substrate, width and length of the patch geometry. For a conventional rectangular microstrip antenna, the parameters for the fundamental resonant TM10 mode as a function of the structure dimensions can be expressed as follows (Balanis, 2015):

a) Width of the patch W:

$$W = \frac{c_0}{2f_r}\sqrt{\frac{2}{\varepsilon_r + 1}} \tag{2.1}$$

where c_0 is velocity of light, ε_r is relative permittivity of substrate material and f_r is resonance frequency.

b) Effective relative permittivity ε_{reff}:

$$\varepsilon_{reff} = \frac{\varepsilon_r + 1}{2} + \frac{\varepsilon_r - 1}{2}[1 + 12\frac{h}{W}]^{-\frac{1}{2}}, \tag{2.2}$$

where h is height of the patch substrate.

c) Effective length of the patch at resonance frequency L_{eff}:

$$L_{eff} = \frac{c_0}{2f_r\sqrt{\varepsilon_{reff}}}, \tag{2.3}$$

d) Length of the patch dimension L:

$$L = L_{eff} - 2\Delta L, \tag{2.4}$$

where ΔL is an incremental length of the patch that can be calculated as,

$$\Delta L = 0.412h\frac{(\varepsilon_{reff} + 0.3)(\frac{W}{h} + 0.264)}{(\varepsilon_{reff} - 0.258)(\frac{W}{h} + 0.8)}. \tag{2.5}$$

An initial design of microstrip antenna for operation at a frequency f_r can be straightforwardly implemented following the equations (2.1) to (2.5).

2.1.2 Reconfigurable antennas

As is well known, the fixed geometry of an antenna imposes restriction on its radiation performance. Since modern communications request operation over various bands and with different radiation characteristics which are difficult (or even physically impossible) to achieve with a single compact antenna, researchers have found solutions to adapt the behavior of antennas by introducing dynamic reconfigurability features.

A reconfigurable antenna is a unique device which can acquire the radiation performance of a multi-antenna system by exploiting a geometry that can be adjusted dynamically. In this case, the optimisation of the antenna design for particular specifications should aim at improving the system effective performance and power utilisation by eliminating unnecessary additional radiating components. This in principle allows to minimise cost, volume and complexity, while simplifying integration. The antenna reconfigurability can be implemented to adapt to changing requirements or environmental conditions and therefore provides an additional level of functionality. Practically, the resonant operation of the antenna can be controlled by altering its effective electrical length, which in turn will modify the current distribution on the antenna and may allow to tune the frequency band of operation, adapt the polarisation or steer the radiation pattern in a desired direction. Traditionally, the reconfigurability properties have been classified into 4 generic categories, which include reconfigurability of the frequency response, radiation pattern, polarisation state and combination of these modalities (known as a compound reconfiguration) (Bernhard, 2007b; Christodoulou *et al.*, 2012; Costantine *et al.*, 2013). Figure 2.2 shows the advantages and disadvantages of a concept of multiple antennas versus reconfigurable antennas for communications applications.

Features	Multiple Antennas	Reconfigurable Antenna
Model	Single-band antennas each operating with single resonance frequency and functionality	Single antenna structure operating with multiple functionalities
Space requirement	Space requirement to accommodate several antennas	Minimal space requirement
Individual radio performance	Very good performance optimised for each band	Acceptable performance, additional loss introduced by electrical switches
Cost	High cost required	Low cost required with low power consumption

Figure 2.2. Static vs. reconfigurable antenna systems. The advantages and disadvantages of configurations including multiple antennas and reconfigurable antennas.

In this context, there are several challenging questions that researchers need to address in reconfigurable antenna designs. The first question that needs to be assessed is what is the most significant reconfiguration property for the antenna design in the targeted application? It could be frequency, radiation pattern, polarisation or combined properties. Then, the potential of a particular antenna geometry to achieve the required reconfiguration of the property needs to be considered as well. Finally, what are the reconfiguration mechanisms and techniques that can be used to reduce the negative effects of the reconfiguration mechanism on the antenna in term of losses, unstable radiation patterns and mismatched impedance characteristics? With these important questions in mind, this chapter reviews several practical examples of reconfigurable antenna implementations based on current technologies.

2.2 Reconfiguration mechanisms

Figure 2.3 provides a brief overview of various mechanisms and advanced techniques that can be adopted into reconfigurable antenna designs. It includes the conventional reconfiguration mechanisms through electrical and mechanical/physical processes, which are most commonly used in antenna technology, as well as optical and material changes.

Every approach has associated practical techniques which should be considered in view of their advantages and disadvantages for the intended application.

In this section, the electrical tuning methods will be described in more detail since they are the most relevant today, and they are the subject of this thesis. Electrical reconfigurability techniques include different switching modalities enabled by Radio Frequency MicroElectroMechanical Systems (RF MEMS) switches, PIN diodes and varactors.

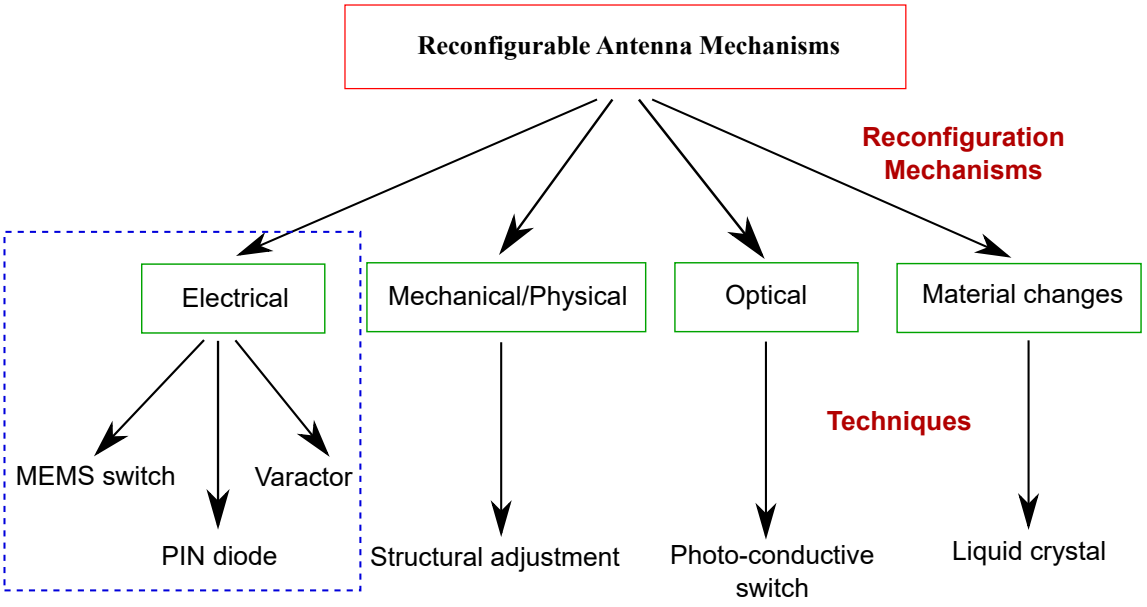

Figure 2.3. Reconfiguration mechanisms. Reconfiguration mechanisms adopted in antenna design.

2.2.1 Radio-Frequency MicroElectroMechanical System (RF MEMS) switch

A RF MEMS switch is a standard mechanical semiconductor-based switching system based on VLSI circuit fabrication technology. Basically, the switch involves a microelectromechanical movement controlled by electronic components to provide the switching functionality at radio frequencies. In an antenna design, the RF MEMS switch can be used to control the surface current flow either through short circuit or open circuit operation. In addition, a RF MEMS switch can be fabricated directly onto the antenna structure, i.e. printed on a glass or ceramic dielectric substrate. Figure 2.4 shows an equivalent circuit model and an example of RF MEMS switch. Since the device has low up state capacitance, this results in wideband performance in the antenna design.

The typical advantages of RF MEMS switches are their low power consumption and high tuning speed (from $1 - 100$ ns), low cost, high isolation and low insertion loss. However, the switch has limitation in poor quality factor, nonlinear behavior, non-continuous tunability and high DC bias current requirement in the "ON" state.

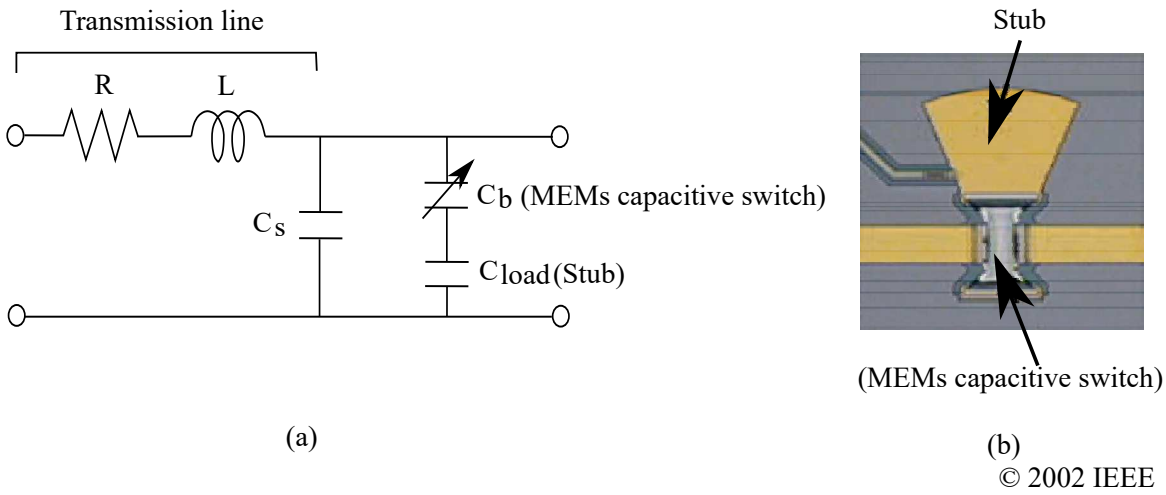

Figure 2.4. RF MEMS. Equivalent circuit and RF MEMS switch model. (a) Equivalent circuit model and (b) example of integrated RF MEMS switch (Rebeiz *et al.*, 2002)

2.2.2 PIN diode

A PIN diode is a semiconductor component including P-type and N-type regions, separated by an Intrinsic region. A PIN diode provides the ability to control low to high RF signals in different applications with a low level of DC biasing. The diode can be a good RF switching mechanism that can be integrated into the antenna design. It enables two modes of operation that will let RF signals pass or block them. The diode is in "ON" state when it is in forward bias DC current, and in "OFF" state when the diode is on reverse bias DC current. Figure 2.5 illustrates a PIN diode fundamental model and equivalent circuit in two mode of operations.

The main advantages of the PIN diodes are their low DC actuation voltage combined with high tuning speed ($1 - 100$ ns), high-speed response, and a high reliability since they include no moving parts. Their simplicity and wide availability results in a low cost of production. The disadvantages of the PIN diode are non-continuous tunability and high reverse recovery time due to power loss.

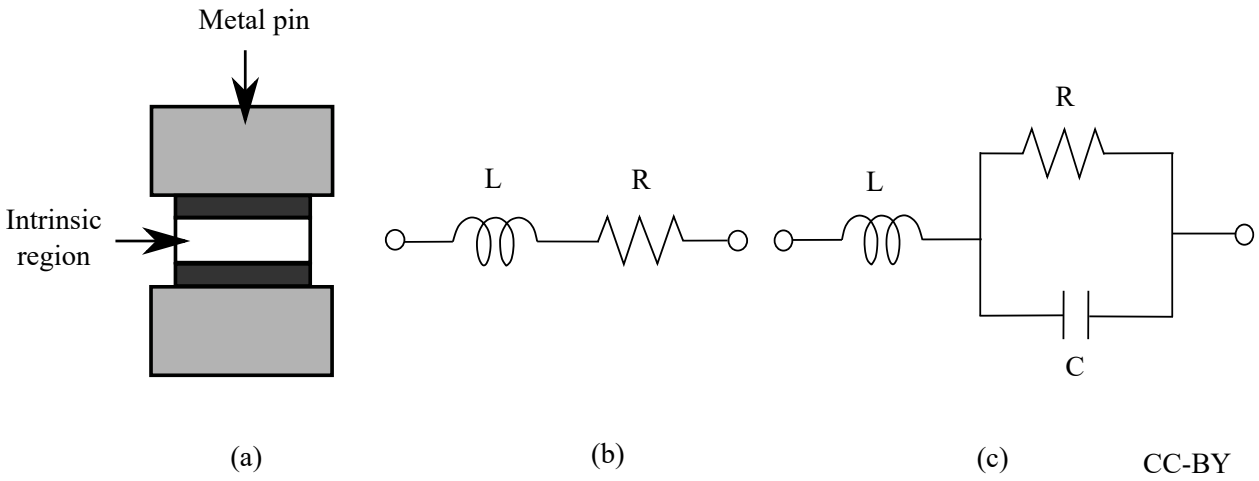

Figure 2.5. PIN diode. PIN diode equivalent circuit, (a) cross-section of basic PIN diode, (b) "ON" state operation and (c) "OFF" state operation (Doherty and Watertown, 2015).

2.2.3 Varactor

A varactor diode (also sometimes referred to as varicap diode) is a semiconductor component that normally consists of a P-N junction. The varactor is considered as a special type of diode which provides a variable junction capacitance controlled by a bias voltage. Generally, the values of the variable capacitance can be up to tens or even hundreds of picofarads depending on the type and model of varactor. The operation of the varactor is relying on the reverse biased state voltage and therefore nearly no DC current will flow through the component. Figure 2.6 shows an equivalent circuit of a varactor diode.

According to an example of a varactor datasheet (MACOM, 2015), the variable junction capacitance $C(V)$ can be calculated as:

$$C(V) = \frac{C_{JO}}{(1 + V/V_J)^M} + C_{par}, \tag{2.6}$$

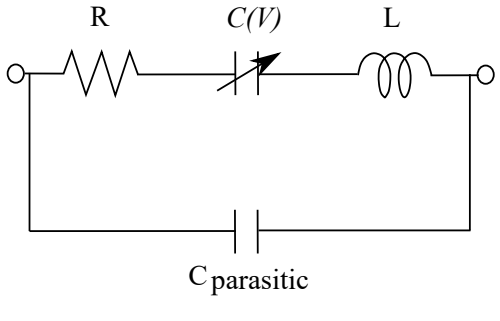

Figure 2.6. Varactor. Equivalent circuit of varactor diode (MACOM, 2015).

R	L	C_{JO}	V_J	M	C_{par}
2 Ω	0.05 nH	1.2 pF	4.155 V	1.97	0.1044 pF

Table 2.1. Varactor parameters

where C_{JO} is the hyperabrupt junctions capacitance, V_J is the built in potential voltage, M is parameter of the abrupt junction and C_{par} is the parasitic capacitance of the varactor. The parameters for the varactor MA46H120 used in this thesis are shown in Tab. 2.1. Figure 2.7 shows the varactor capacitance $C(V)$ varying from 1.304 to 0.149 pF when changing the reverse bias voltage from 0 to 18 V.

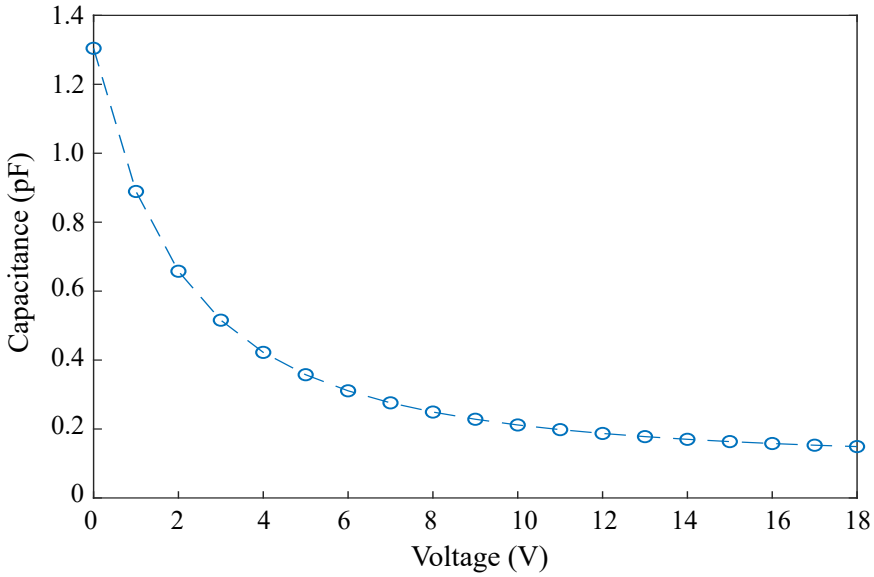

Figure 2.7. Variable junction capacitance of MA46H120 varactor. Variable junction capacitance of MA46H120 varactor corresponding to the change of reverse bias voltage.

The advantages of the varactors compared to other switches are firstly that they allow very small current flow through them, thus minimising DC power consumption; secondly, they have a relatively high quality factor; and thirdly, they are also suitable for antenna designs that request a continuously tunable operation. However, the varactor is a non-linear component which has limited RF power capability and requires a complex bias circuitry.

2.3 Type of reconfigurable antennas

This section introduces the fundamental approaches to reconfigurable antenna technology, putting emphasis on electrically tunable implementations with diodes and switches as described in the previous section. It begins with a detailed explanation and summary of reconfigurable properties with some examples from the literature. For each modality of reconfiguration, the selected examples will sequentially cover actuation using RF MEMS, PIN diodes or varactors.

2.3.1 Frequency-reconfigurable antennas

In the literature dedicated to microwave technology, frequency reconfigurability is defined as the tunability of the operation frequency band with acceptable matching, and is often described through the variation of the central resonance frequency. This functionality should be usually obtained for one or more resonance frequencies without any substantial changes to the antenna radiation pattern and polarisation properties in the operation band.

The frequency reconfigurability of the antennas can be implemented with the mentioned electrical tuning elements (RF MEMS switch, PIN diode and varactor) to attain a reliable system performance. An example in (Zohur *et al.*, 2013) proposed a reconfigurable RF MEMS integrated antenna with the ability to achieve two frequency modes of operation. A RF MEMS is embedded at a strategic location in the bottom layer of the antenna geometry, allowing to change the current path between a meander and a T-shaped structure. Figure 2.8 shows the photographs of the frequency-reconfigurable antenna operated by “ON” and “OFF” state of the RF MEMS switch. The antenna provides two modes with central frequencies of 0.718 GHz and 4.96 GHz. Another example was presented by (Wright *et al.*, 2018) who proposed a reconfigurable patch antenna

with RF MEMS switches directly integrated onto the patch antenna to provide three reconfiguration states of operation frequencies. The antenna supports frequency in lowband, midband and highband at 1.16 GHz, 1.28 GHz and 1.6 GHz, respectively which are appealing to different applications.

The use of PIN diodes as a switch for frequency reconfiguration has been extensively explored in the literature (Majid *et al.*, 2013; Pazin and Leviatan, 2013; Bansal *et al.*, 2018). For example in (Han *et al.*, 2016), a reconfigurable slotted rectangular compact patch antenna with a set of PIN diode working as switches is presented. The operation of the antenna is controlled based on the ON-OFF states of three switches that provide switchable subbands between two single-band modes (2.3 and 5.8 GHz) and two dual-band modes (2.3/4.5 GHz and 4.5/5.8 GHz). With a similar operating principle, another example is found in (Borhani *et al.*, 2016), who also presented a wide range of frequencies that can be modified extensively, with three switchable multiband frequency response at $2.3 - 2.51$ GHz, $3.35 - 3.75$ GHz and $4.95 - 5.53$ GHz for Bluetooth, WiMaX and WLAN applications, respectively. Another impressive design of frequency tuning reconfiguration is demonstrated in (Zadehparizi and Jam, 2018), where a rectangular microstrip patch antenna including a slot with optimised shape and switchable PIN diodes in the ground plane was proposed to increase reliability performance. There were two categories of antenna designs in this paper: Firstly, a design with a single diode mounted in the antenna structure had an "OFF" state corresponding to a frequency with higher priority. Secondly, with an increase to three diodes in the optimised structure, the reliability of the antenna was improved by adding four different switchable band of operations. The manufactured antenna and tunable frequencies of the antenna are shown in Fig. 2.9, with a performance validating the concept.

The integration of varactor diodes in frequency-reconfigurable antennas can be found in numerous publications (Khidre *et al.*, 2015b; Huang *et al.*, 2016; Ge *et al.*, 2017). In (Nguyen-Trong *et al.*, 2017a), the variable capacitance from two sets of varactors was selected as tuning mechanism that independently controls the resonance frequencies in two distinct bands for a low-profile monopolar antenna. In this case, the antenna provided continuously tunable dual-frequency bands. The lower band was achieved by an equivalent magnetic-current loop through a center-fed patch with shorting rods. Then, four symmetrical slot on the patch created another magnetic-current loop that define the radiation in the upper band. In another publication from the same group, (Nguyen-Trong and Fumeaux, 2018), a further analysis of design tradeoffs on a

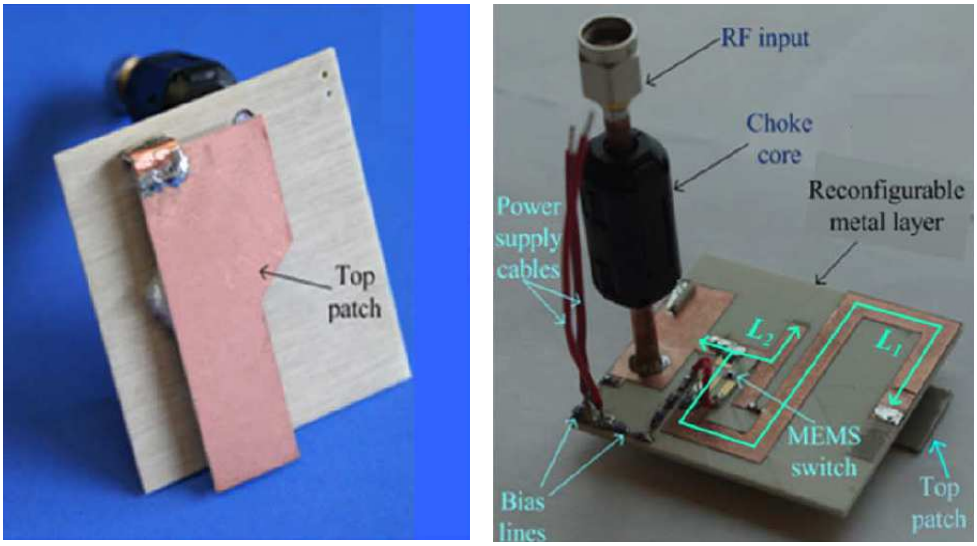

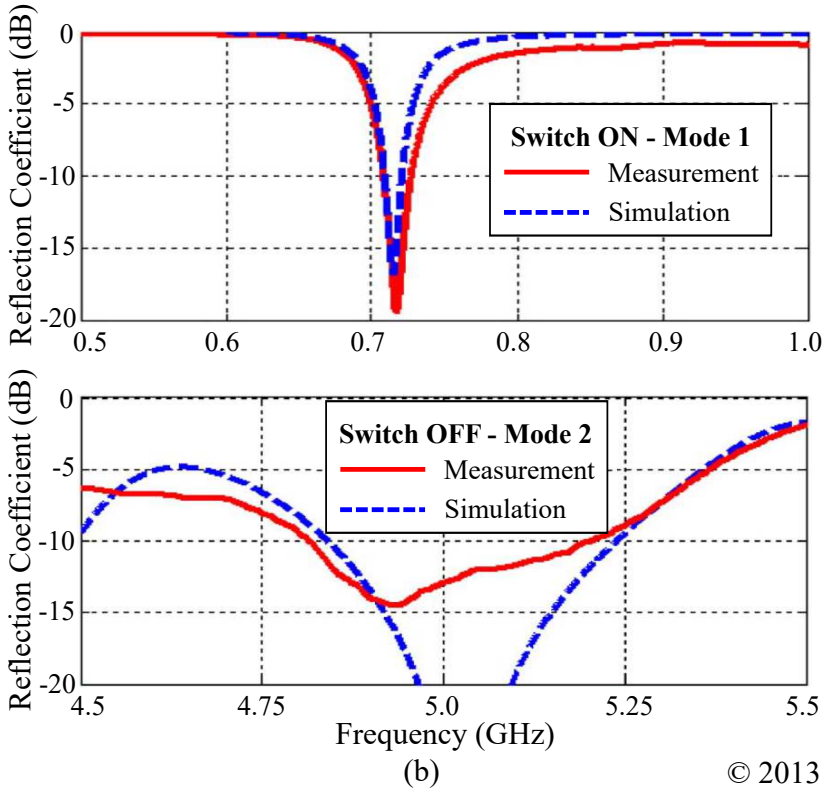

Figure 2.8. Example of RF MEMS frequency-reconfigurable antenna. An example of reconfigurable antenna design using RF MEMS switch (Zohur *et al.*, 2013). (a) Photographs of the antenna in top and bottom views. (b) Frequency response of the antenna controlled by the switch state.

frequency-reconfigurable microstrip antenna based on varactor tuning was conducted in order to maximise the antenna tuning range and efficiency. The article investigated several different antenna design structures and demonstrated how to obtain the appropriate capacitance range for optimal design. Figure 2.10 shows the examples of the reconfigurable antenna, together with the frequency reconfigurable reflection coefficient.

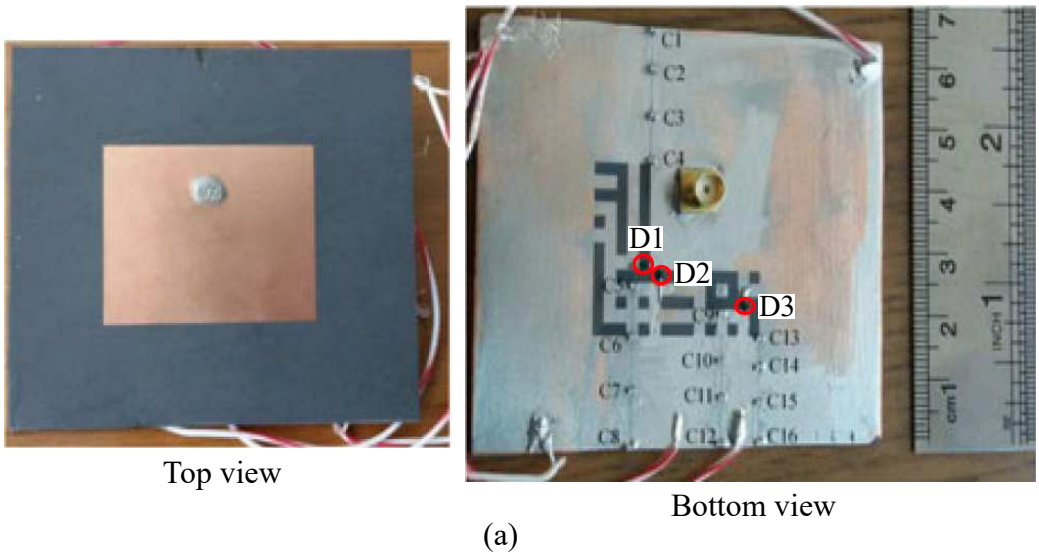

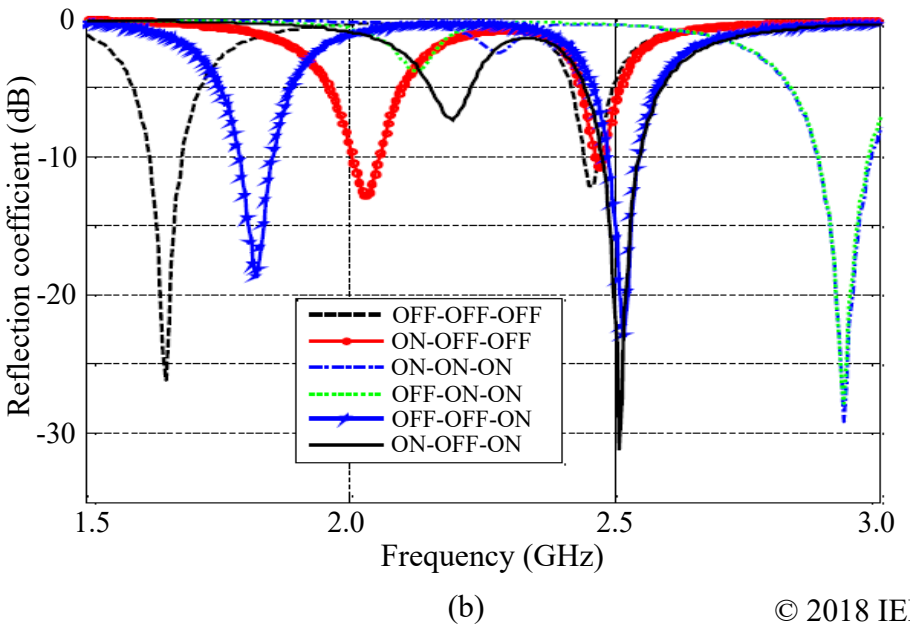

Figure 2.9. Example of PIN diode frequency-reconfigurable antenna. An example of frequency-reconfigurable antenna design using three PIN diodes. (a) Manufactured antenna and (b) reflection coefficients of the antenna at different states of diodes (Zadehparizi and Jam, 2018).

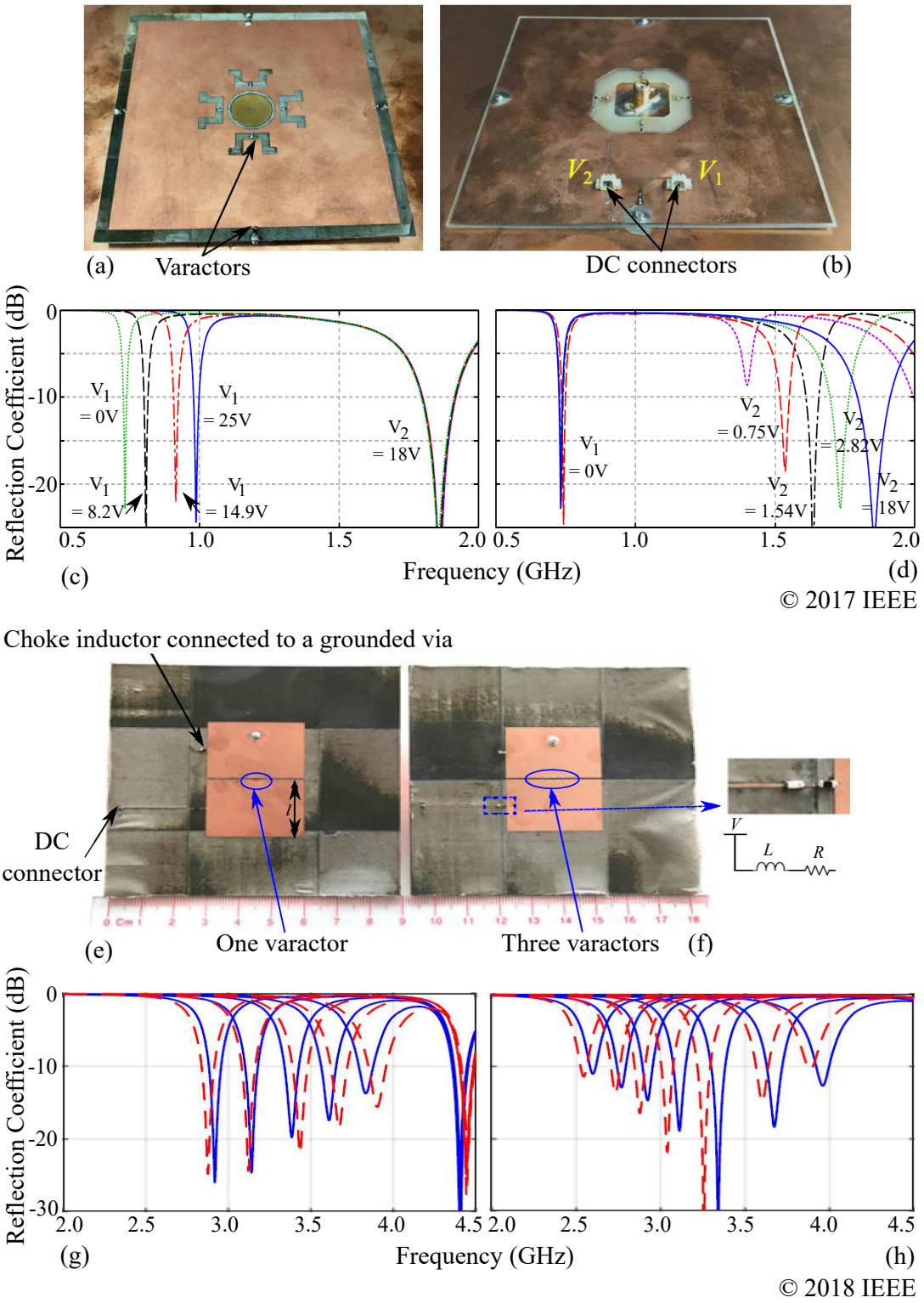

Figure 2.10. Examples of varactor-controlled frequency-reconfigurable antenna. Examples of frequency-reconfigurable antenna designs using varactors. (a)(b) Top and bottom views of the proposed antenna structures in (Nguyen-Trong *et al.*, 2017a) with independent tuning in the (c) lower band and (d) upper band. (e)(f) Photographs of the reconfigurable antenna loaded with one and three varactors onto the aperture (Nguyen-Trong and Fumeaux, 2018) with (g) reflection coefficient for the one varactor design and (h) reflection coefficient for the three varactors design.

2.3.2 Pattern-reconfigurable antennas

In order to increase the reliability of a communications link, it is desirable to adapt the radiation patterns of the antenna to direct transmission/reception in preferred directions. In this context, the design of pattern-reconfigurable antennas aims to change the structure of the antenna radiation pattern in term of direction, shape or gain (Jin *et al.*, 2018; Chen *et al.*, 2018a), without significant changes in the resonance frequency and polarisation of the antenna. Generally, the fundamental principle of a pattern-reconfigurable antenna relies on a variation of the antenna current distribution including magnitude and phase in the radiating aperture. The relationship between the current distribution and the reconfigurable radiation pattern is somewhat challenging to directly comprehend, but it is nevertheless possible to control the currents by applying some of the tuning mechanisms that have been mentioned in 2.2. The antenna can be developed with a single radiating element, or alternatively with several antenna elements in an array configuration. In the latter case the radiation pattern is determined by the multiplication of a unit of single antenna element radiation pattern with the array factor of the antenna (Mailloux *et al.*, 1981; Balanis, 2015), and as such, the reconfiguration mechanism has to aim at modifying the array factor, e.g. by controlling the inter-element phase difference.

Over the last decades, several designs with switching techniques to change the radiation pattern of antennas have been proposed based on MEMS switches. For example, the antenna proposed in (Besoli and Flaviis, 2011) has introduced a multifunctional reconfigurable pixeled antenna using MEMS technology as active switching devices. The MEMS devices were embedded directly onto a printed circuit board substrate to achieve switching of orthogonal radiation patterns corresponding to either the antenna fundamental excitation or higher order modes. Towards a compact antenna configuration and control architecture, (Deng *et al.*, 2016) focused on a low profile and small size of reconfigurable patch antenna which was operated at a resonance frequency of 35 GHz and comprised two RF MEMS switches. The antenna provided three different directions of radiation pattern controlled by switching modes of the RF MEMS switches. Figure 2.11 shows the photograph of the reconfigurable antenna with its radiation pattern characteristics.

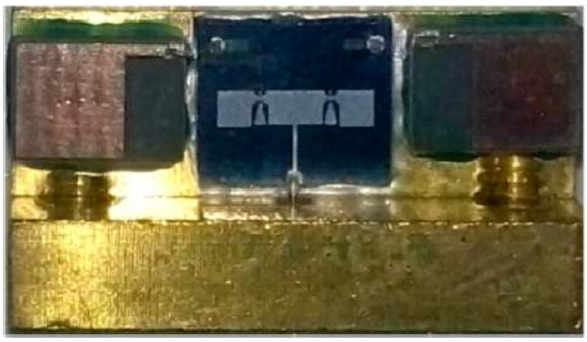

(a)

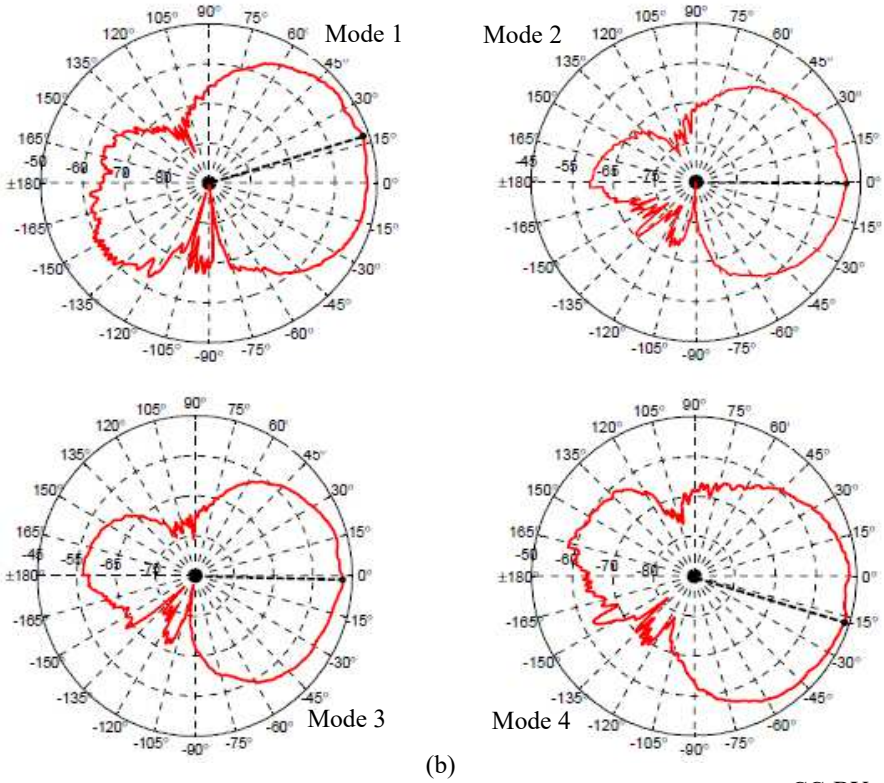

(b)

Figure 2.11. Example of RF MEMS pattern-reconfigurable antenna. (a) The low-profile pattern-reconfigurable RF MEMS antenna with testing holder. (b) Pattern reconfiguration characteristics at different states of the RF MEMS switches (Deng *et al.*, 2016).

Another type of the electrical switching typically used for pattern-reconfigurable antennas is PIN diodes which received wide attention in recent years (Jusoh *et al.*, 2014a; Lin *et al.*, 2017b). The article by (Yang *et al.*, 2018) presented a switchable feeding network realised through a PIN diode located at the feed. This arrangement allows to produce two different antenna excitations of in-phase and out-of phase modes which in turn provide a pattern reconfigurability to a patch antenna. In this case, the antenna will produce a conical radiation pattern when the switchable feed has an in-phase excitation and a broadside radiation pattern when the feed has an out-phase excitation. As most recent design of pattern-reconfigurable antenna, a compact microstrip antenna with multidirectional beam is reported in (Yang *et al.*, 2019). The antenna consists of six PIN diodes that are placed in between two metal walls and the antenna ground plane. By controlling the different switching modes (ON and OFF states) of the diodes, six different directions of radiation patterns are realised within the operating frequency band from 3.5 GHz to 3.9 GHz. Figure 2.12 shows examples of the pattern-reconfigurable antennas using PIN diode switches.

With basic concepts similar as implemented with RF MEMS and PIN diode switching, the varactor diodes are in addition able to modify the effective electrical length of resonant structures continuously by variation of the variable capacitance of the varactor. Examples illustrating this ability can be found in (Farzami *et al.*, 2017; Row and Wu, 2018; Tian *et al.*, 2019). A linear phased array with pattern-reconfigurable microstrip Yagi-Uda antenna elements is demonstrated in (Xiao *et al.*, 2015a). The antenna consists of varactors loaded onto all antenna elements to provide flexibility at wide scanning angles. This is illustrated in Fig. 2.13(a) where the prototype of the array antenna is shown with illustration of its pattern reconfiguration. In addition, the attractive antenna design in (Shi *et al.*, 2019) demonstrated that multibeam characteristics can be achieved in a variation of beamwidth in E-plane, H-plane and also both planes. The paper introduced a single magnetoelectric dipole antenna with two tunable parasitic patches loaded with a varactor into each of them. This realised a continuously varying radiation pattern beamwidth by adjusting the varactor capacitance within a frequency band of 2 GHz to 2.1 GHz. The functionality of the reconfigurable magnetoelectric dipole antenna with variable beamwidth is illustrated in Fig. 2.13 (b).

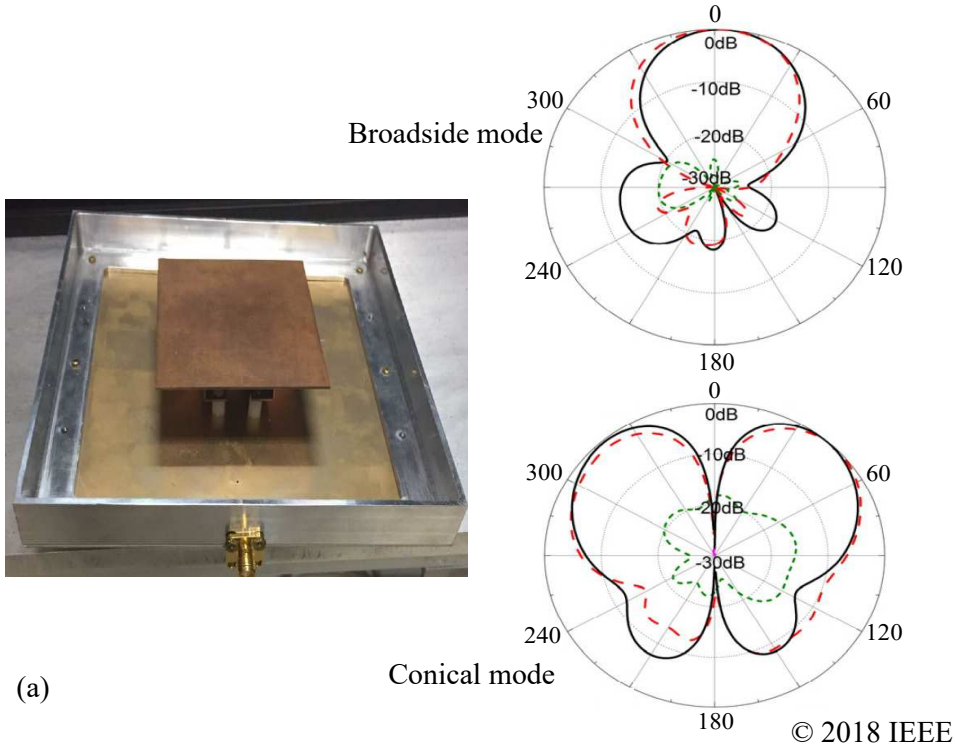

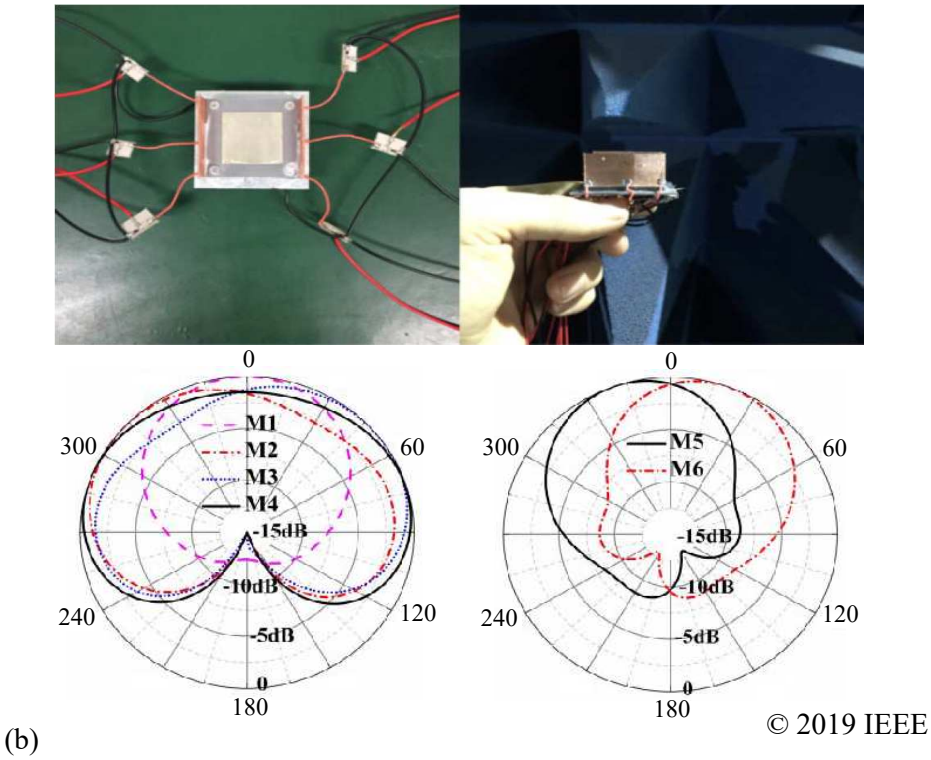

Figure 2.12. Examples of PIN diode pattern-reconfigurable antennas. Examples of PIN diode switching for the pattern reconfigurations in (a) (Yang *et al.*, 2018) and (b) (Yang *et al.*, 2019), respectively.

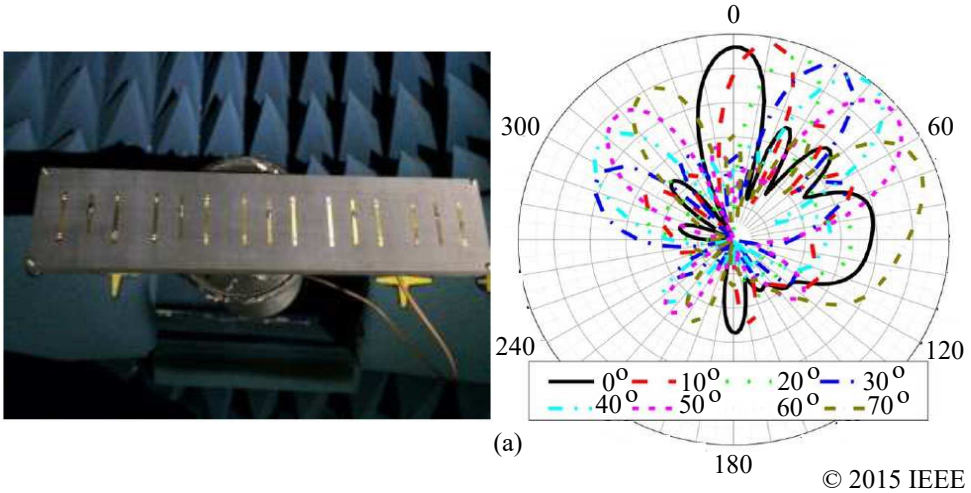

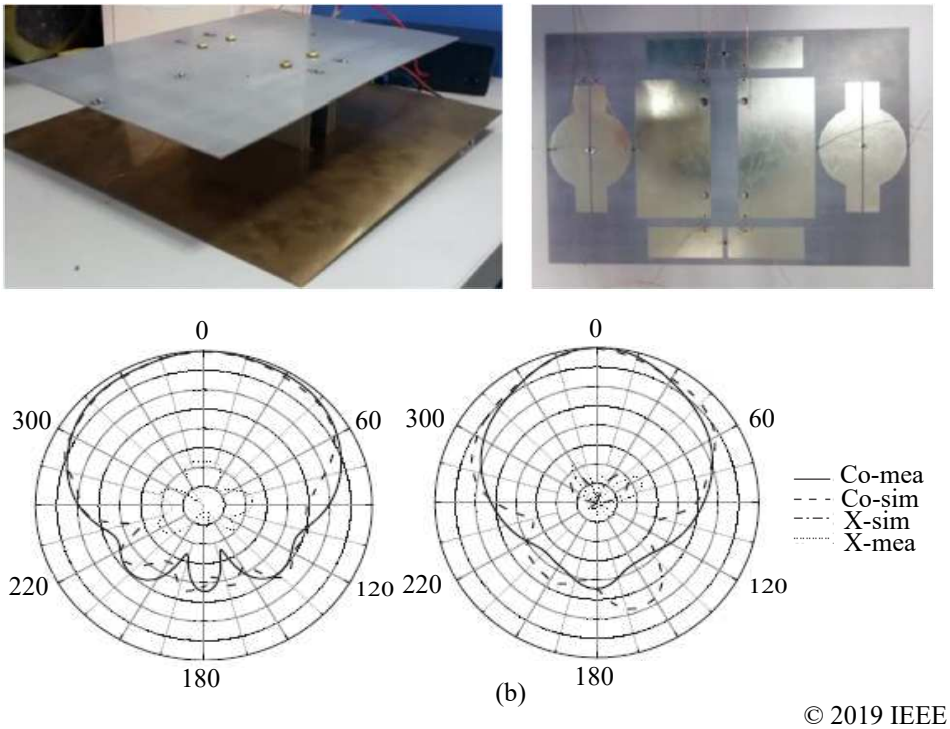

Figure 2.13. Examples of varactor-controlled pattern-reconfigurable antennas. Examples of varactor diode switching for the pattern reconfigurations in (a) (Xiao *et al.*, 2015a) and (b) (Shi *et al.*, 2019), respectively.

2.3.3 Polarisation-reconfigurable antennas

Polarisation-reconfigurable antennas are generally realised with two primary methods, namely through changes in the antenna structure or through the variation of the material properties. This type of reconfigurable antennas offers the capability to switch between different polarisation characteristics, e.g. between various angles of linear polarisation (LP), or between right-hand circular polarisation (RHCP) and left-hand circular polarisation (LHCP), or even between linear and circular polarisations in one integrated device. Practically, linearly polarised radiation characteristics occur when the antenna has its radiating currents in a plane bearing the direction of propagation. In contrast, if the antenna currents experience well-defined rotation perpendicular to the direction of radiation during one frequency cycle, the radiation characteristics will correspond to a state known as a circular polarisation. In this situation, the RHCP sense of rotation has a transverse electric field rotation in clockwise sense in the direction of propagation. On the other hand, the LHCP has a transverse electric field rotation in anti-clockwise sense in the direction of propagation.

In the literature, a number of solutions for polarisation-reconfigurable antennas have been developed and some examples can be found in (Row *et al.*, 2012; Lin and Wong, 2015b; Gu *et al.*, 2016; Lin and Wong, 2017; Hao *et al.*, 2017). Among these examples, (Kovitz *et al.*, 2015) has put forward the theoretical and practical basis for actuation using RF MEMS switches integrated into a reconfigurable E-shaped patch array antenna, as illustrated in Fig. 2.14. In this work, the radiation characteristics were influenced by the switch states, which allowed effective polarisation reconfiguration of RHCP and LHCP characteristics.

Apart from RF MEMS, polarisation-reconfigurable antennas found in the literature have also widely used PIN diodes as actuator to achieve the functionality. The reference (Lee and Sung, 2014) presented a simple structure of a reconfigurable rhombus-shaped patch antenna that is electrically controlled by two PIN diodes embedded between the microstrip patch and the Y-shaped antenna feed line. A bias circuit network was used to drive the diodes switchable states that determined the two operation modes of polarisation between the LHCP and RHCP. Meanwhile (Sun and Sun, 2016) presented a polarisation-agile aperture-coupled patch antenna with a reconfigurable feeding network. The uniqueness of the antenna is a reconfigurable quad-polarisation ability, which is achieved through PIN diodes embedded into the feeding network. The state of the PIN diodes determine the desired operation between two orthogonal linear

polarisations and two orthogonal circular polarisations. Similarly to (Lee and Sung, 2014), the proposed antenna in (Mak *et al.*, 2017) was also able to switch between vertical and horizontal polarisation characteristics to improve the reliability of the communication systems. Figure 2.15 shows examples of a polarisation-reconfigurable microstrip antenna using beam lead PIN diodes.

Figure 2.16 shows a tunable circular polarisation microstrip Yagi-Uda antenna proposed in (Khidre *et al.*, 2015a). The antenna consists of two square patches where one patch is for circular polarisation and is driven by two orthogonal feeds, while the other patch is used as a reconfigurable parasitic patch loaded with a group of varactors for beam scanning. In this study, the antenna works at a resonance frequency of 2.45 GHz and a changing of the capacitance of the varactors through reverse DC bias voltage in the parasitic patch allows to scan the main beam.

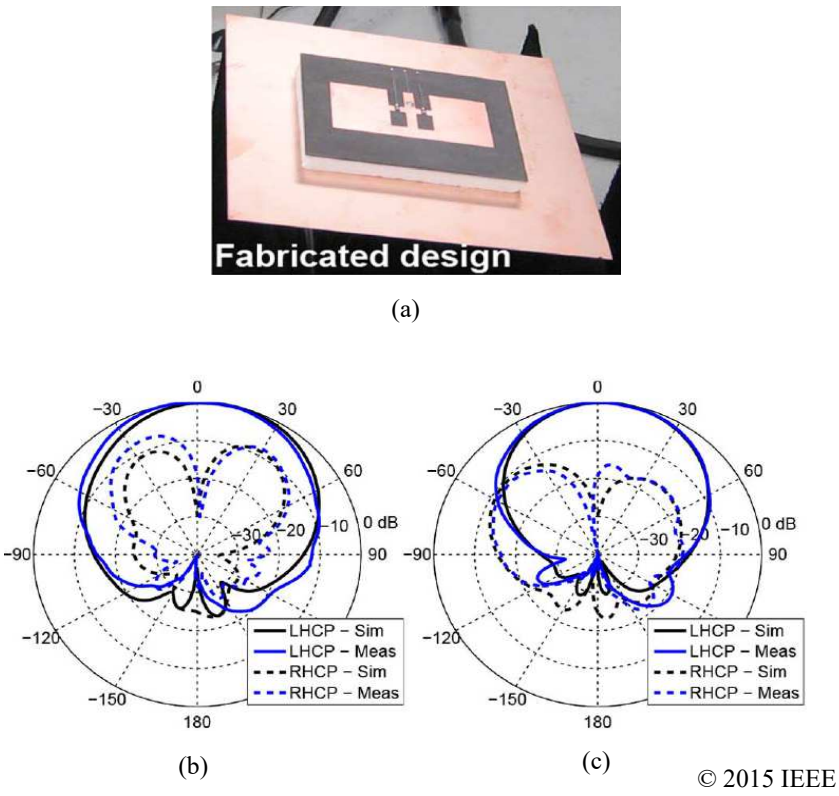

Figure 2.14. Example of RF MEMS polarisation-reconfigurable antenna. (a) Photograph of the RF MEMS reconfigurable circular polarisation E-shaped antenna. The LHCP radiation pattern in (b) E-plane and (c) H-plane at the operation frequency of 2.45 GHz (Kovitz *et al.*, 2015).

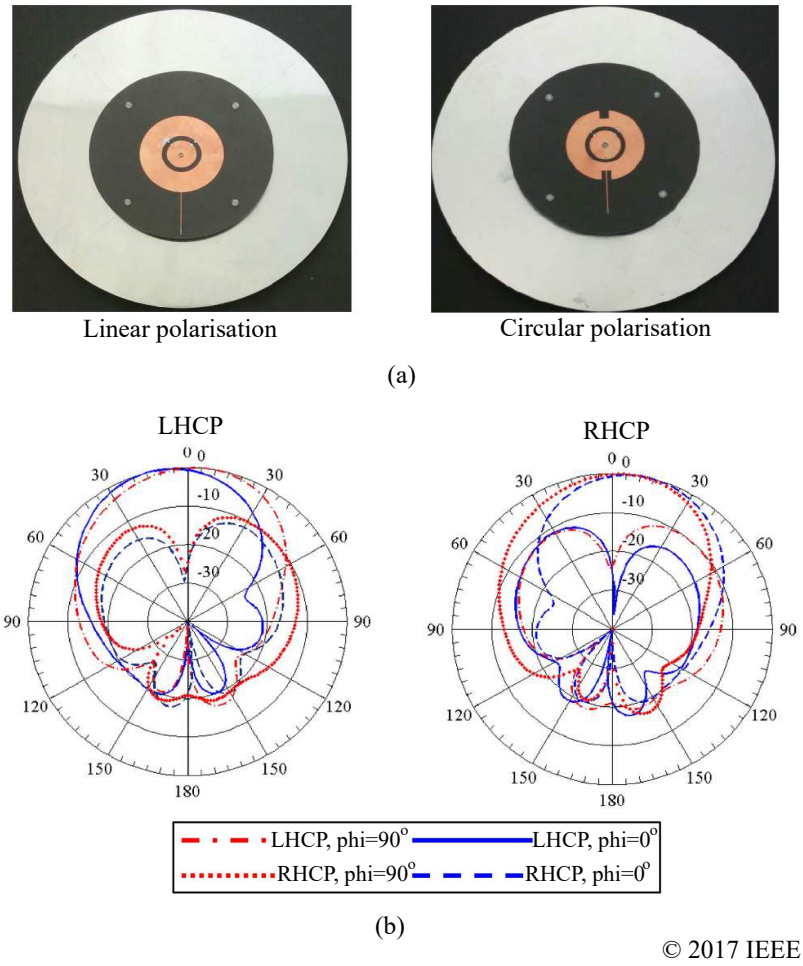

Figure 2.15. Example of PIN diode polarisation-reconfigurable antenna. (a) Prototypes of split ring slot antenna configuration for linear and circular polarisation in (Mak *et al.*, 2017) and (b) the antenna radiation pattern characteristics driven by PIN diode switching states.

2.3.4 Compound-reconfigurable antennas

In addition to the reconfiguration of a single antenna characteristic, as described above, a most desirable feature of reconfigurable antennas is to achieve a combination between two or more reconfiguration types in a single device. This is referred to as compound reconfiguration properties and typically includes frequency and pattern reconfiguration, or frequency and polarisation reconfiguration. These properties can be found in (Rodrigo *et al.*, 2014b; Selvam *et al.*, 2017; Chen *et al.*, 2017a).

In the recent literature, (Patel *et al.*, 2018) demonstrated a compound-reconfigurable microstrip antenna loaded with three square split ring resonators, illustrated in Fig. 2.17, to achieve pattern and frequency reconfigurable properties. The multifunctionalities performance of the antenna is obtained by controlling RF MEMS switches placed in

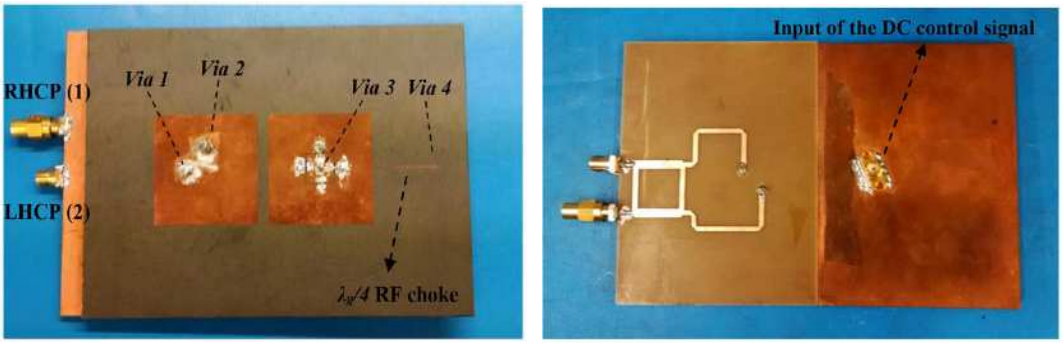

Front view Back view

(a)

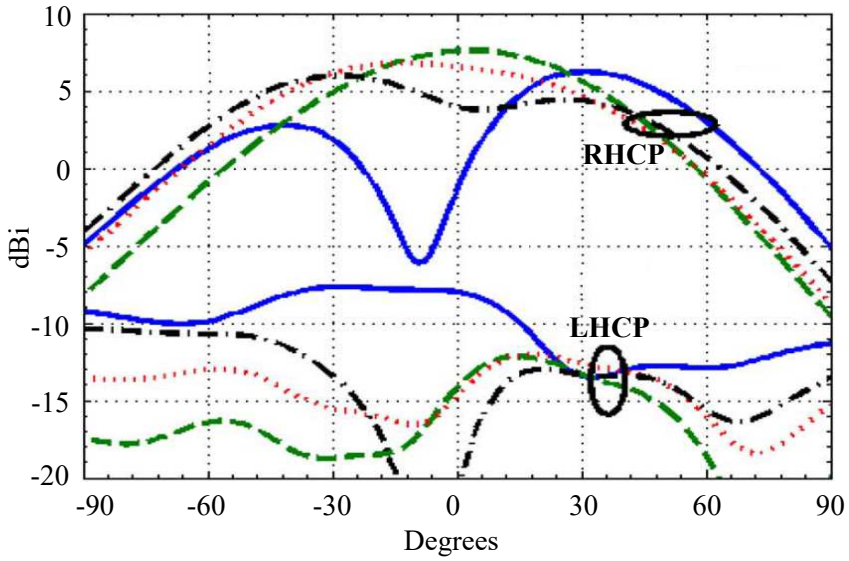

(b)

Figure 2.16. Example of varactor-controlled polarisation-reconfigurable antenna. Configuration of reconfigurable circular polarisation beam scanning antenna associated with varactor tuning devices and biasing networks (Khidre *et al.*, 2015a).

between the gap of the split ring resonators. The tuning of the operating frequency relies on the RF MEMS operation states in term of various combination of switches states. Meanwhile, the radiation patterns are also changed corresponding to the states of the switches.

A design of a frequency- and pattern-reconfigurable antenna with slot transition is also reported in (Majid *et al.*, 2014). The antenna consists of PIN diodes switches integrated into a feeding slot in order to obtain three adjustable frequency bands while slits at the edge of the ground plane procure pattern reconfiguration of the antenna. The article

by (Nguyen-Trong *et al.*, 2017b) demonstrated a reconfigurable circular cavity with 6 tunable groups of PIN diodes switches along its outer edge where each group was controlled by a DC bias network. In accordance with the state of the switches, the antenna realised a reconfigurability of polarisations at discrete resonance operation frequencies. Figure 2.18 shows the fabricated reconfigurable antenna design with good performance results.

In addition, other techniques using varactor diodes also been highlighted in (Nguyen-Trong *et al.*, 2016b) for compound-reconfigurable antennas by controlling the variable junction of the varactor capacitances loaded with matching stub. With the same operating principle design approach in (Nguyen-Trong *et al.*, 2016b), the authors (Nguyen-Trong *et al.*, 2015a) have developed a design of reconfigurable microstrip antenna with frequency and polarisation properties using varactor diodes. There are two independent voltages used to drive the antenna varactors loaded into the stubs that determines the frequency tuning range and also allows the selection of polarisation between circular and linear characteristics. In contrast to varactor loaded with stub, the same reconfigurability of frequency and polarisation can also be designed using active electromagnetic band gap (EBG) structure loaded with varactors. Figure 2.19 shows a wideband monopole antenna placed above the surface of the EBG structure. The surface provides independently tunable of the reflection phases for the orthogonal incident waves. With proper tuning of the varactor bias voltages, circular polarisation can be generated within the resonance frequency range (Liang *et al.*, 2015).

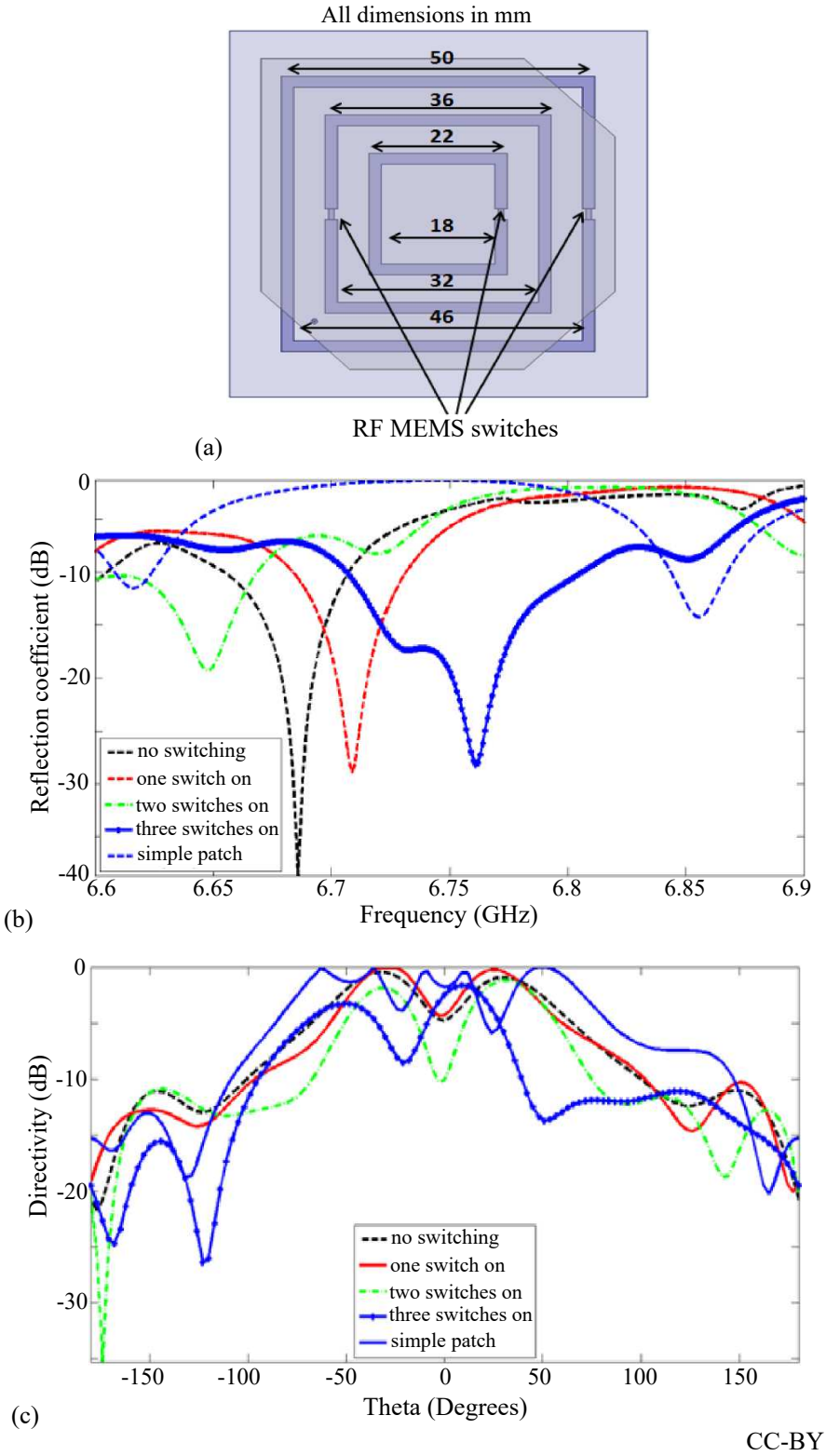

Figure 2.17. Example of RF MEMS compound-reconfigurable antenna. (a) Three square split-ring resonators configuration with RF MEMS switches in (Patel *et al.*, 2018). (b) The frequency tunability and (c) radiation patterns of the antenna corresponding to switches states.

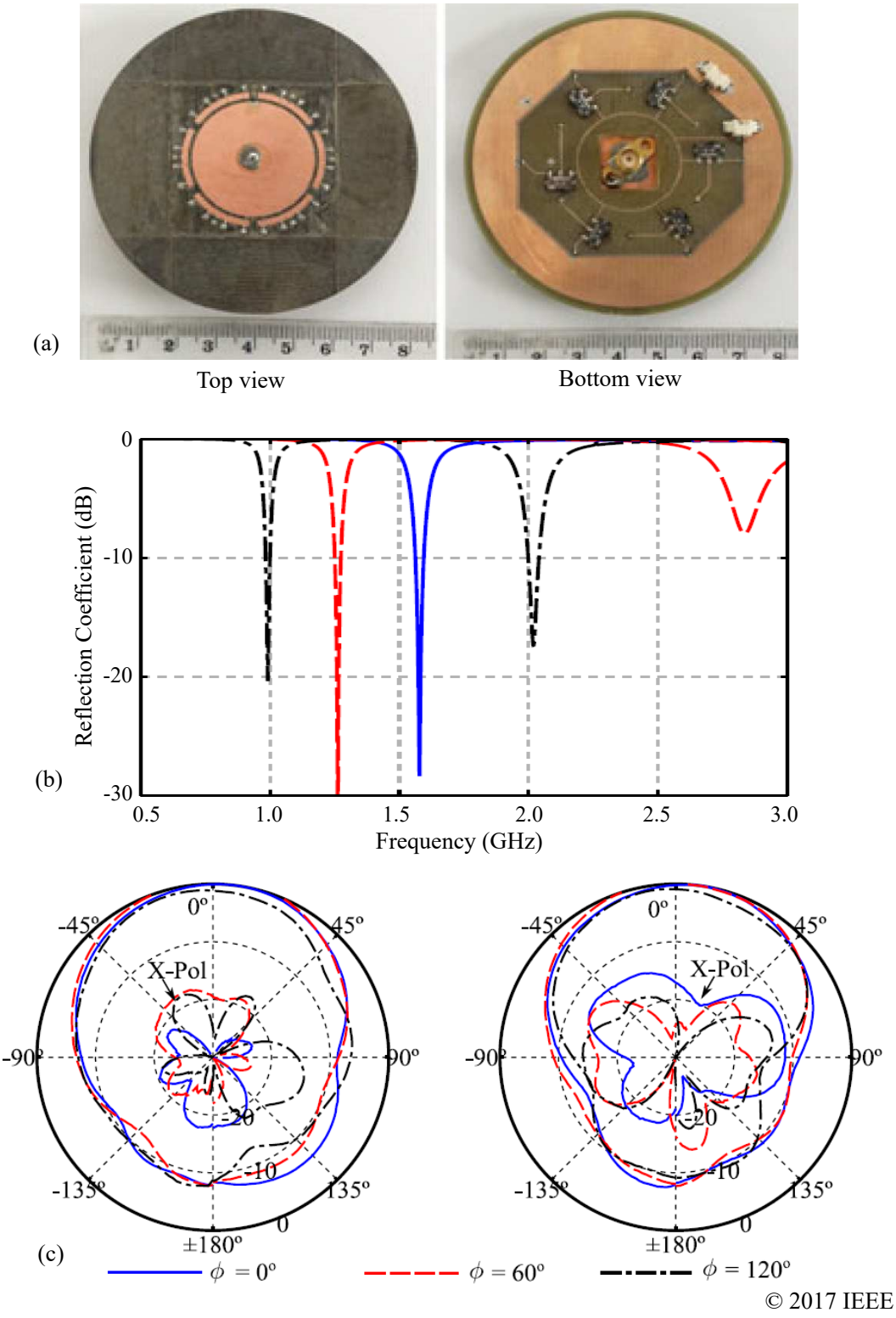

Figure 2.18. Example of PIN diode compound-reconfigurable antenna. (a) Prototypes of the top and bottom view of a reconfigurable circular cavity antenna. (b) The reflection coefficient and (c) the radiation pattern characteristics of the antenna at different polarisation states $\phi = 0°$, $60°$ and $120°$ (Nguyen-Trong *et al.*, 2017b).

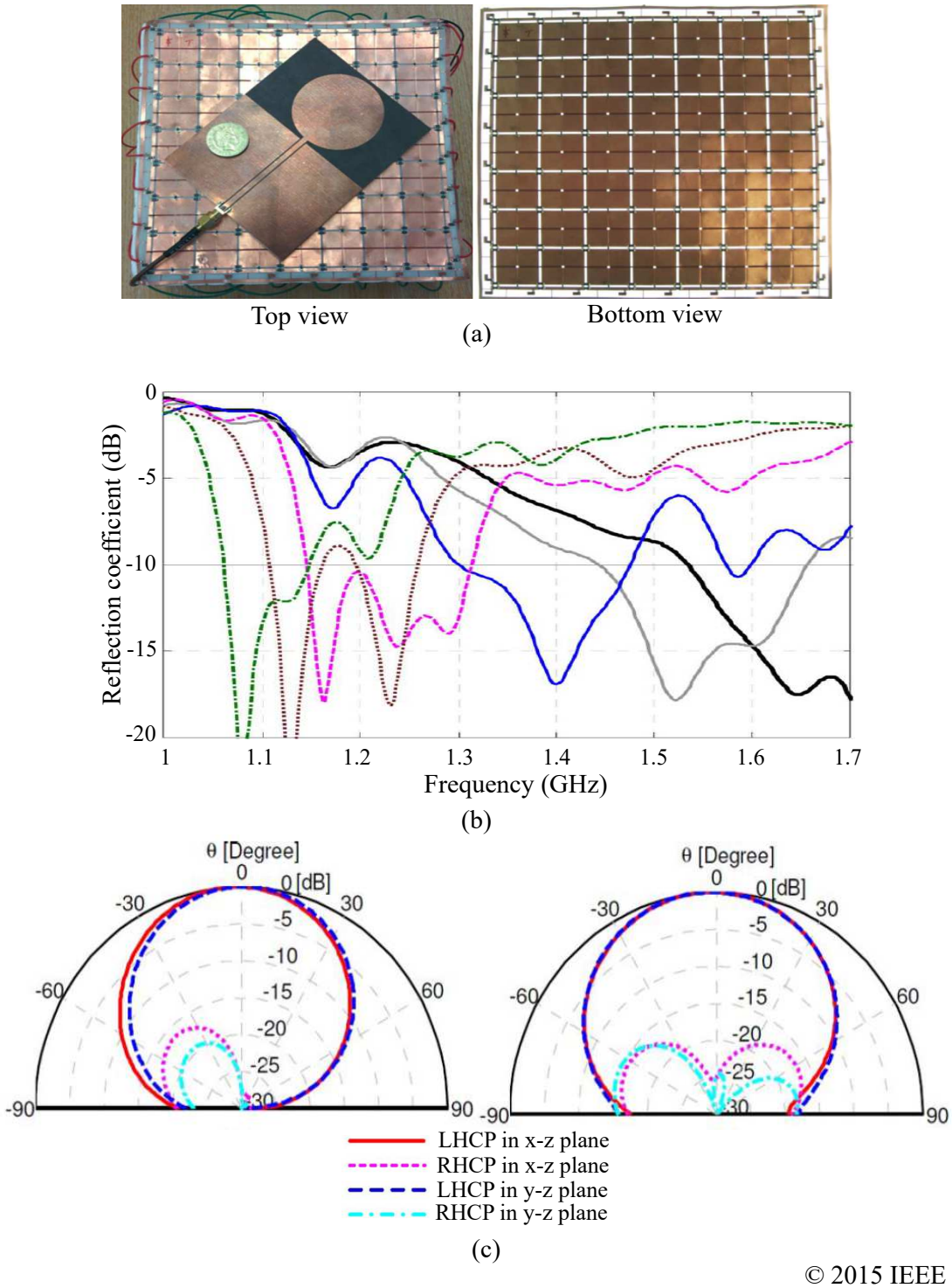

Figure 2.19. Example of varactor-controlled compound-reconfigurable antenna. (a) An example of a wideband monopole antenna above an active of dual-polarised tunable EBG structure in (Liang *et al.*, 2015). (b)(c) The reflection coefficient and the radiation patterns of the antenna.

2.4 Conclusion

This chapter presented the basic concepts of reconfigurable antennas with emphasis on planar designs that can adapt their radiation properties to meet the requirements of future communication applications. The review discussed the reconfiguration mechanisms and techniques that can be used in order to achieve the desired reconfiguration properties. While the actuation of reconfigurable antennas can be implemented through electrical, mechanical, optical and material changes, this chapter has put emphasis on the electrical switching mechanisms compared to the others, because of their advantages in producing simple designs compatible with planar technologies, low manufacturing cost and low power consumption. Selected examples from the available literature for different type of reconfigurations were also presented.

Based on the requirements for the research work of this thesis, the use of varactor diodes is chosen as a technique to achieve frequency- and pattern-reconfigurable antenna designs. This technique selection was made because varactor diodes can provide a continuously tunable range based on the varactor variable junction capacitance. This is a significant advantage when compared to other techniques based on RF MEMS and PIN diodes. The rest of this thesis will continue with descriptions of the contributions towards designing reconfigurable antennas and periodic structures in Chapters 3 to 6.

Chapter 3

A Frequency- and Pattern-Reconfigurable Two-Element Array Antenna

THIS chapter starts by providing a brief overview of the operation principle of two-element array antennas, where beam steering is obtained from a phase shift between the antenna elements. The design proposed in this chapter will obtain this phase shift by detuning the resonances of the elements. Therefore, a detailed analysis of a frequency-tuning mechanism of a single-element antenna using an open stub loaded varactor diode is then presented, where the impedance matching is maintained along the tuning range. The analysis of relative phase shift of the antenna obtained by slightly detuning the resonances of the patch is also presented in this chapter, thus introducing a beam-steering relative phase difference for the two element antennas. The two-element array antenna is then equipped with two independent bias networks giving control to the relative phase of the elements, and thus providing beam-steering pattern reconfigurability. This chapter also elaborates on the tradeoffs associated with the mutual coupling between the array elements that can degrade the beam-steering performance, expressed in beam-steering angle and gain. Based on this studies, a reconfigurable two-element array antenna with continuously H-plane beam-steerable radiation pattern and frequency-reconfigurable operation is discussed.

3.1 Introduction

The requirements for multi-functional abilities of advanced antennas are continuously increasing for wireless communications, sensing and radar systems, which provides new additional capabilities and challenges to the antenna designs. However, the challenges are not only with respect to enhancing existing antenna functionality, but also to add and unify various functionalities into an entire system, while maintaining efficiency and relatively inexpensive cost. In this context, reconfigurable antennas have emerged as an effective solution that allows an integration of multiple radio access networks into a single platform, often implemented in microstrip technology (Yang *et al.*, 2009; Haupt and Lanagan, 2013). A number of physical mechanisms, including electrical, mechanical and material processes, can be used to change the performance of the antenna by switching or tuning selected operation characteristics. Usually, the electrical tuning mechanisms are preferred compared to the other traditional switches to obtain simple and compact antenna configurations. There are several approaches that has been taken to develop reconfigurable antenna functionalities, which are mostly based on varactors, PIN diodes, RF switches or Micro-electromechanical Systems (MEMS) as described in the previous chapter. Pattern, frequency and polarisation reconfigurations are the common operation modes of reconfigurable antennas to accommodate their operating requirements independently (Pan *et al.*, 2013; Nemati *et al.*, 2014; Nguyen-Trong *et al.*, 2015b; Kansheng *et al.*, 2016; Chen *et al.*, 2017b; Lin *et al.*, 2017a). The functionality can include a single reconfiguration modality or can be of compound type, for example with both frequency and polarisation in (Ho and Rebeiz, 2014; Babakhani and Sharma, 2015), or frequency and pattern in (Xiao *et al.*, 2015b; Panagamuwa *et al.*, 2006a; Nguyen-Trong *et al.*, 2016b,c).

In an array configuration, the combination of electronically phase-tunable antenna elements can provide higher gain, while offering the ability to scan the main beam. Over the past decade, pattern reconfigurable array antennas have widely become a center of attention in communication systems to overcome the limitation of the radiation pattern requirements. The reconfigurable multi-element antennas offering beam-steering radiation pattern rely on the control of the signal phase and amplitude in each of the array elements (de la Torre and Sierra-Castaner, 2007). A number of pattern reconfigurable antennas have been previously demonstrated to achieve beam-steering functionalities. In (Chen *et al.*, 2018b), the main beam of the antenna is controlled using a switchable director and a switchable reflector. By selecting among a number

of parasitic switches, the pattern reconfigurability can be acquired in five directions, namely -90°, -45°, 0°, 45° and 90°. However, due to the complex structure of the antenna, it is not suitable for array configurations. Meanwhile, another example of beam switching application was reported in (Deng *et al.*, 2017; Jusoh *et al.*, 2014b). The reconfigurability is obtained by switchable directors between two to four parasitic microstrip element antennas, which result in a simple structure. Nevertheless, the antenna size is quite bulky as it requires more than two elements in a device. A two array elements was proposed in (Nemati *et al.*, 2014), where the variation of far-field phases was realised by switching an RF switch into three different branches of 50 ohms feeding networks, allowing to achieve a beam-switchable radiation pattern scanning at broadside, -30° and 30°. However, most of these existing antennas are limited to the pattern reconfigurability at a single operating frequency (Unlu *et al.*, 2013; Majumdar and Esselle, 2016).

In contrast, a frequency- and pattern-reconfigurable array of two microstrip antenna elements is presented in this chapter, for which the phase control is achieved using varactors. The antenna can offer unique advantages to continuously scan the main direction of the radiation pattern. More specifically, the resonance frequency of each element is determined by the capacitance C_1 and C_2 of two varactors, which are additionally loaded with open-circuited rectangular stubs as shown in Fig. 3.1. By considering a particular resonance frequency f_0, corresponding to a capacitance C_0, a relative phase between the two elements near resonance can be introduced by individually adjusting their capacitances C_0 by small respective amounts $+\Delta C_0$ and $-\Delta C_0$. This general principle makes both the resonance frequency of the two-element antenna and the radiation pattern reconfigurable.

This chapter will start by elaborating on the the design and operation principle of the proposed reconfigurable antenna, followed by a detailed optimisation analysis of its tunable frequency and the beam-steering directions.

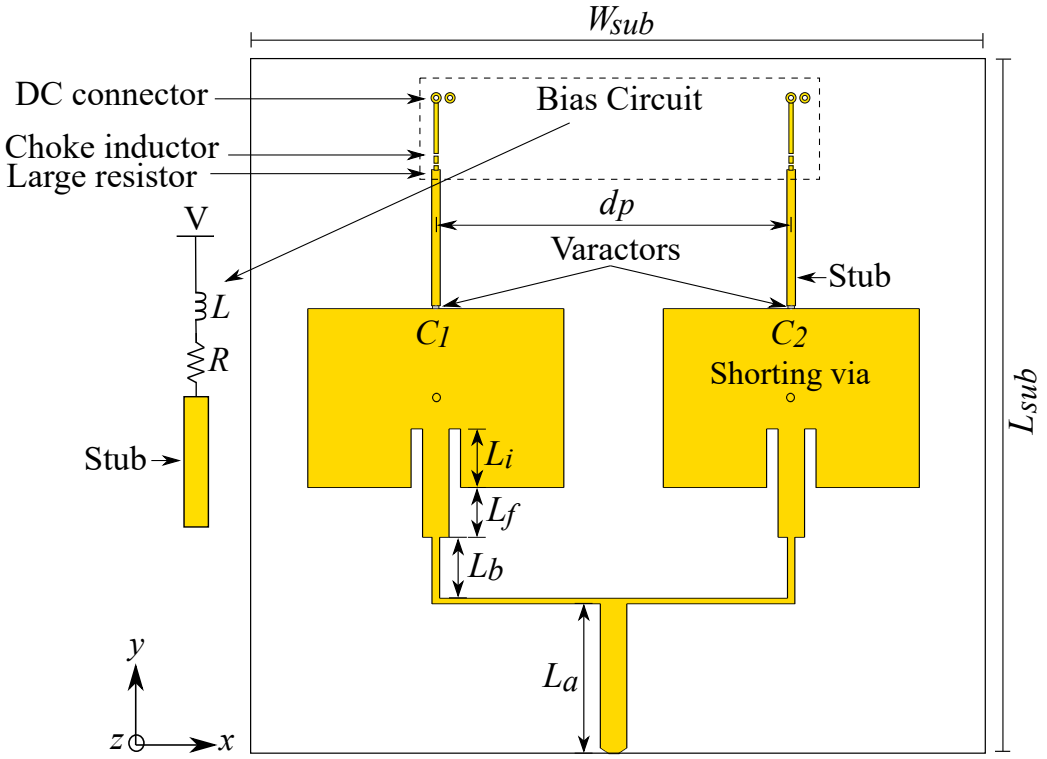

Figure 3.1. The reconfigurable two-element antenna configuration. The reconfigurable two-element antenna based on stub-loaded varactors configuration excited by a T-junction power divider.

3.2 Two elements array principle

To meet the requirement of an antenna with low profile, simple structure and low production cost while retaining efficiency, two microstrip antennas are selected as radiating elements of the reconfigurable array. The patches have their centers located at a distance d_p and they are connected to a feeding network. The distance between the antennas is obtained based on a trade off between the achievable beam-steering angle and the mutual coupling effects. Figure 3.2 illustrates the operation principle of the two-element array antenna positioned along the x-axis. Each radiating element has an electronic phase shifter that can vary the phase of the signal emitted from the antennas. Through electronically adjusting the variable relative phase behavior, ϕ_1 and ϕ_2 respectively, continuous beam-steering in direction theta can be achieved.

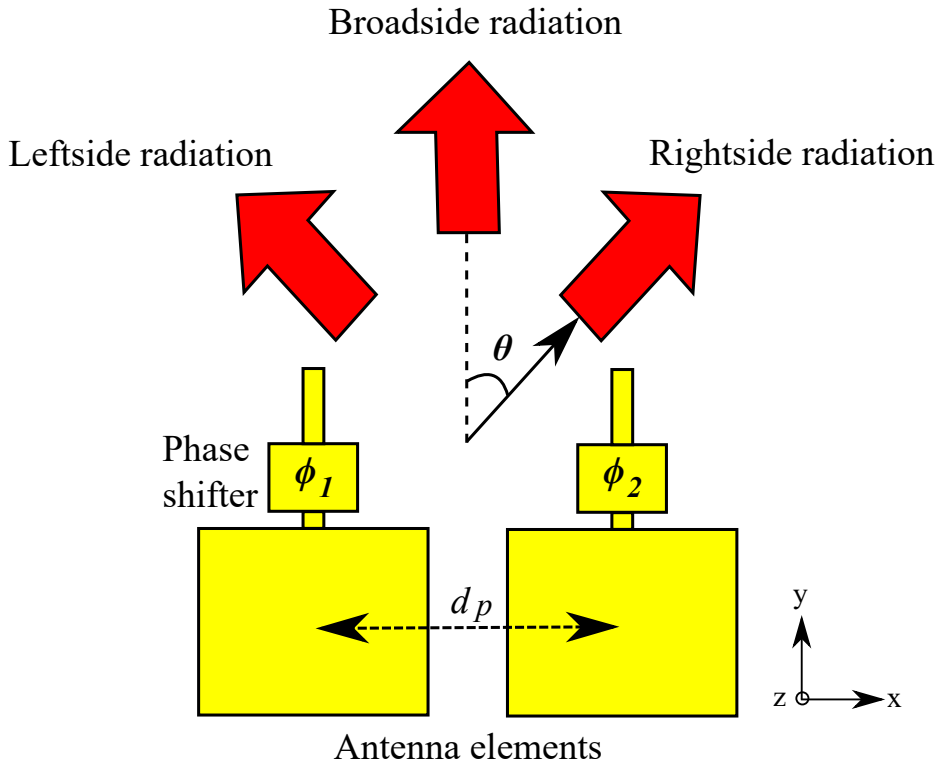

Figure 3.2. Operation principle. The operation principle of the two element array antenna.

3.3 Reconfigurable single-element configuration

In this section, the proposed concept of the reconfigurable array antenna is presented. The design procedure is commenced with a single-element design and evolves into a two-element array configuration as described in the following.

3.3.1 Basic single-element structure

Given that the main design is based on a resonant patch, the first step requires defining the patch dimensions, selecting the appropriate material and substrate thickness. Figure 3.3(a) shows the single-element antenna geometry, with a patch designed based on a standard procedure outlined in Section 2.1.1 (Balanis, 2015). For this design, Rogers Duroid 5880 is selected as dielectric substrate with a relative permittivity of 2.2, loss tangent of 0.0009 and thickness of 1.578 mm. The antenna size is chosen as $L_p = 41.1$ mm and $W_p = 49.5$ mm, yielding a resonance frequency of 2.4 GHz. The inset feed arrangement with line width $W_f = 4.6$ mm, gap $g = 2$ mm and position $L_i = 11.4$ mm is optimised to provide impedance matching between the antenna and a 50-Ω feed network.

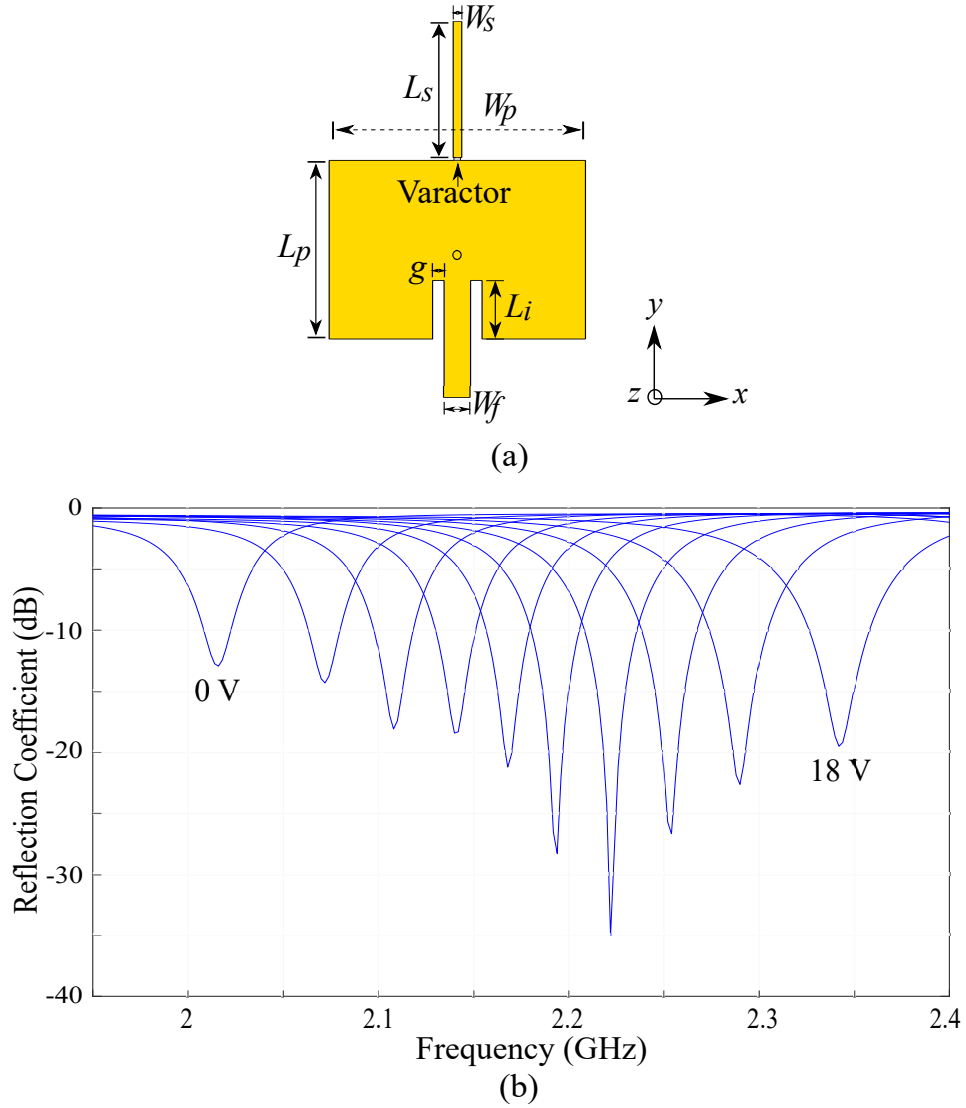

Figure 3.3. Single-element configuration. (a) Single-element configuration used as basis for the design and (b) the tuning range of its resonance frequency at different reverse bias voltages.

3.3.2 Resonance frequency detuning

To introduce reconfigurability, a varactor is placed at the edge of the open patch aperture as shown in Fig. 3.3(a). An additional impedance manipulation is adopted here by adding a rectangular open-circuited stub as discussed in (Nguyen-Trong *et al.*, 2015d). In this process initially the stub length L_s can be parametrically optimised to achieve a desired frequency tuning range. A simple bias circuitry which consists of a large resistor $R = 1$ MΩ followed by a choke inductor $L = 100$ nH is placed at the other end of the stub to block RF current while providing a DC bias voltage for varactor control. A varactor MA46H120 from MACOM Technical Solutions (MACOM, 2015) is used with a measured

capacitance ranging from 0.149 pF to 1.304 pF, controlled by a reverse bias voltage from 18 V to 0 V. This varactor capacitance range is chosen for maximum frequency variation, using the generic method outlined in (Nguyen-Trong *et al.*, 2015d). To set the antenna as the DC ground, a shorting via is added in the center of the patch, where it does not affect the resonant patch mode. At this stage, frequency-reconfigurability with a relative tuning range of 16% is straightforwardly obtained for L_s = 32 mm and W_s = 1.5 mm in the single antenna element as illustrated in Fig. 3.3(b).

3.4 Reconfigurable two-element array configuration

As shown in Fig. 3.1, two reconfigurable patch elements with inter-element distance d_p are fed by a T-junction power divider. The feed network is designed with 50-Ω microstrip line, then divided up into two 100-Ω splitting in-phase feed lines. The size of the substrate is selected to $L_{sub} \times W_{sub}$ = 151.5 mm × 160.9 mm. According to linear array theory (Balanis, 2015), beam steering can be realised by adding a progressive relative phase shift between the individual elements.

3.4.1 Relative phase of cavity mode

In the proposed geometry, the phase difference between the two elements is obtained by adjusting the effective electrical length of the individual patches through variation of the varactor capacitance. As a starting point, a particular resonance frequency f_0 can be tuned by adjusting the varactor capacitance C_0. Then, if a slight capacitance variation $\pm\Delta C_0$ is introduced for the two elements (one positive, one negative), the patches become slightly detuned from their resonance. As the result, the introduced non-zero reactances at f_0 cause a relative phase shift between the two elements, while their magnitude remains nearly the same. In this scenario, a continuously steerable beam around broadside can be achieved, with this pattern reconfigurability covering the frequency tuning range. More explicitly, when the two individual elements share a same value of capacitance C_0, they radiate in phase resulting in a broadside beam at f_0. By detuning both elements through changing their varactor capacitance C_0 by small amounts of opposite signs $\pm\Delta C_0$, a continuously steerable beam can be obtained. The maximum beam-steering angle is obtained with the maximum achievable phase difference $\Delta\phi_{max}$, provided that the input impedance at the considered frequency is still satisfactorily matched.

As an illustration, Fig. 3.4 shows the simulated reflection coefficient of the single antenna element when varying the varactor capacitance around a nominal value. The middle graph shows the reflection coefficient for a varactor capacitance C_0 arbitrarily chosen for resonance at $f_0 = 2.27$ GHz. While, the top and bottom graphs show the two extreme cases for variations $\pm\Delta C_0$, so that the reflection coefficient at f_0 is just at the -10 dB level. For both cases of detuning, the field distribution underneath the patch remains nearly unchanged compared to the resonant case (as shown on the right-hand side of Fig. 3.4), except for phase shifts of $\pm 19°$, respectively. The phase shift as a function of the varactor capacitance around resonance is shown for this case in Fig. 3.5, with illustration of the maximum achievable phase difference $\Delta\phi_{max}$. Based on this phase difference, one can easily calculate the maximum achievable beam steering. It is noted that due to the symmetry of the structure, the beam can be steered to both sides from broadside by swapping the values of bias voltage for both antenna elements.

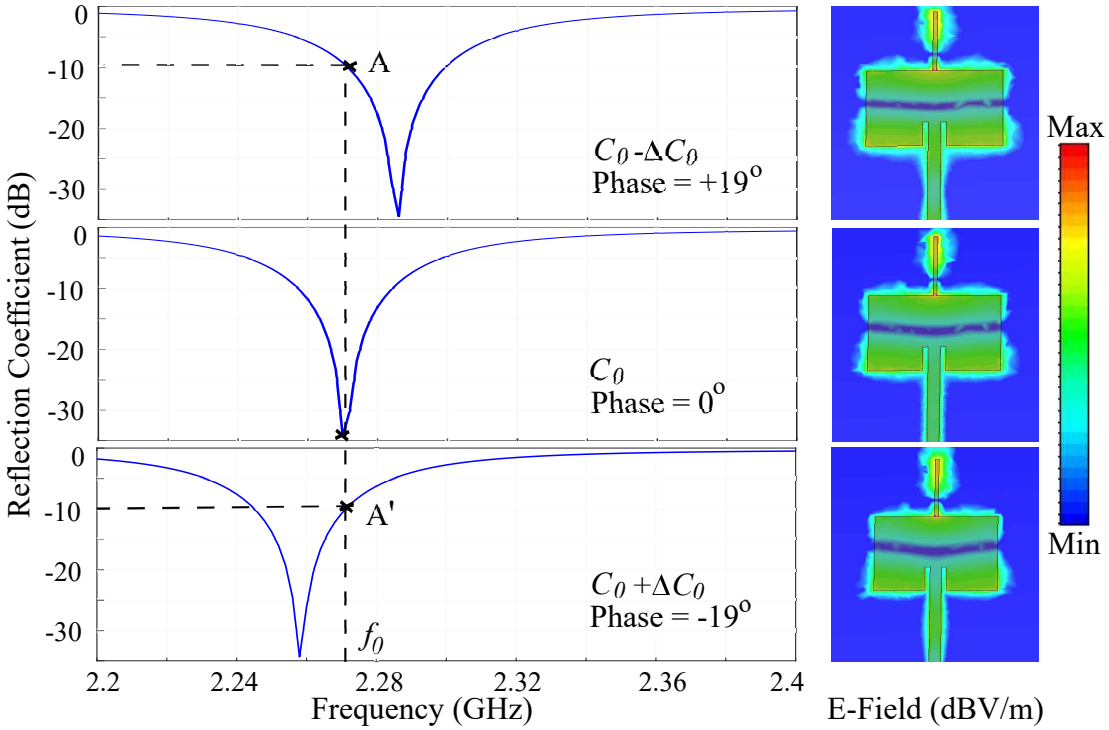

Figure 3.4. Detuning of the patch from resonance frequency. Detuning of the patch from resonance frequency f_0 obtained by adapting the capacitance of the varactor around its original value C_0. The detuning capacitances (altered by $\pm\Delta C_0$) are chosen such that the upper and lower -10 dB point A and A' occur at f_0. The right-hand side figures show the field distribution underneath the patch at the frequency f_0.

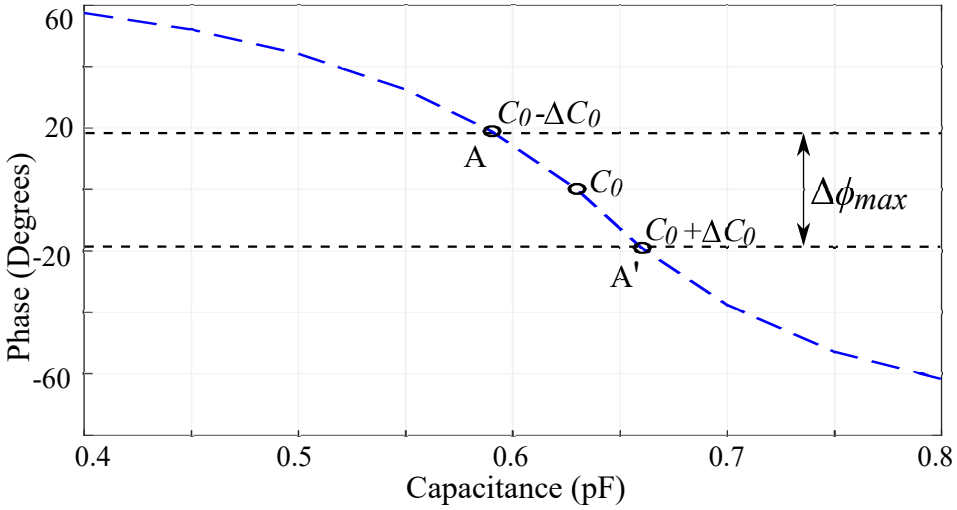

Figure 3.5. Relative phase of the cavity mode. Relative phase of the cavity mode at f_0 for the detuned patches as a function of the varactor capacitance. The maximum achievable phase diference $\Delta\phi_{max}$ is highlighted for the -10 dB points A and A' shown in Fig 3.4.

To improve the beam-steering capability, the inter-element distance d_p can be fixed and the achievable phase shift $\Delta\phi_{max}$ needs to be maximised. It is noted that a smaller distance d_p will increase the antenna beam scanning angle for a fixed phase tunability of the elements. However, a closer distance will reduce the effective aperture of the antenna, and thus its directivity. Since this trade-off is well-known, the distance between two elements is fixed at half free-space wavelength at 2.4 GHz which is $d_p = 62$ mm that yields high directivity while avoiding grating lobes.

In the initial consideration to get a better understanding of the phase shifting effect of detuning the resonance, the maximum phase difference $\Delta\phi_{max}$ in Fig. 3.5 has been determined by considering a single isolated element. In practice, this value is however significantly influenced by the mutual coupling between the two patches. The next Section 3.5 will consider the main physical causes of coupling and, on that basis, it will describe how to maximise the range of scanning angles.

3.5 Mutual coupling optimisations

In order to obtain the maximum scanning angle for the wider range of resonance frequency, the two main mutual coupling effects between the two antenna elements are investigated. The first coupling mechanism is the direct electromagnetic coupling between the two patches. Meanwhile, the second mechanism is the coupling through

the feeding line of the T-junction power divider. Controlling the coupling level and balancing their effects allows to achieve best performance for the two-element antenna.

3.5.1 Direct coupling between elements

The direct coupling between the two antenna elements includes both coupling through the air and through surface waves in the dielectric substrate. Typically, these coupling effects tend to decrease the scanning angle range as the addition of the coupling field causes a reduction in the phase difference between the two patches. In order to reduce the direct coupling for a fixed inter-element distance d_p, the patch width W_p should be reduced. However, since the width W_p of the patch influences both its matching and directivity (Balanis, 2015), configurations of narrower patches tend to result in reduced beam steering, higher losses and smaller directivity/gain (Yong and Bernhard, 2009). Figure 3.6 shows the simulated achievable scanning angle at different frequencies and the corresponding gain for three values of patch width W_p. The results in Fig. 3.6(a) show that reducing the coupling effect by narrowing the patch obviously helps in obtaining a uniformly high beam-scannning angle. However, reducing the patch width also reduces the antenna gain as shown in Fig. 3.6(b), due to a higher loss and smaller size of the antenna. For this reason, an intermediate value of W_p (here 44.55 mm) is chosen as trade-off between maximum angular scanning range and gain.

3.5.2 Coupling through the feeding network

By contrast to the direct coupling, the coupling through the feeding network can improve the scanning angle range if optimised appropriately. This is because the phase of the associated coupling coefficient can be conveniently controlled by varying the length L_b (defined in Fig. 3.1). Figure 3.7 shows the maximum scanning angle at different frequencies when no T-junction is used (i.e. with just two antenna elements fed independently from two ports) and for different values of L_b. The results demonstrate that the coupling through the feeding line can partly compensate the direct coupling. Based on these results, the feeding dimension is chosen as $L_b = 14$ mm for a maximum scanning angle across the whole tuning range.

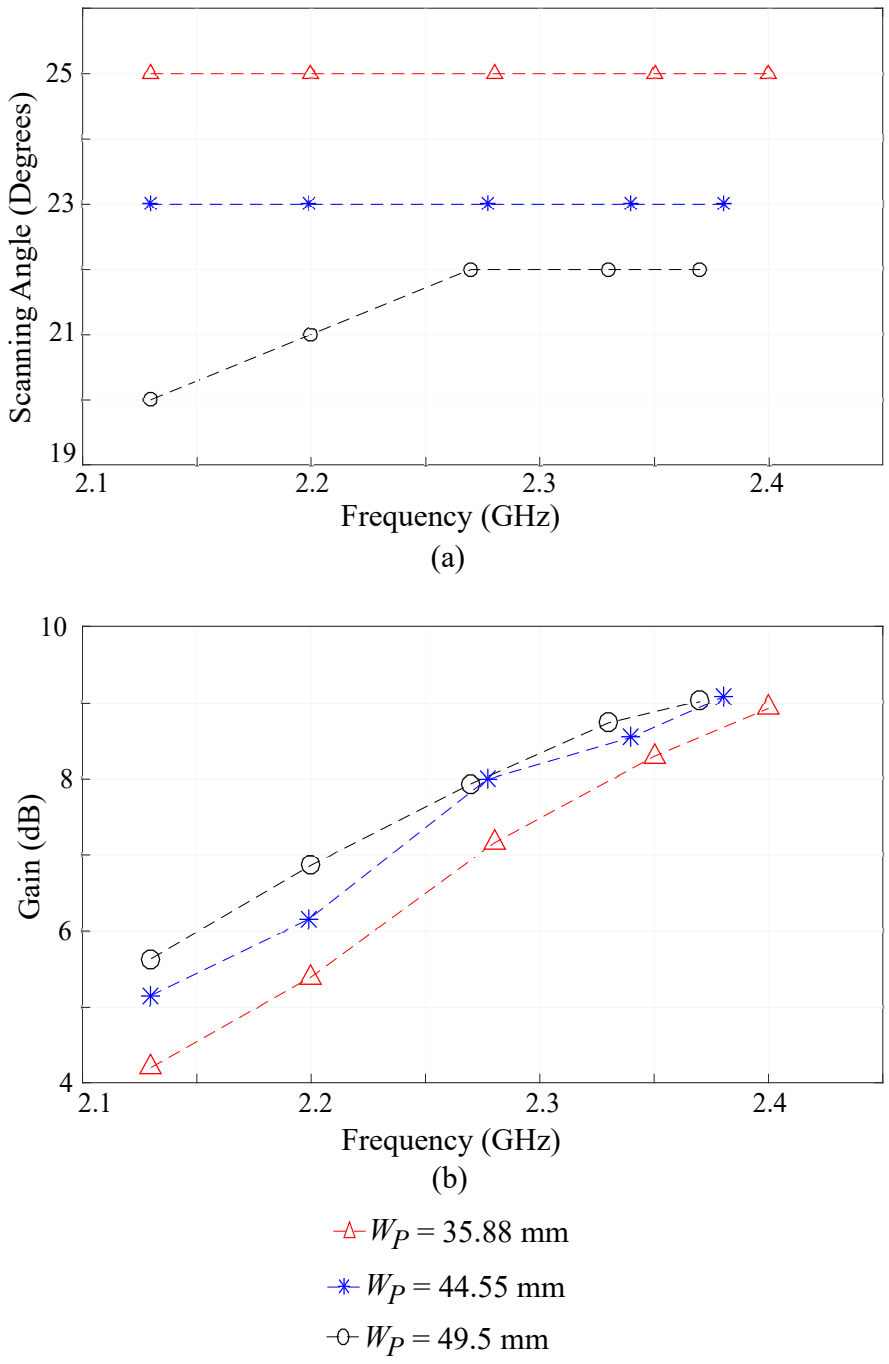

Figure 3.6. Parametric study of the patch width. Parametric study of the patch width W_p: (a) maximum scanning angle and (b) corresponding antenna gain as functions of resonance frequency obtained by varying varactor capacitances.

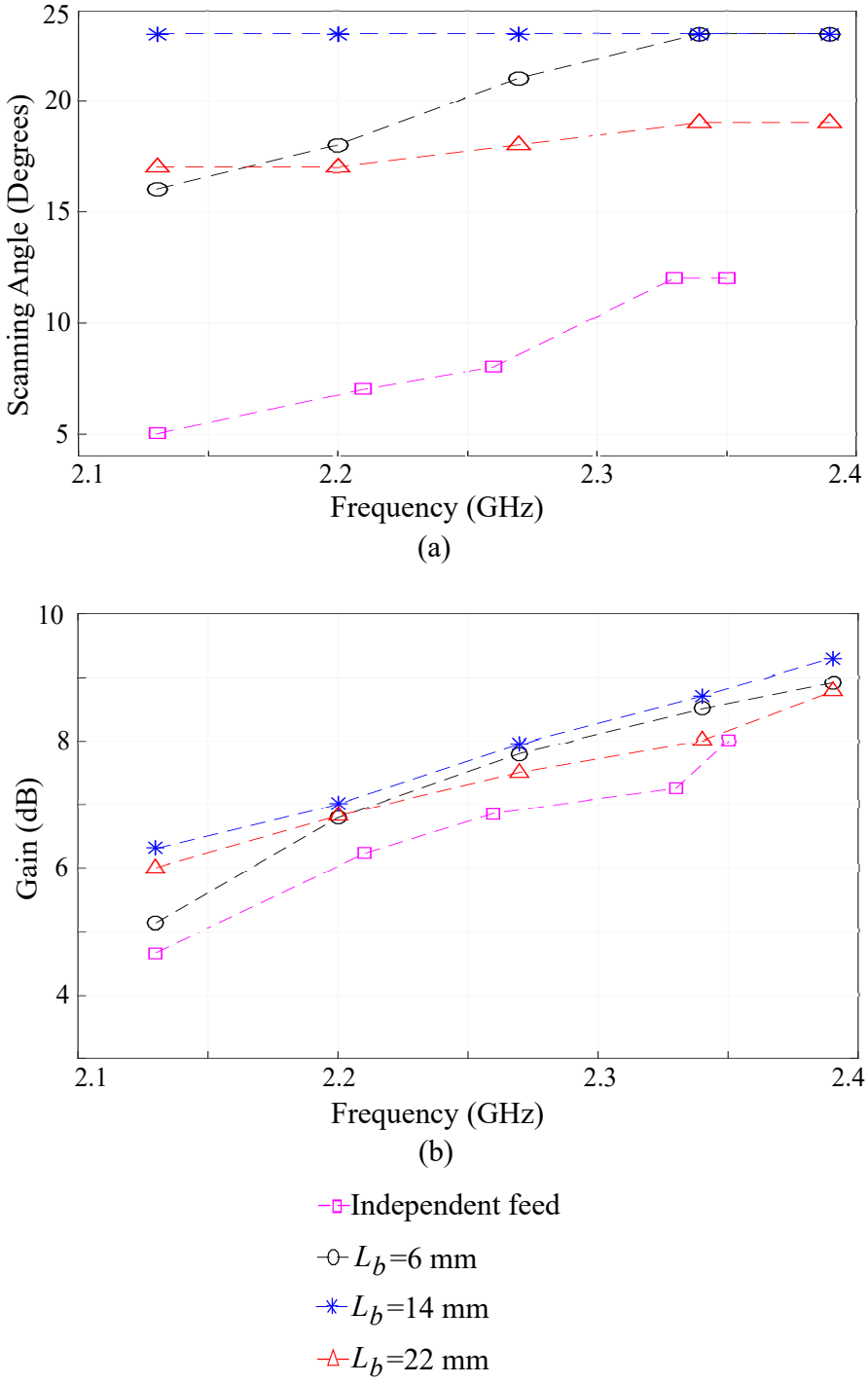

Figure 3.7. Parametric study of feed line length. Parametric study of feed line length L_b: (a) maximum scanning angle and (b) corresponding antenna gain as functions of resonance frequency obtained by varying varactor capacitances.

3.6 Full-wave simulation of beam steering

For validation of the final structure with full-wave electromagnetic simulation, the optimal parameters of L_p = 41.1 mm, W_p = 44.55 mm, L_f = 12 mm, L_a = 33 mm and L_b = 14 mm are selected. As an example, a center frequency of f_0 = 2.27 GHz within the frequency tuning range is chosen to validate the antenna performance. The simulation result demonstrates a reflection coefficient for a combination of two bias voltages that slightly detune the resonance of the two elements in Fig. 3.8. In further detail, Fig. 3.8(a) shows the reflection coefficient of the isolated antennas at the two capacitance values, where the curves are intersecting to each other within −10 dB cross point at the resonance frequency of 2.27 GHz. From this fundamental result, the curve in Fig. 3.8(b) illustrates the combination of the two bias voltages for the two-element array where the near-by resonances which refer to the capacitor values $C_0 + \Delta C_0$ and $C_0 - \Delta C_0$.

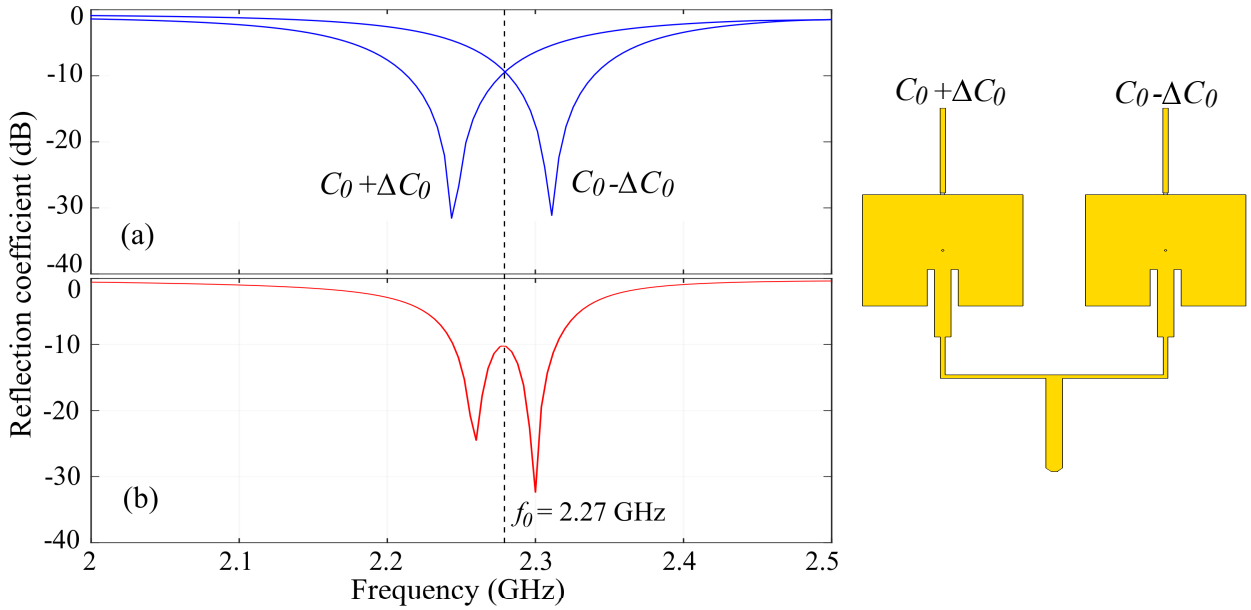

Figure 3.8. Reflection coefficient. Reflection coefficient of the resonance frequency of 2.27 GHz at different reverse bias voltages for the two elements, as indicated on the right-hand side. (a) Reflection coefficient, $|S11|$ for isolated antennas at the two capacitance values and (b) $|S11|$ for the two-element array with the two indicated voltages.

For this example, Fig. 3.9 shows the electric field distributions for three selected scenarios where the two-elements are tuned at or near the resonant frequency of 2.27 GHz. As described in the Section 3.4.1, when the two-elements antennas have the same value of capacitor C_0, they will radiate in phase. This will result in a broadside beam at the

selected operating frequency of the antenna as illustrated in the Fig. 3.9(b). However, if both elements are slightly detuned through changing the varactor capacitance C_0 by $\pm\Delta C_0$, a continuously beam-steering capability can be obtained as shown in Fig. 3.9(a) and Fig. 3.9(c), respectively.

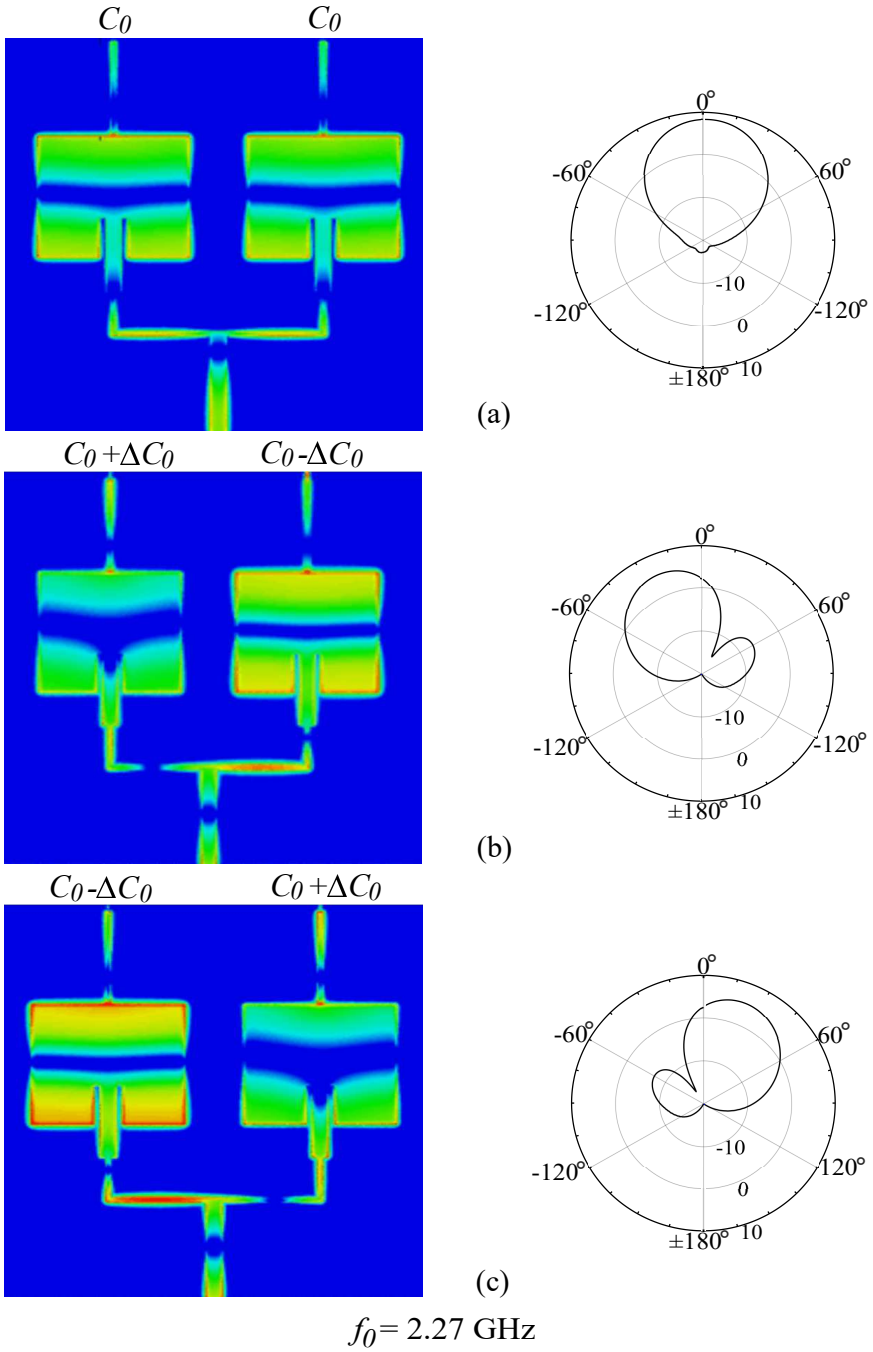

Figure 3.9. Instantaneous electric-field distribution. Instantaneous electric-field distribution at 2.27 GHz for three cases. (a) Same value of capacitor C_0 corresponding to broaside radiation pattern. (b) and (c) Detuned values of capacitors by $\pm\Delta C_0$, corresponding to the beam-steering cases.

3.7 Prototype and measurement results

This section compares the prediction of analysis and simulation with measured data obtained with a prototype. A photograph of the fabricated antenna is illustrated in Fig. 3.10. The zoomed regions on the right-hand side of the figure show close-ups of the biasing circuitry, including a large resistor and choke inductor, as well as a view on the varactor and shorting via in the centre of the patch.

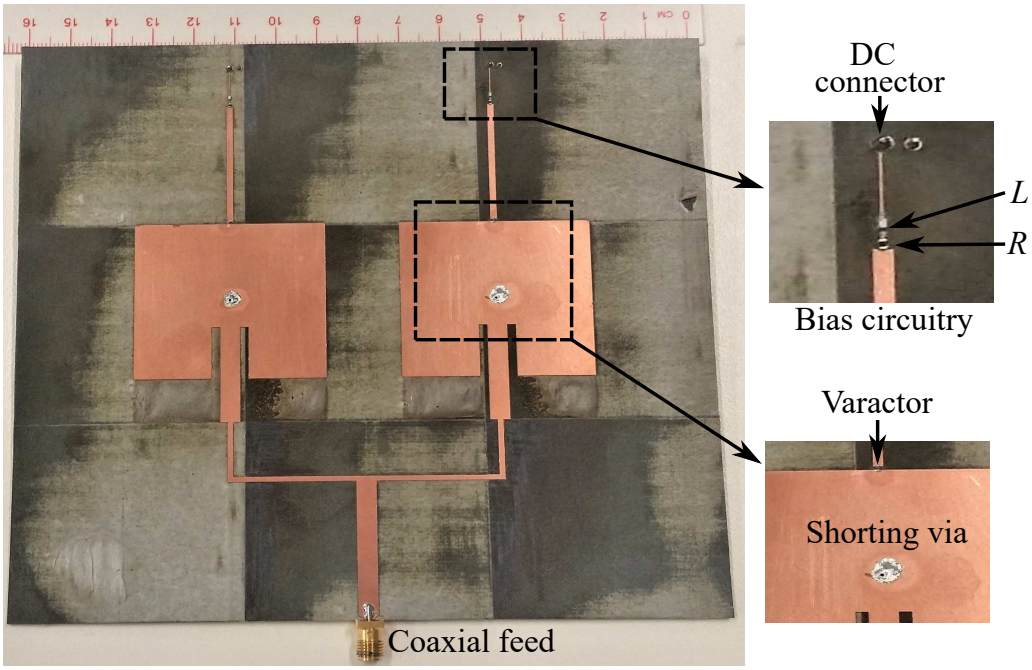

Figure 3.10. Photograph of the fabricated prototype. Photograph of the fabricated reconfigurable two-element antenna array.

3.7.1 Frequency reconfigurability

The reflection coefficients for different combinations of bias voltages covering the tuning frequency band are shown in Fig. 3.11. The curves in the graph each clearly show two nearby resonances associated with the detuned patches. The examples are selected for the limit cases where the mid-point reflection coefficient between resonances reaches -10 dB, which corresponds to operation with the maximum beam steering angle. The overall achievable tuning range is between 2.15 GHz and 2.38 GHz with good agreement between simulated and measured results. Ideally, the frequency tuning range of a single antenna of this type can reach up to 40% as shown in (Nguyen-Trong *et al.*,

2016b). However, in the present case, due to the difficulty in the impedance matching of the structure with two patches and a T-junction, the effective frequency tuning range becomes limited to about 10%. The minimum instantaneous −10 dB impedance bandwidth across the tuning range for all scanning angles is 1.5%. A second numerical study with the reflection coefficient of the combination of bias voltages reaching a less stringent value of −6 dB has has also been considered, since this specification is practically relevant to mobile application systems. The tuning frequency bands are found to increase to 13% as illustrated in Fig. 3.12. From this perspective, the minimum operation point of −6 dB provides an additional angle of 3° to the maximum beam scanning performance of the antenna.

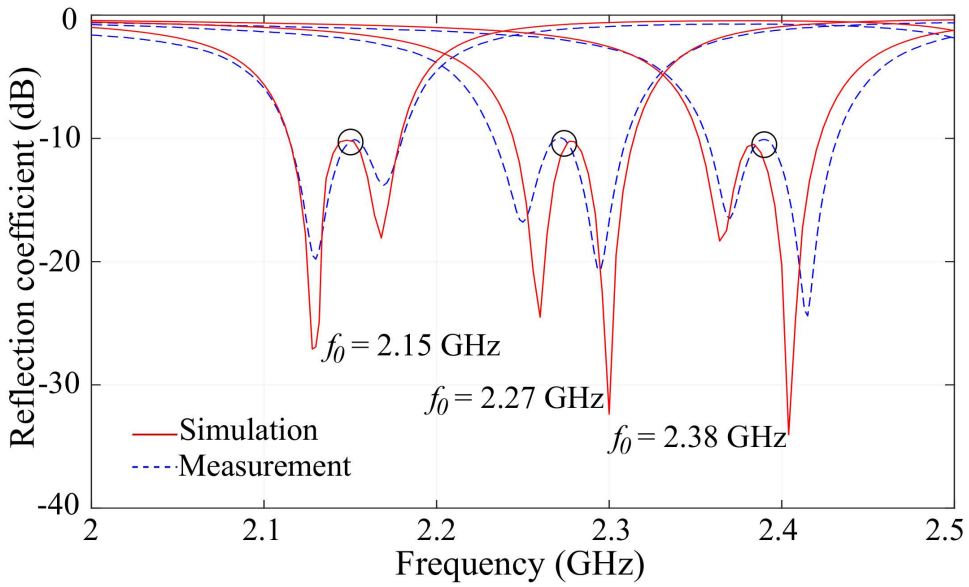

Figure 3.11. Reflection coefficient for different combinations of bias voltages. Reflection coefficient for different combinations of bias voltages for scanning operation. The circles indicate the operation points within −10 dB for the maximum beam steering cases.

In addition, Fig.3.13 shows a function of the antenna reflection coefficient in a three-dimensional (3-D) plots corresponding to the varactor capacitances variation across the resonance frequencies. Each row of the figure corresponds to a fixed capacitance value C_1, namely, 0.149, 0.713 and 1.304 pF, while capacitance C_2 is varied in the whole range of the varactor capacitances in each graph. The near vertical dark line is representative of the operating resonance frequency of the element with fixed capacitance C_1, and therefore it is not altered when C_2 is varied. The dark slanted lines diagonal are

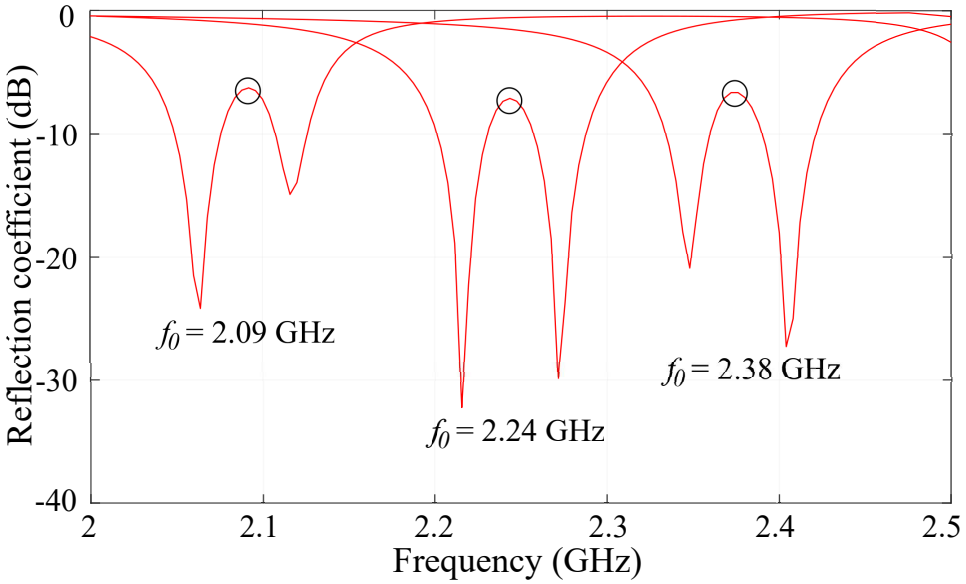

Figure 3.12. Simulated reflection coefficient for different combinations of bias voltages. The simulated reflection coefficient for different combinations of bias voltages for scanning operation. The circles indicate the operation points within −6 dB for the maximum beam steering cases.

representative of the resonance frequency change in the second element when the value of C_2 is changed. The relevant region for beam scanning is where the antenna operates with C_2 nearly equal to C_1 (the intersection point in the graphs).

3.7.2 Pattern reconfigurability

The realised gain patterns at three selected resonance frequencies, within the frequency tuning range are illustrated in Fig. 3.14. Three different directions of the antenna radiation patterns are presented, including broadside patterns and the maximally achieved scanning angles for a reflection coefficient better than −10 dB, respectively. These particular cases are shown as illustrations, but it is emphasised that the antenna is capable to continuously steer the beam in between these extremes. A good agreement is observed between simulated and measured results, which validates the antenna operation. The results also illustrate that the antenna pattern can be simply switched between right and left direction by swapping the values of C_1 and C_2, i.e. by swapping the bias voltages. The simulated realised gain patterns for the minimum operation point of −6 dB also been analysed as shown in Fig. 3.15.

Figure 3.16(a) shows the gain of the antenna as a function of the frequency for broadside and beam-steerable operations. The results show a reasonable agreement between simulation and measurement with a slightly lower measured gain compared to prediction. For the continuously beam-steerable radiation patterns, the gain decreases from the broadside values as expected for beam-steering arrays, with a worst-case degradation by 1.3 dB at the lowest frequency of operation. The antenna efficiency increases from

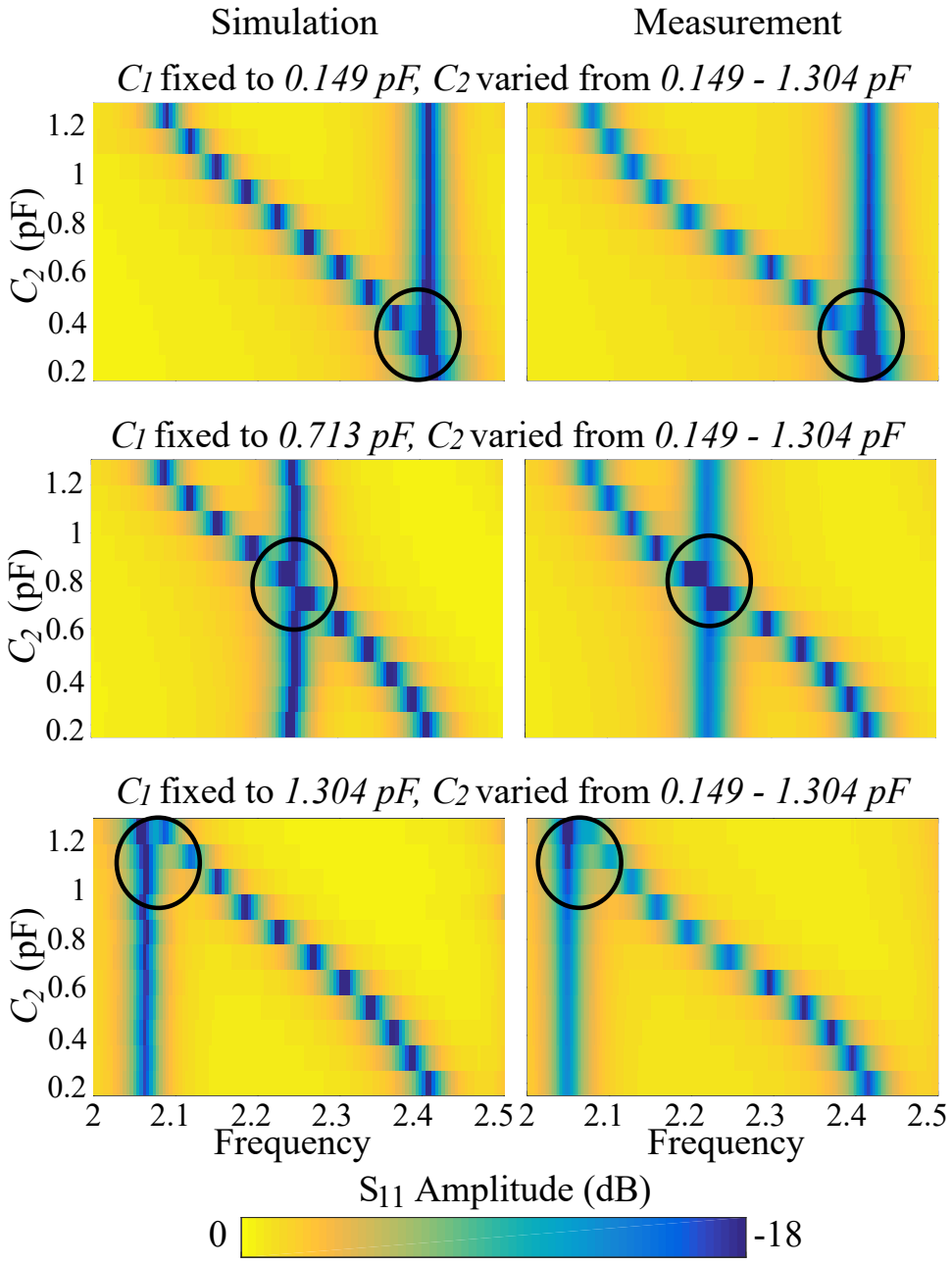

Figure 3.13. 3-D plot of reflection coefficient. 3-D plot of the simulated and measured reflection coefficient of varying C_2 with fixed C_1 at 0.149, 0.713, and 1.304 pF, respectively from top to bottom.

41% to 87% with increasing frequency through the operation range as illustrated in Fig. 3.16(b).

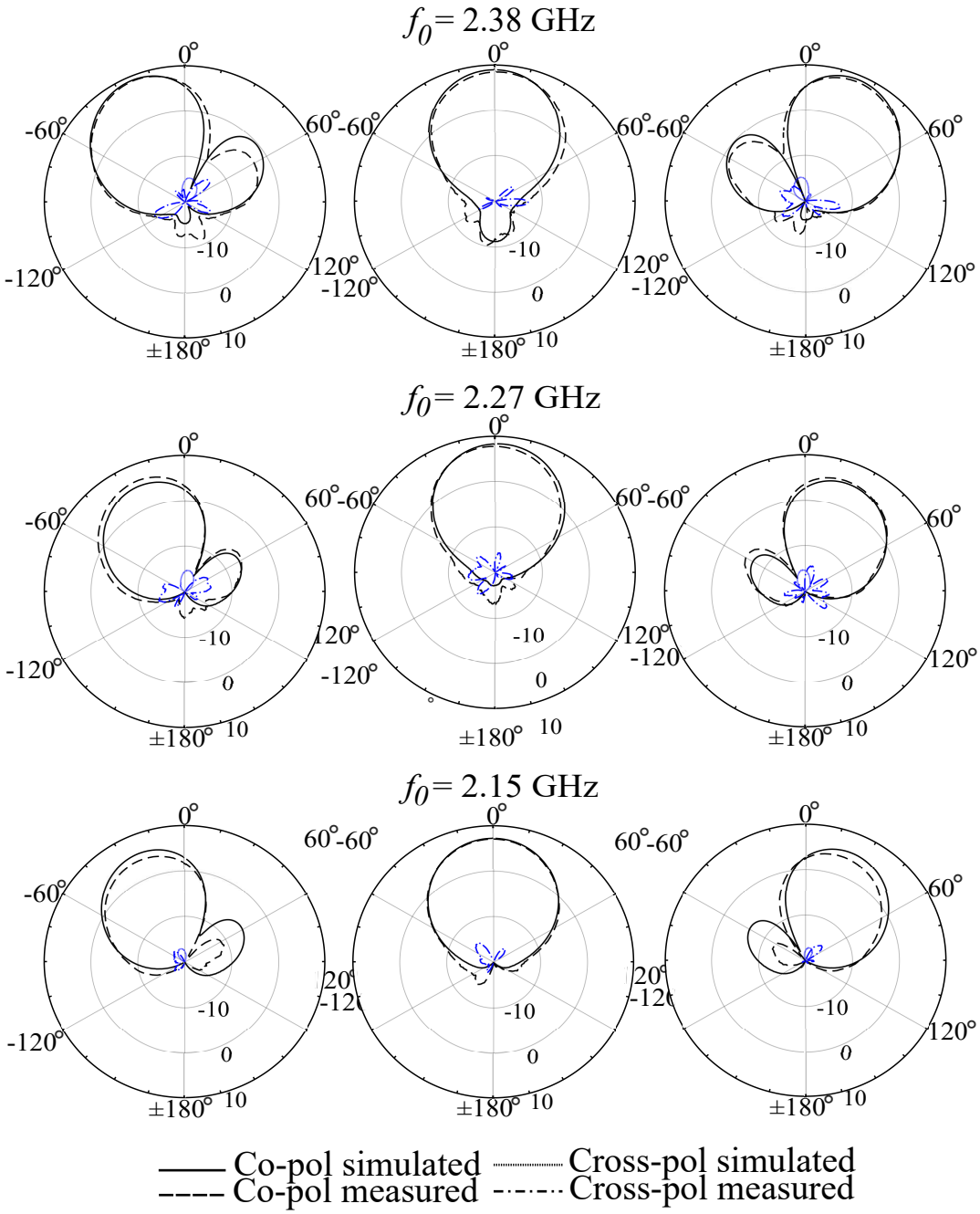

Figure 3.14. Realised gain patterns. Realised gain patterns within operation point of −10 dB at f_0 = 2.38, 2.27 and 2.15 GHz from top to bottom.

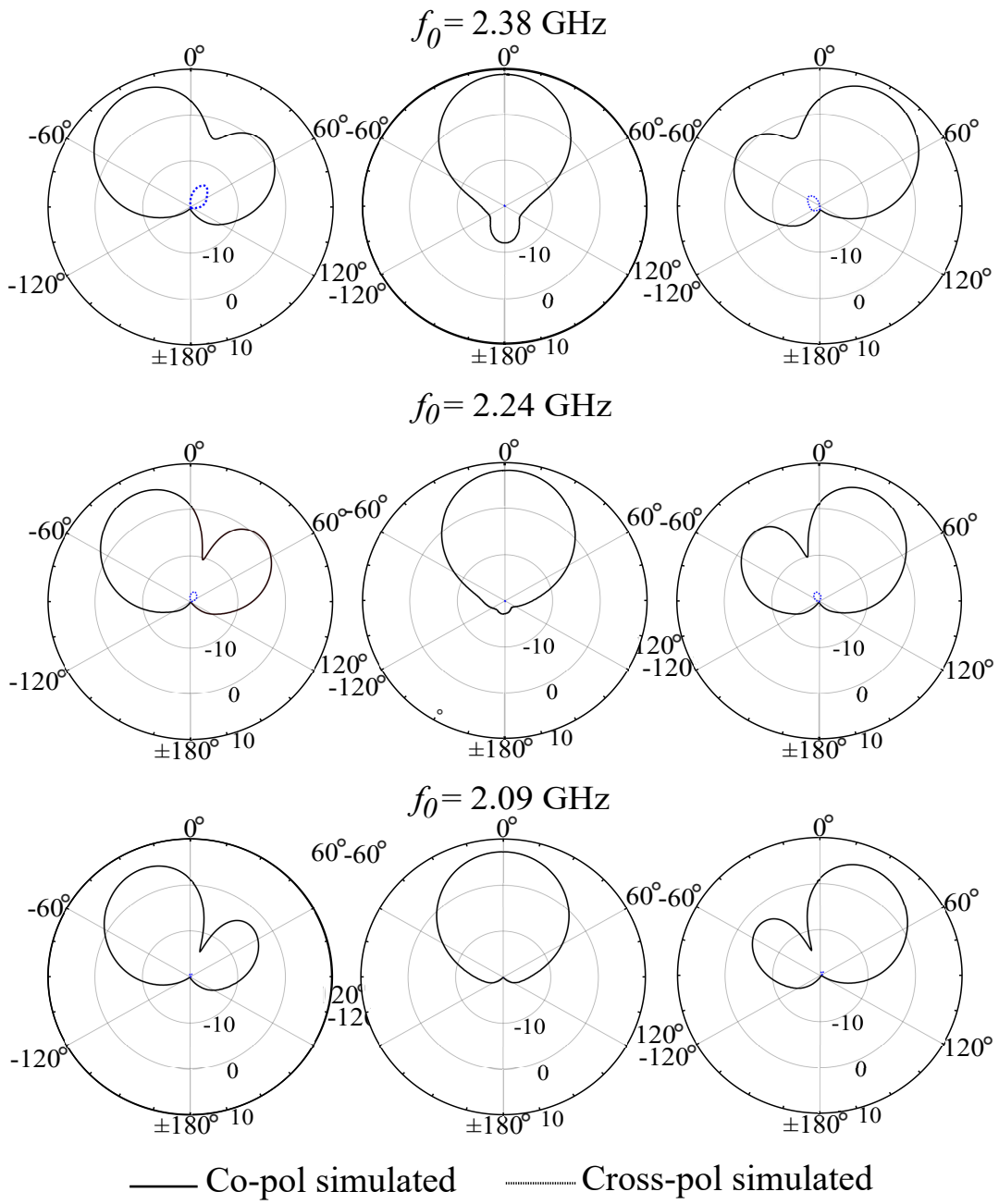

Figure 3.15. Simulated realised gain patterns. The simulated realised gain patterns within operation point of -6 dB at $f_0 = 2.38$, 2.24 and 2.09 GHz from top to bottom.

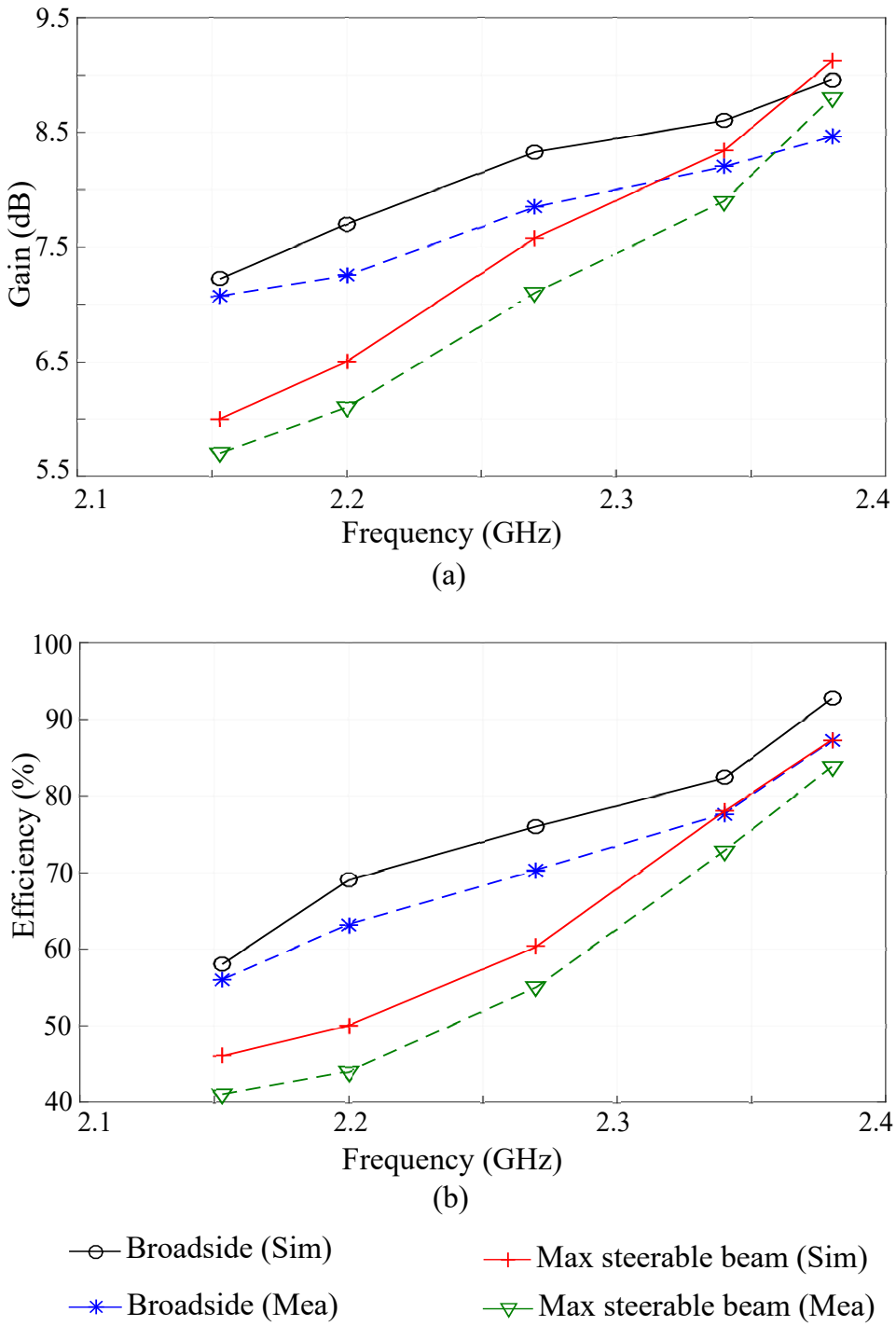

Figure 3.16. Antenna realised gain and efficiency. (a) Antenna realised gain and (b) Antenna efficiency.

3.8 Conclusion

In this chapter, a two-element array antenna with frequency and pattern reconfigurability has been proposed. A tuning mechanism based on stub-loaded varactors has been adopted to realise a phase shift between two slightly detuned antenna elements. Based on this principle, the antenna has been parametrically optimised to reach a continuous beam scanning in the H-plane from -23° to 23° across a relative frequency tuning range of 10% extending from 2.15 to 2.38 GHz.

Chapter 4

A Pattern-Reconfigurable Single-Element Microstrip Antenna

IN the previous chapter, the beam-steerable characteristics of a two-element antenna array were discussed and analysed. Usually this functionality can be obtained though an arrangement of two or more elements in array antennas, where the phase shift of each element provides the beam steering ability. With the same fundamental application, this chapter first describes a unique approach to pattern reconfigurability achieved by a single-element antenna configuration. The description of the concept is followed by the antenna structure design, the operating principle and the fundamentals of the tunability in the next section. Finally, the experimental validation of the simulation results related to frequency response and scanning range as a function of the varactor capacitance variations are also presented.

4.1 Introduction

Pattern-reconfigurable antennas can provide reconfigurability in their radiation characteristics to adapt to changing system requirements in the propagation environments (Genovesi *et al.*, 2014; Lin and Wong, 2015a; Nguyen-Trong *et al.*, 2016b; Tian *et al.*, 2018a). The ability of far-field beam steering through reconfiguration has recently received attention to increase the performance of communication systems. Technically, reconfigurable antennas can change their radiation pattern by electrical switching through various tuning mechanisms with components that can affect the electric or magnetic currents. Based on the traditional microstrip patch antenna, the control of the currents can for example enable to achieve variation between the fundamental even and odd modes of operation. This means that if the antenna cavity can be separated in two radiation parts which support an odd mode and an even mode, the maximum electric field on both side can be made to be in-phase or have a phase difference of 180°. In such cases, once a dual mode topology of phase or current distribution is determined, an antenna configuration management can be implemented by adding a tuning component and various desired beam-steerable patterns can be generated.

In general, the existence of diverse reconfigurable beam-steering capabilities at a single frequency has been developed in various past implementations (Yang and Luk, 2006; jefors *et al.*, 2007; Topalli *et al.*, 2008; Qin *et al.*, 2012). One good example is in (Ouyang *et al.*, 2018) where the antenna introduced a pattern reconfigurability through a careful design of the radial slots on the ground plane which allow selecting the operation mode of the antenna. Even though the antenna does not necessarily meet the requirements of reconfigurability which has been described in Chapter 3, the article provides an overview of the general approaches to developing reconfigurable designs. In addition, other examples in (Vaughan, 2004; Yang *et al.*, 2006, 2007; Jiang *et al.*, 2014) also introduced designable functionalities that are achieved through characteristic modes frequency-dependent operation. The beam steering is realised by radiating energy gradually as the wave propagates along the structure.

However, these antennas usually possess sophisticated structures and bias circuits. Simpler designs that can achieve similar reconfigurabilities would be desirable. Various techniques have been proposed to realise multiple patterns in a single antenna (Huff *et al.*, 2003; Chen *et al.*, 2007; Tian *et al.*, 2018b). This chapter proposes a simple concept of single-element microstrip antenna with a stub-loaded varactor at one of the radiating apertures to realise beam scanning.

4.2 Antenna design

The proposed antenna configuration is shown in Fig. 4.1. The antenna is inspired by the structure in (Tian *et al.*, 2018b) and is combined with the principle of (Zainarry *et al.*, 2018) elaborated in Chapter 3, based on the two-element phased array theory (Balanis, 2015). It consists of a probe-fed rectangular microstrip patch printed on the top of a dielectric substrate of the type Rogers Duroid 5880 with a relative permittivity of ε_r = 2.2 and a thickness of h = 1.58 mm, as shown in Fig. 4.1(b) and (c). Furthermore, there is a series of vias that are placed near the center of the patch with their spacing and diameter are selected as d_s = 2 mm and d = 0.9 mm. This metallic wall allows to realise two coupled cavities with nearly independent resonance frequencies. A stub-loaded varactor is connected to the edge on one side of the patch in the center of the y-axis aperture to tune the effective electrical length of one of the cavities. This can create a relative phase difference between the two radiating slots of the patch, thus providing a mechanism to achieve a reconfigurable beam squint.

As illustrated in Fig. 4.1(a), the stub is introduced to attain a maximum tuning range (Nguyen-Trong *et al.*, 2015d) with the chosen varactor of MA46H120 from MACOM Technology Solutions. Referring to the varactor datasheet (MACOM, 2015), the maximum reverse leakage current of 100 nA is expected over the tuning range, which implies low DC power consumption of the antenna. In this initial stage of the design procedure, the size of the antenna is chosen with the two radiation slot lengths L_p = 39 mm, and width W_p = 39 mm corresponding to an operating frequency of 2.4 GHz. An additional length, ΔL_p = 0.7 mm, is introduced on one side to compensate imbalance caused by the feed. In addition, a reverse DC bias circuit with a resistor of 1 MΩ and an inductor of 100 nH placed at the end of the stub are used to control the tunable varactor capacitances C_0 from 0.15 to 1.3 pF for a voltage varying from 18 to 0 V. Noting that the DC power consumption of the antenna (based on the chosen values of the bias circuit) can be calculated as

$$P = {I_v}^2 R, \tag{4.1}$$

where P is the DC power consumption of the antenna, I_v is the maximum reverse leakage current of the varactor and R is the large resistor of the bias circuit.

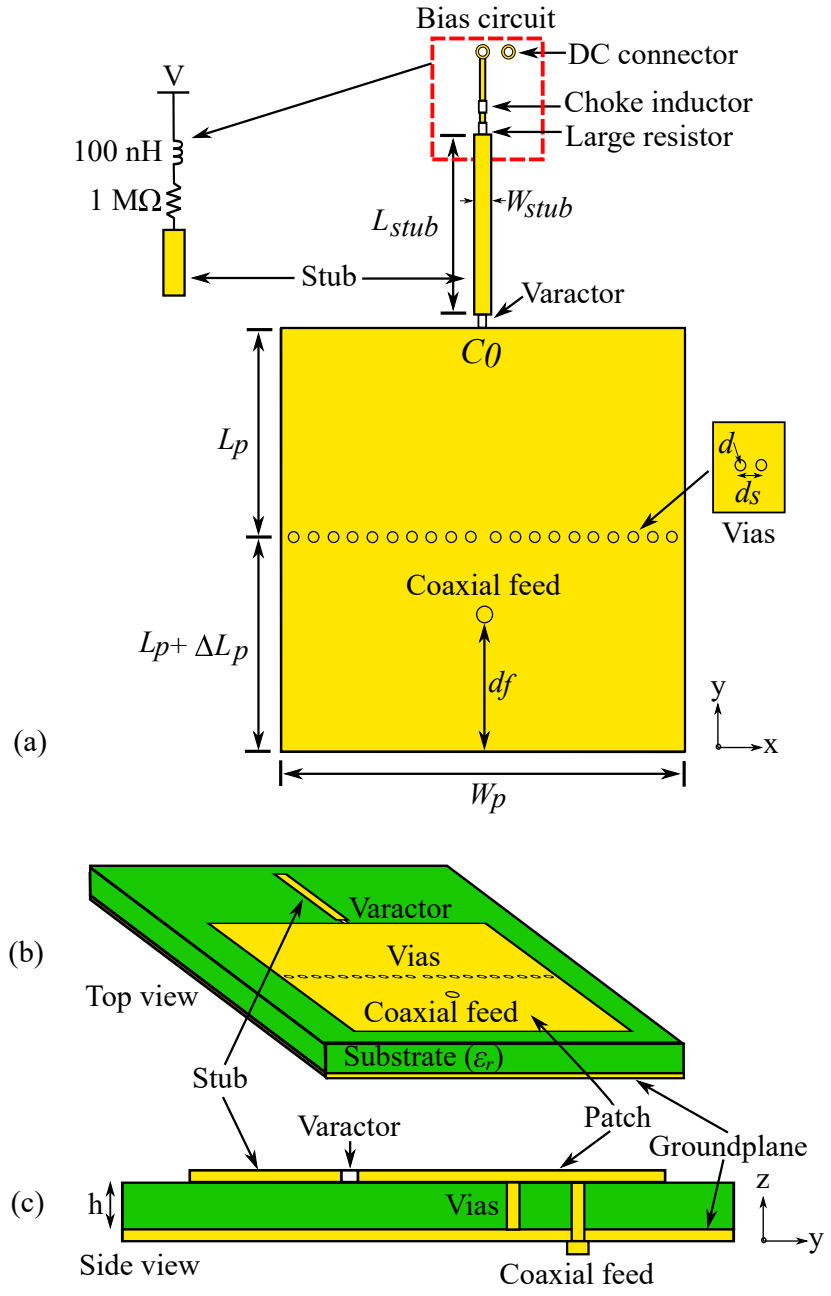

Figure 4.1. A reconfigurable single-element microstrip antenna structure. (a) A reconfigurable single-element microstrip antenna structure, (b) top view - consisting of a probe-fed rectangular microstrip patch on the top of a dielectric substrate (ε_r) backed by a metallic ground plane and (c) side view.

4.3 Operation principle

According to the design, the antenna frequency tuning range is strongly related to the varactor capacitance C_0 together with the width and length of the stub, since they determine the reactance loaded at one of the radiating apertures. The optimisation of the stub length can be performed as described in (Nguyen-Trong *et al.*, 2015d) for a fixed stub width. As a result of this study, the stub width, W_{stub} = 1.5 mm and the length, L_{stub} = 17 mm are selected. In addition, the patch with the center metallic wall can be seen as two coupled back-to-back quarter-wave patches, which can have slightly detuned resonance frequencies depending on their resonance lengths. The largely independent resonance frequencies can be tuned by varying C_0.

For excitation, the antenna is fed by a coaxial probe in one of its half cavities located at d_f = 13 mm. The resonant mode on the second half cavity of the patch is excited by direct coupling to the fed cavity. In order to compensate the imbalance caused by this feeding probe, the patch is made slightly longer by ΔL_p on the feeding side. In practice, within the impedance bandwidth ($|S_{11}| < -10$ dB), the main beam direction at a particular frequency can be continuously adjusted within a certain angular range, determined by the phase difference between the two radiating slots.

To further study the direct coupling between the two coupled cavities, Fig. 4.2 demonstrates the schematic electric field distribution of the antenna for two different operation conditions which are defined as an odd mode (refer to Fig. 4.2(a)), caused by the coupling of magnetic currents, and an even mode (refer to Fig. 4.2(b)), caused by the coupling of electric currents. These two conceptual modes can be seen through the two lines of current flow in an electromagnetic situation, where the pair lines are conducted differentially. The odd mode excitation is associated with the two lines of the electric current that have an opposite polarity with respect to each other and same polarity plane between the magnetic current. Meanwhile, the other mode of the current flow (even mode excitation) is associated with the same polarity of the electric current in both sides with opposite polarity between the magnetic current.

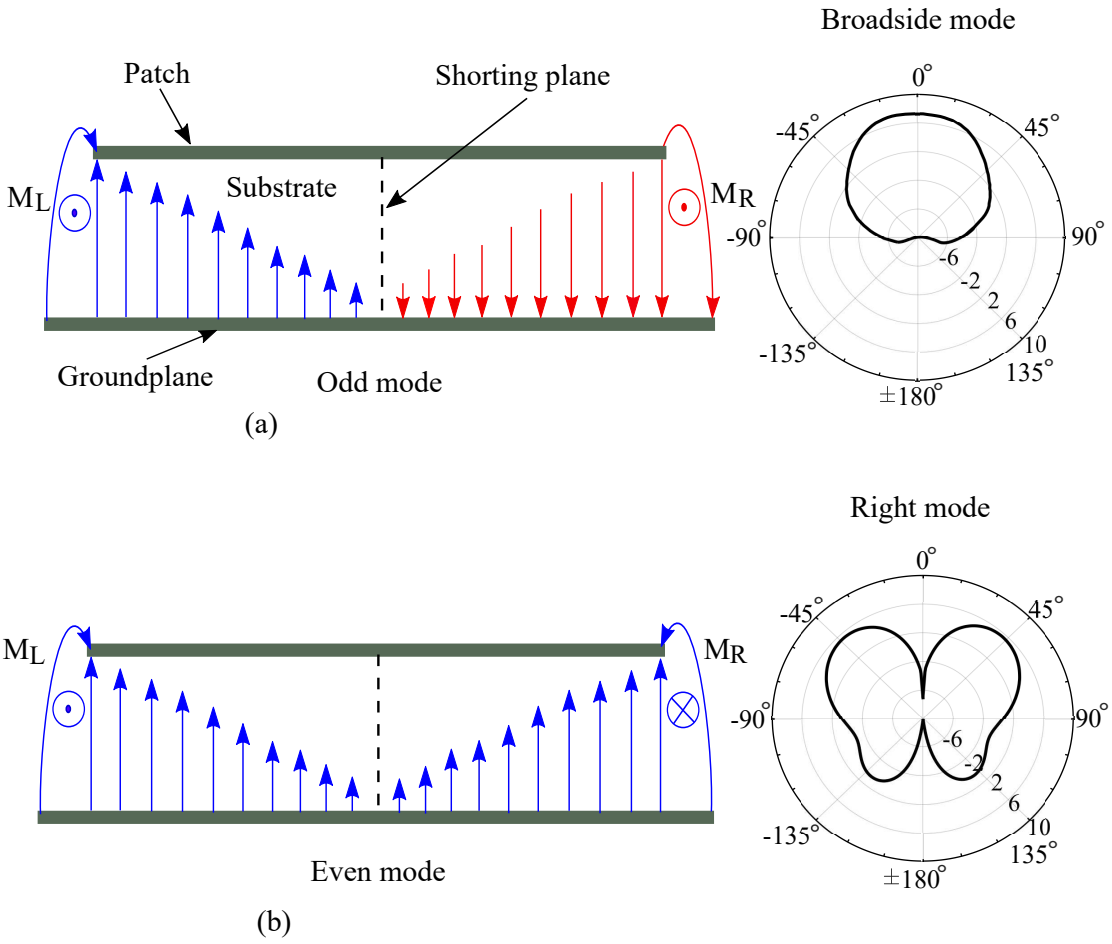

Figure 4.2. The electric-field distribution of two modes. The electric-field distribution of the shorted patch in (a) odd mode and (b) even mode operation.

The two modes can indeed exist independently of each other since the shorting plane at the center of the patch is forced to be zero. Thus, two half mode cavities can be defined with the electric field between these cavities having symmetrical or antisymmetrical distributions. In this analysis, the antenna structure can be identified as a two-element array similarly as in (Zainarry *et al.*, 2018), where the elements are two equivalent magnetic currents that possess different phases and similar amplitudes. The far-field pattern of the antenna can be calculated corresponding to array factor as (Balanis, 2015)

$$Array factor, AF = 2cos\left(\frac{1}{2}(k_0 dsin\theta + \Delta\phi)\right), \tag{4.2}$$

where k_0 is the free-space wavenumber, meanwhile d is the distance between the array elements and $\Delta\phi$ is relative phase between the two magnetic currents formed in the two patch apertures, respectively. For the odd mode in Fig. 4.2(a), the field distribution corresponds to the traditional fundamental mode of the patch. Since the equivalent magnetic currents, M_L and M_R, are in phase along the left and right side of the cavities, this results in broadside radiation pattern. In contrast, for the even mode in Fig. 4.2(b), the M_L and M_R are essentially out of phase along the two side cavities. This mode generates a pattern with a zero towards broadside, as the radiation from the two equivalent currents cancel each other out in this direction.

4.4 Pattern reconfigurability

This section describes an approach for beam steering operation of the antenna, together with an investigation of the main design parameters. In short, the operation is achieved when detuning the resonance on one side of the patch, by which the phase difference between the two radiating slots is obtained. This is analogous to the principle presented in the previous chapter (Zainarry *et al.*, 2018) where a variation in varactor capacitances detuned the two resonances and thus provided beam scanning at a fixed frequency. In the present case, this principle also leads to a frequency-dependent beam steering within the operation band, because the relative phase varies with operation frequency. However, the beam steerable angle is limited both by the impedance bandwidth and the achievable phase difference between the two radiating apertures. Theoretically, a wider impedance bandwidth can lead to a wider beam scanning angle, due to the larger phase difference that can be created between the two half patches. Therefore, the antenna reconfigurability is largely restricted by the achievable impedance bandwidth.

4.5 Numerical optimisation

In order to evaluate the proposed antenna, this section represents an optimisation of different design parameters to achieve satisfactory matching performance for excitation of the two cavities and increase the maximum scanning angle of the antenna. As mentioned in the previous Section 4.2, the presence of the series of vias near the center of the antenna does not affect the resonance frequency of the conventional resonant mode, provided the vias have a small radius. Therefore, the resonance frequency remains almost the same as the resonance frequency of a single quater-wave patch antenna. From this perspective, the operation of the antenna is numerically calculated when varying a number of vias to control the coupling level, which allows to achieve best performance of the two cavities antenna. Figure 4.3 shows the simulated reflection coefficient of the antenna for various numbers of via, N introduced in the asymmetric cavity, for a fixed additional length $\Delta L_p = 0.7$ mm on one side (See Fig. 4.1a). As seen in the figure, increasing the number of vias helps improving the performance of two coupled cavities performance corresponding to the antenna matching level. In this study, the maximum number of vias, $N = 20$ provides a good matching level of the antenna within -10 dB for beam scanning functionality.

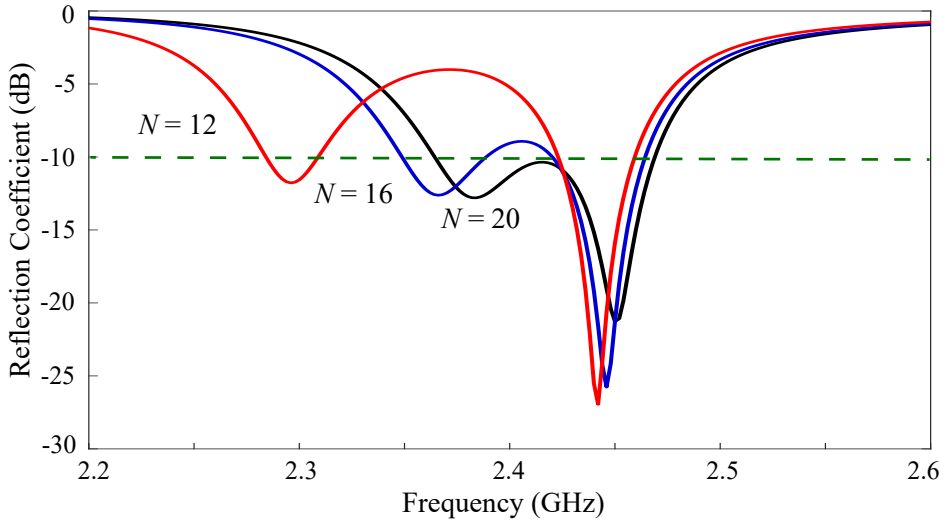

Figure 4.3. Simulated reflection coefficient for different number of vias. Simulated reflection coefficient for different number of vias placed near the center of the aperture at a fixed ΔL_p.

For optimisation of the maximum beam-steerable performance, the additional length ΔL_p plays an important role to compensate the imbalance of the effective electrical length of the two cavities, which is introduced by the single-sided asymmetric feeding. It is noted that the antenna matching still needs to be considered since varying the length ΔL_p can cause the matching condition to change, thus affecting the range of beam steering patterns attainable within matching specifications. Figure 4.4 illustrates the antenna maximum scanning angle at different length of ΔL_p along the capacitance range of the varactor. According to these results, the selected minimum and the maximum additional length are observed to yield a more limited beam scanning range compared to the middle value. In addition, there is is a mismatch in the antenna reflection coefficient at the highest capacitance when ΔL_p = 1 mm. Therefore, an optimised value of ΔL_p = 0.7 mm is chosen to provide in the maximum beam steering angle.

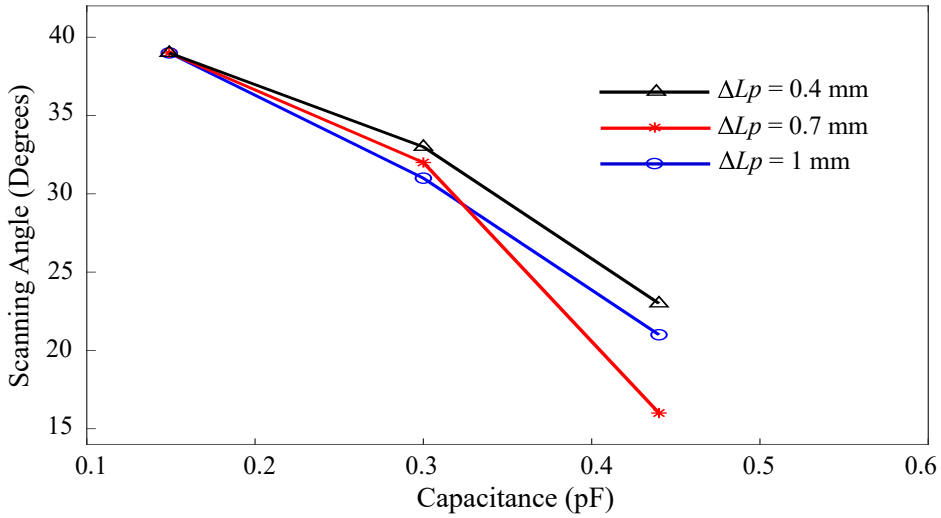

Figure 4.4. Parametric study of the additional length. Parametric study of the additional length, ΔL_p of one cavity side. The results allow to determine maximum scanning angle as functions of the varactor capacitance values.

4.6 Experimental results

In order to verify the pattern reconfigurability, an antenna prototype has been fabricated which is illustrated in Fig. 4.5. The simulated and measured reflection coefficients of the antenna with three different cases of bias voltages, V_1 = 3.8, V_2 = 6.3 and V_3 = 18 V corresponding to fixed frequency of 2.4 GHz are shown in Fig. 4.6. The curves in the graph indicate two resonances associated with the two half-cavity sides of the patch. The variation of the capacitance C_0 influences the detuning of the two coupled resonances, with lower values of C_0 leading to increase in frequencies. In this context, the maximum beam steerable angle is achieved by the limit cases for which the mid-point of the reflection coeficient of every case is reaches -10 dB. A good agreement between simulated and measured result is observed. Furthermore, the measured operation bandwidth is achieved from frequencies of 2.34 to 2.44, 2.35 to 2.45 and 2.36 to 2.46 GHz respectively, when bias voltage is V_1 (C_0 = 0.44 pF), V_2 (C_0 = 0.30 pF) and V_3 (C_0 = 0.15 pF).

The simulated and measured radiation patterns shown in Fig. 4.7 suggest that the beam can be squinted on one side by an angle dependent on the varactor capacitance. The range of scanning angle is primarily limited by the impedance matching for a particular frequency. In Fig. 4.7(a), the radiation patterns in the E-plane at 2.40 GHz indicate that the measured beam squint varies from 20°, 32° and 39° with bias voltages of 3.8, 6.4 and 18 V, respectively. Correspondingly, at a fixed bias voltage of 6.3 V, the beam steers as a function of the frequency. This can be seen in Fig. 4.7(b), where the E-plane radiation patterns are shown at frequencies f_1 = 2.35 GHz, f_2 = 2.40 GHz and f_3 = 2.45 GHz, with a good correspondence between the simulated and measured data. Within the impedance bandwidth of 4.6% (denoted as BW in Fig. 4.7) for this voltage setting, the antenna has a scanning beam from 8° at 2.35 GHz to 43° at 2.45 GHz.

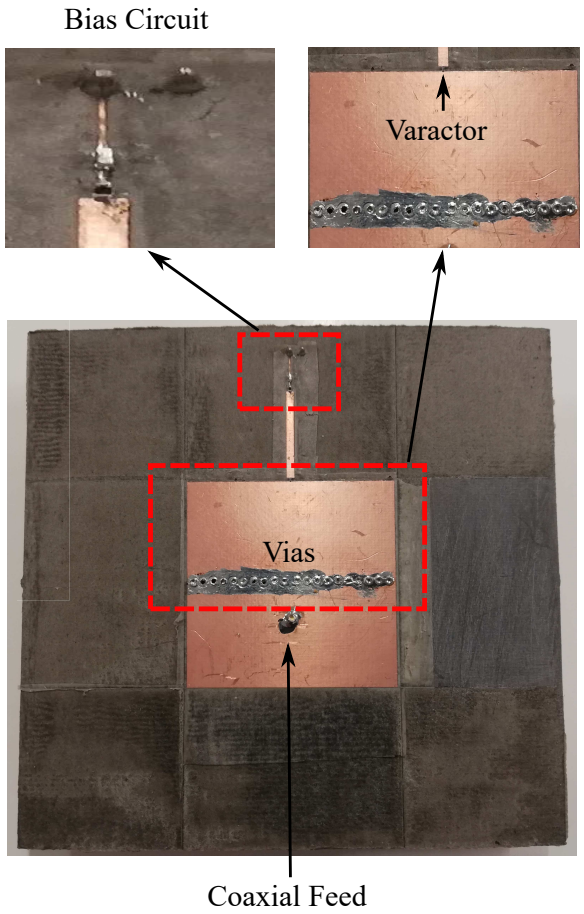

Figure 4.5. The photograph of the fabricated antenna. The photograph of the fabricated single-element pattern-reconfigurable antenna.

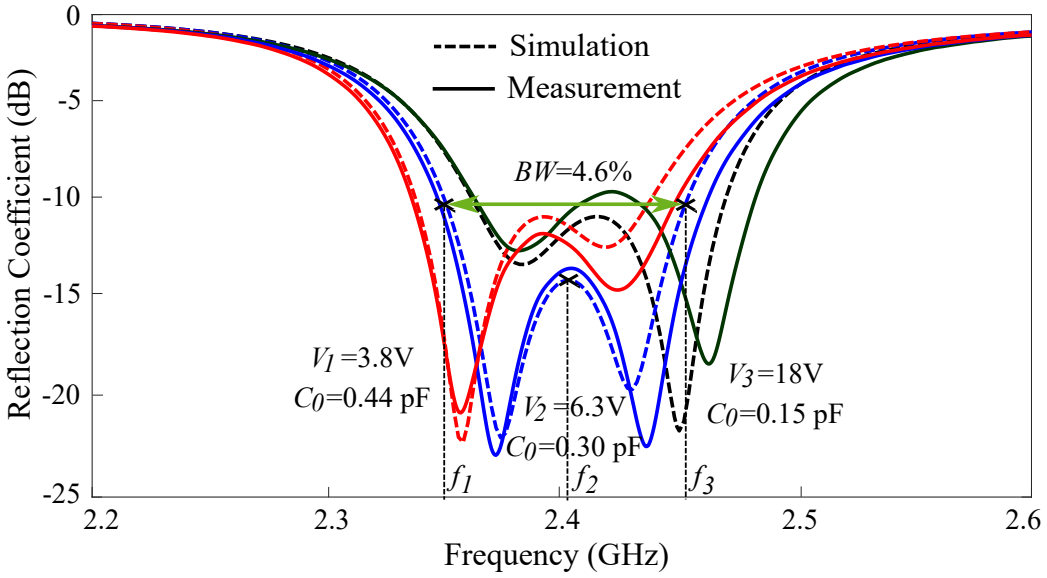

Figure 4.6. Reflection coefficients with three different bias voltages. Reflection coefficients with three different bias voltages for beam scanning operation.

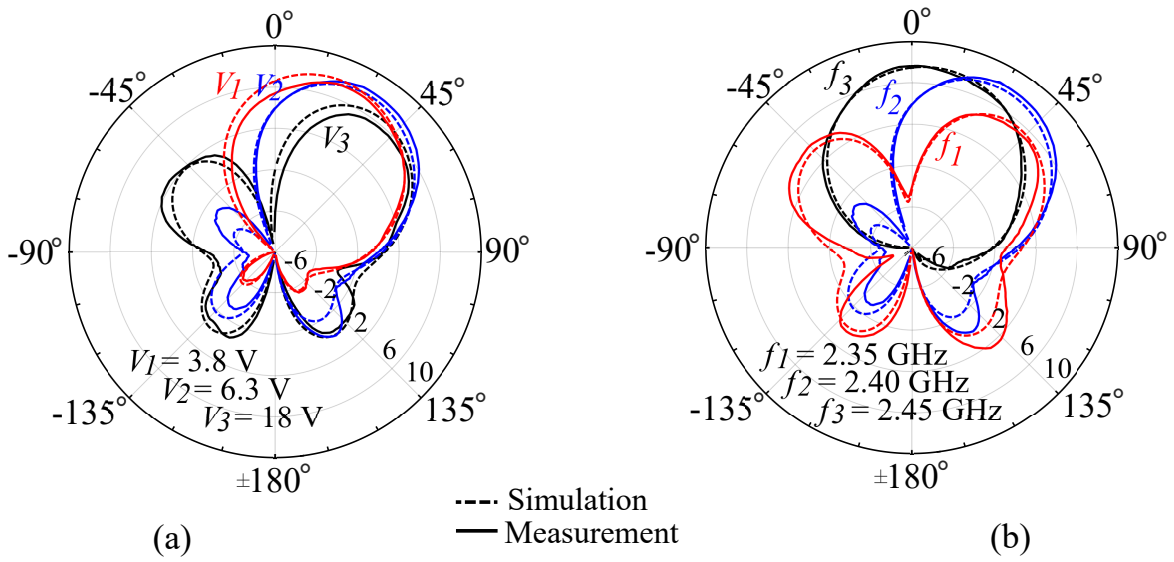

Figure 4.7. Normalised radiation patterns. (a) Normalised radiation patterns at 2.40 GHz in the yz-plane with different bias voltages $V_1 = 3.8$ V, $V_2 = 6.3$ V and $V_3 = 18$ V. (b) Normalised radiation patterns with bias voltage of 6.3 V in the yz-plane at different operating frequencies, $f_1 = 2.35$, $f_2 = 2.40$ and $f_3 = 2.45$ GHz.

Figure 4.8(a) shows the realised gain of the antenna as a function of the bias voltage at 2.40 GHz. The measured results show that the antenna gain at 3.8, 6.3 and 18 V are 7.4, 8.0 and 6.2 dBi, respectively. The corresponding efficiencies are depicted in Fig. 4.8(b), where the maximum and minimum efficiencies of 98% and 83% are observed at 3.8 and 6.3 V, respectively. Since the gain variations reflect both the directivity and efficiency differences, these results imply that the directivity at 3.6 V is similar to that at 6.3 V, while the one at 18 V decreased.

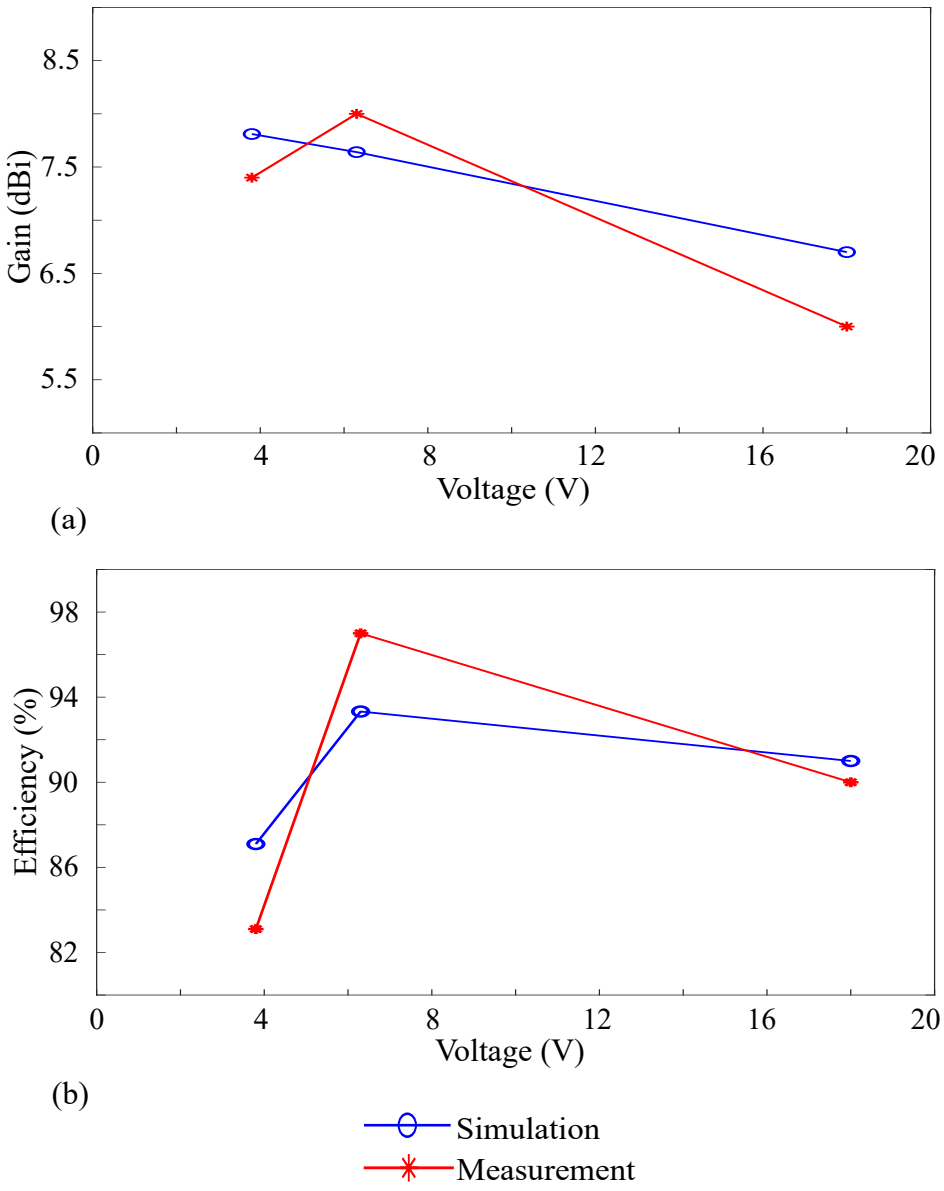

Figure 4.8. Antenna gain and efficiency. (a) Antenna gain and (b) antenna efficiency at 2.40 GHz with various voltages of 3.8, 6.3 and 18 V.

4.7 Conclusion

A concept of a simple single-element microstrip antenna with pattern reconfigurability has been presented. The antenna consists of two back-to-back quarter-wave patch cavities separated by a metallic wall made of a row of vias. A stub-loaded varactor connected to one of the radiating slots has been utilised as the tuning mechanism to obtain pattern reconfigurability, by electronically detuning the frequency of one of the resonances. Varying the varactor capacitance allows to primarily manipulate the effective cavity length on one side, and thus yields a tunable phase difference between the two radiating slots of the patch to obtain beam steerability. An antenna prototype has been measured and results demonstrate that the antenna exhibits beam squint up to 39° on one side of the patch at the center frequency of 2.40 GHz, when the bias voltage is tuned from 18 to 3.8 V. Also for a fixed bias voltage of 6.3 V, the beam can scan from 8° to 43° as a function of frequency within the operation bandwidth from 2.35 to 2.45 GHz.

Chapter 5

Concept of a Stub-Loaded Reconfigurable Reflectarray Unit Cell

THIS chapter deals with general procedures for designing a printed reconfigurable reflectarray unit cell based on a concept of a stub-loaded varactor-controlled tunability. The rationale of the design is in the impedance transformation characteristics of the stubs which are exploited to achieve the unit cell reconfigurability. In that context, the optimisation of the length of the stub loaded with varactors is presented, which provides an enhancement of the frequency agility feature. To satisfy the space requirement of a unit cell, a potential design of the reconfigurable reflectarray unit cell with T-shaped stubs is proposed. Futhermore together with a varactor connected at the two edges of the unit cell along one direction, a good performance of reflection coefficient and phase tuning range is achieved. This chapter also presented the comparison between T-shaped stubs and straight-line stubs geometries as a contribution to the unit cell's performance.

5.1 Introduction

Reflectarray antennas are receiving increasing attention in various applications, especially in satellite communications and radar systems since they are providing remarkable functionality features that other antennas cannot support. Indeed, reflectarray antennas combine some advantages of microstrip array technology with those of conventional reflector antennas (Carrasco *et al.*, 2016), leading to a reflector structure characterised by flatness, low profile, light weight, ease of fabrication, ease of circuitry integration and high efficiency (Venneri *et al.*, 2003; Sarshar and Tabari, 2013; Hum and Perruisseau-Carrier, 2014; Costanzo *et al.*, 2015b). Figure 5.1(a) shows a printed antenna array which has its elements arranged in a grid that, with a feeding network that can offer designable complex amplitude for excitation of the individual elements for a particular functionality. Practically, if the elements are equipped with phase shifters, arrays can have a capability of a steerable beam pattern in real time. However, the presence of a large number of phase shifters lead to high cost of implementation, and there are significant power losses in the antenna transmission-line feeding networks especially at high frequency. On the other hand, Fig. 5.1(b) illustrates a conventional reflector antenna which has a simple and developed configuration structure. The antenna provides a solution to achieve high antenna gain in a relative inexpensive cost. The disadvantage of the antenna is a bulky structure and limited ability for electronic beam steering.

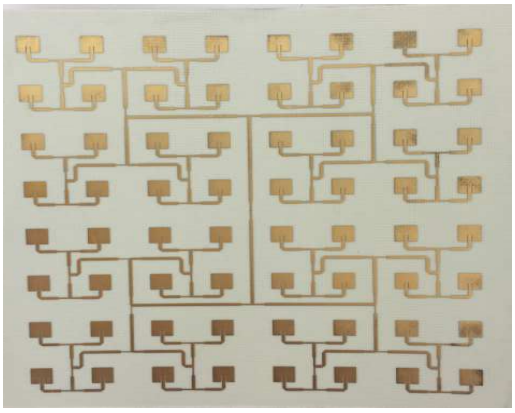

(a) CC-BY

(b) CC-BY

Figure 5.1. Microstrip and parabolic antenna. (a) Microstrip antenna array (ATcodi Co., n.d.) and (b) parabolic reflector (University, n.d.).

Since the reflectarray antenna can be considered as an hybrid between these antennas (arrays and reflectors), the combined features ideally allow to obtain flexibility in beam shaping (Elsherbiny *et al.*, 2004; Pozar *et al.*, 1999) or multiple beam (Johansson, 1990; Nayeri *et al.*, 2012) performance while maintaining implementation cost. Generally, a standard reflectarray antenna consists of an array of passive microstrip patches printed onto the top layer of a dielectric substrate and located in the far field of a feed. Each unit cell of the array is uniquely designed by varying parameters of a given structural shape to achieve an individual prescribed phase on reflection. This localised control of the phase allows to synthesise a reflecting surface that determines a predefined radiation pattern. Hence, scattering characteristics response of the unit cell, such as reflection coefficient amplitude and reflection phase range, as function of design parameters, are important performance measures for a unit cell in a periodic configuration. Figure 5.2 shows an example of a reflectarray antenna that is composed of an array printed elements and illuminated by a feed-horn antenna.

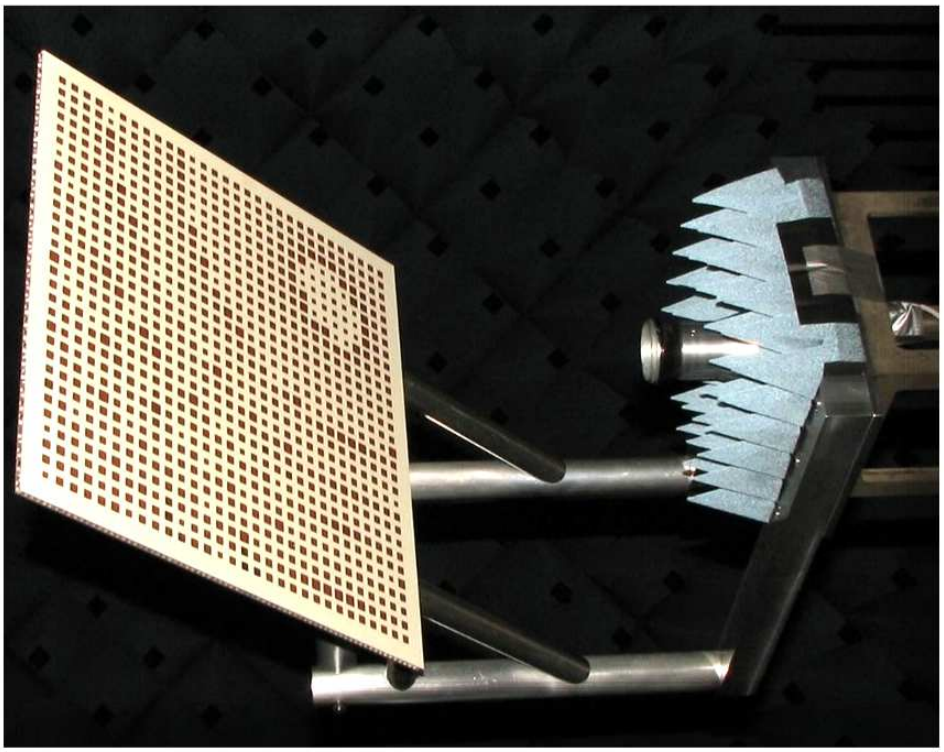

Figure 5.2. Example of reflectarray antenna system. A printed reflectarray antenna illuminated by a feed-horn antenna in anechoic chamber (Zhou *et al.*, 2011).

More recently, the concept of reconfigurable reflectarray antennas (Hum *et al.*, 2005b; Gianvittorio and Rahmat-Samii, 2006a; Venneri *et al.*, 2012) has emerged as pathway to multi-functional reflectors with enhanced capabilities compared to a fixed reflectarray antenna. Indeed, a reconfigurable reflectarray antenna should be capable of providing flexibility in tuning the frequency of operation and adapting its beam in scanning applications. The reconfiguration can be achieved by applying electronically tunable components, e.g. PIN diodes (Kamoda *et al.*, 2009; Carrasco *et al.*, 2010), varactors (Hum *et al.*, 2005b; Sievenpiper *et al.*, 2003; Hum *et al.*, 2005a) or MicroElectroMechanical Systems (MEMS) switches (Gianvittorio and Rahmat-Samii, 2006b; Legay *et al.*, 2003, 2007), to adapt the complex impedance characteristics of each antenna unit cell. In this chapter, a reconfiguration based on varactor diodes is considered. The intrinsic imperfection and limitations of varactors lead to constraints and challenges towards achieving a satisfactory performance in term of reflection coefficient and phase range across a wide frequency tuning range and thus a careful analysis and design method is required.

According to the principles studied in (Nguyen-Trong *et al.*, 2015c, 2016d,a), a stub-loaded configuration of unit cell appears attractive. In this context, a reconfigurable reflectarray unit cell antenna with two varactors connected at the edges of a square patch is proposed. A modification of the geometry is investigated in form of a T-shaped stub to adapt straight-line stub geometries to the restriction of a unit cell, while maintaining performance in view of a wider frequency tuning range behavior.

This chapter will begin with a description of the operation principle and unit cell design in Section 5.2 and 5.3, respectively. Then in Section 5.4, parameter studies and the unit cell's optimisation based on the open stub-loaded configuration concept are discussed in detail. Finally, the simulation results related to scattering characteristic response corresponding to the variation of the varactor capacitance are presented in Section 5.5.

5.2 Principle of reflectarray

For the fundamental design of the reflectarray antenna, the most important step to be highlighted is the characterisation of their elements in periodic settings. In case that the single element is not properly optimised, the excitation signal from a primary feed will not be scattered effectively in order to achieve a desired beam steering. Figure 5.3

illustrates the general architecture of the reflectarray antenna, where the antenna reflecting surface is located in the far-field of the feed. In the reflectarray antenna design, the reflection loss will directly translate into loss performance for the antenna, meanwhile full phase 360° tuning is ideally required as a reflection phase range of the antenna. Generally, the excitation amplitude of each elements is introduced by the primary feed illumination. On the other hand, phase technique is implemented to provide the phase distribution on the reflectarray surface.

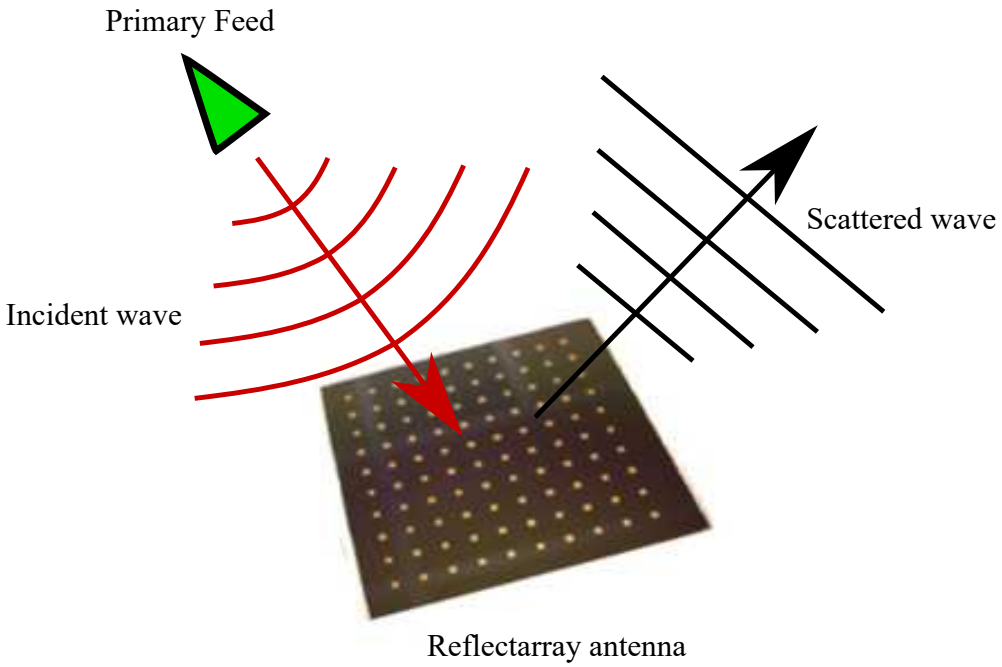

Figure 5.3. Reflectarray architecture. General architecture design of the reflectarray antenna

To further understand the concept of the antenna, the operation principle for a off-specular reflection angle of radiation pattern is shown in Fig. 5.4. This configuration consists an array of microstrip patch elements which has a progressive phase change applied to them. This array is designed to steer the scattered plane wave to a desired direction. For specific implementation, the geometry of the patch elements can be any type (e.g. rectangular, square, triangular, dipole, etc) depending on the desired element characteristics. According to this principle of progressive phase, the incident wave fed by a feed to the reflectarray antenna surface will be reflected in direction of θ. This direction θ may be designed to depend on the incident wave polarisation. For

the elements with progressive phase change, the following condition will define the steering angle (Niu *et al.*, 2013):

$$\Delta\Phi = \frac{360^\circ \times d \times sin\theta}{\lambda}, \tag{5.1}$$

where $\Delta\Phi$ is the progressive phase change introduced by corresponding to the array elements, d is the spacing between the element, θ is the reflection angle of scattered plane wave and λ is the wavelength of the operating frequency.

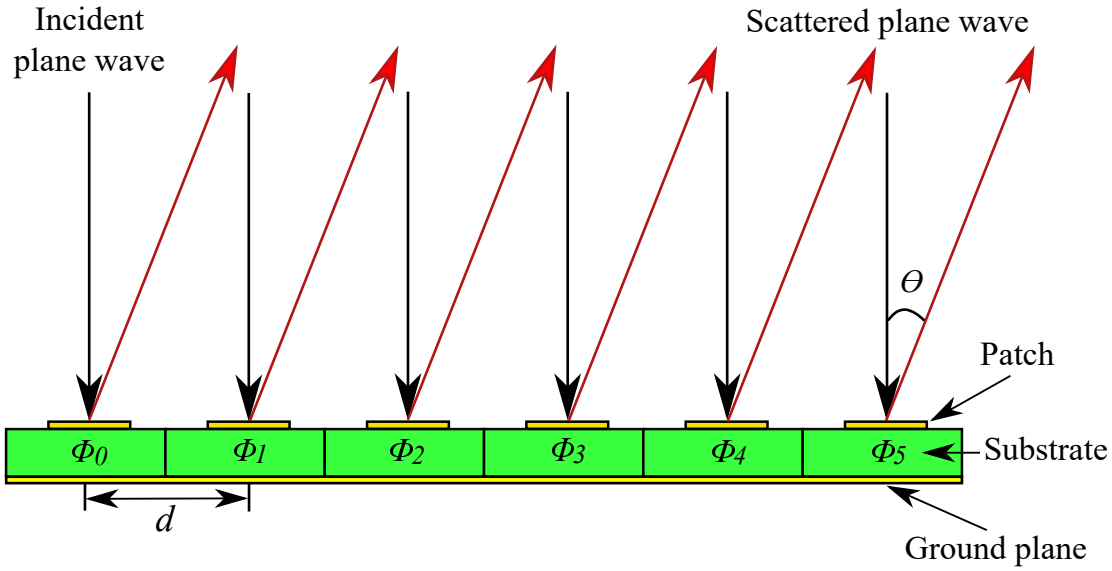

Figure 5.4. Operation principle. Operation principle of the designed reflectarray. The phase distribution results in desired scattered plane wave with designed angle θ by excitation from normal incident plane wave.

5.3 Unit cell design

Figure 5.5 shows a generic configuration of a stub-loaded reconfigurable reflectarray unit cell. The operation principle is inspired by stub-loaded varactor control as demonstrated for a half-mode cavity (Nguyen-Trong *et al.*, 2015c) and a patch antenna in (Nguyen-Trong *et al.*, 2016a). In these works, an optimisation of the stub length is used to maximise the tuning range offered by the variable capacitance of the varactor. Based on the concept, an initial configuration of the unit cell is designed as shown in Fig. 5.5.

The unit cell consists of three material layers namely a square microstrip patch printed on the top of a dielectric substrate backed by a metallic ground plane. Two varactors are placed at the opposite radiating edges of the patch, creating a symmetrical loading condition to the unit cell. Both varactors are then loaded with a straight stub, whose length can be optimised to achieve best tuning performance. However, the design in this stub configuration will require a large area of dielectric substrate on each side of the patch, making it no longer suitable for a unit cell design because of grating lobes appearing when the cell size L_s becomes larger then $\lambda/2$. Thus, a new configuration of T-shaped stub-loading is proposed as shown in Fig. 5.6. The configuration provides a compact structure and a more efficient design. A bias circuit consisting in a large isolating resistor and a choke inductor is straightforward to implement in this open stub configuration, as shown in (Nguyen-Trong *et al.*, 2015c, 2016a).

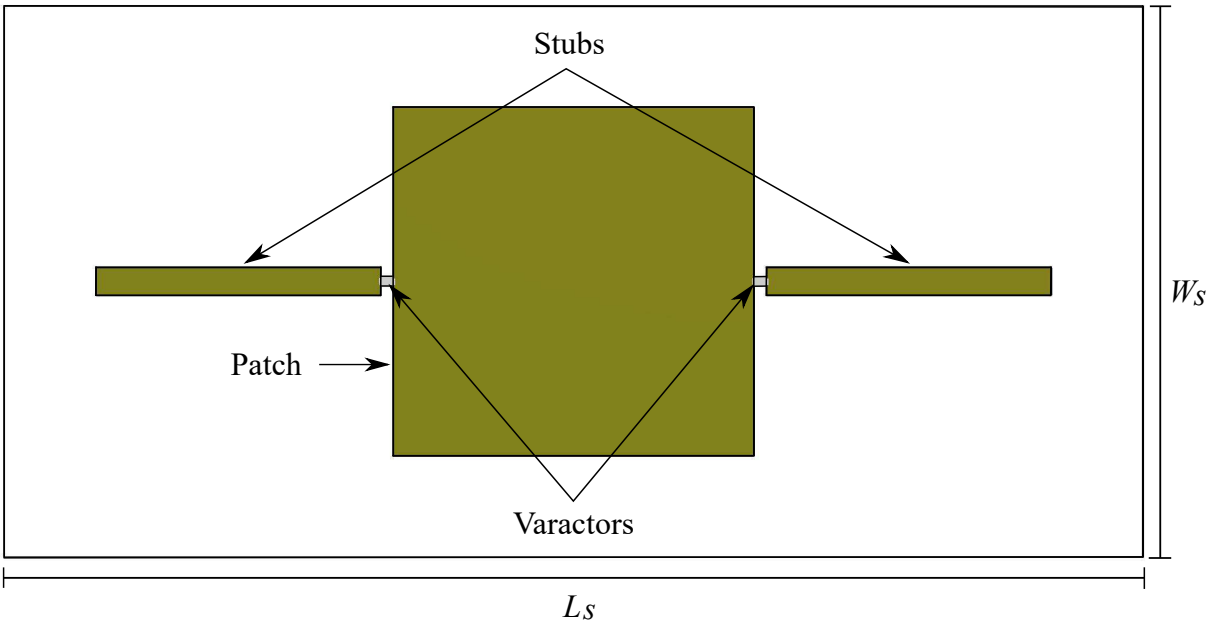

Figure 5.5. Unit cell straight-line stub-loaded configuration. Straight-line stub-loaded configuration of a reconfigurable patch unit cell, as basis for the investigation.

As a first step, the primary unit cell parameters L_p and W_p can be determined based on the rectangular patch standard design procedure discussed in Section 2.1.1 (Balanis, 2015). Here, the dimensions of a square patch are derived for operation frequency around 3 - 4 GHz where $L_p = W_p = 19$ mm. The patch is printed on a Rogers Duroid 5880

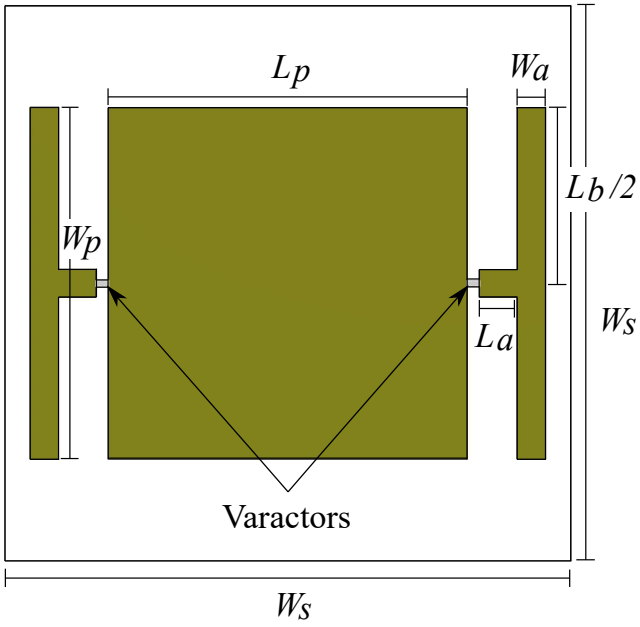

Figure 5.6. Unit cell T-shaped stub-loaded configuration. T-shaped stub-loaded configuration of a reconfigurable patch for implementation as reflectarray unit cell.

substrate with a relative permittivity ε_r = 2.22 and thickness of 3.175 mm. As a practical varactor type, a model MA46H120 from MACOM Technical Solutions (MACOM, 2015) is considered. This particular varactor provides a tunable variable capacitance in the range of 0.149 pF to 1.304 pF for a reverse bias voltage varying from 18 V to 0 V. The reconfigurability of the unit cell can be achieved by electrically adjusting the varactor variable capacitance to tune the resonance frequency of the patch. However due to the limitation of the varactor capacitance range, this approach usually does not provide a large tuning range of frequency. Therefore, an additional open stub is loaded to the varactor as a solution offering additional impedance manipulation leading to an increase in the tuning range of the patch resonance frequency. The lengths of the T-shaped stub, L_a and L_b together with the width, W_a are optimised as described in the next section.

5.4 Optimisation and parameter study

This section provides a parameter study of the reconfigurable reflectarray unit cell design. The design is analysed using CST Microwave Studio in an infinite array environment using Floquet analysis. In Section 5.4.1, the theoretical basis of the impedance

manipulation using varactor and open stub is discussed. The next Sub-section 5.4.2 explains the optimisation of the stub length associated with different varactor capacitance values.

5.4.1 Impedance analysis of the stub-loaded varactor

Practically, Fig. 5.7 illustrates the unit cell equivalent circuit associated with a stub-loaded varactor at one of the radiating aperture of the patch. According to this equivalent circuit, the varactor provides a tunable variable capacitance that is used to control the behavior of the patch resonance, essentially corresponding to varying the effective length of the patch. Controlling the patch length around resonance allows to obtain an individually prescribed phase for each unit cell, thereby controlling the radiation pattern of a reflectarray. The varactor parasitics and losses are also taken into account by inserting a series resistance and a parasitic inductance in the circuit. The three parasitic capacitances C_s, C_{p1} and C_{p2} are included in the circuit as well as proposed for the equivalent circuit model in (Kirschning *et al.*, 1983). Since the datasheet does not provide the full range of reverse bias voltage for all capacitance values, the capacitance can be calculated as (Cojocaru and Brazil, 1992)

$$C(V) = \frac{C_{JO}}{(1 + V/V_J)^M} + C_{par}, \tag{5.2}$$

where the measured values of the varactor parameters can be seen in Tab. 5.1. The frequency agility of the patch is determined by the presence of the microstrip stub loaded onto the other side of the varactor. This approach is changing the impedance at the radiating slot of the patch, in a fashion relying on the stub length as described in (Collin, 2007)

$$Z = -jZ_{mo}\left(\frac{\cot[\beta_m(L_b/2 + \Delta l)] - 2\tan(\beta_m L_a)}{2 + \cot[\beta_m(L_b/2 + \Delta l)]\tan(\beta_m L_a)}\right). \tag{5.3}$$

R	L	C_{JO}	V_J	M	C_{par}
2 Ω	0.05 nH	1.2 pF	4.155 V	1.97	0.1044 pF

Table 5.1. Varactor parameters

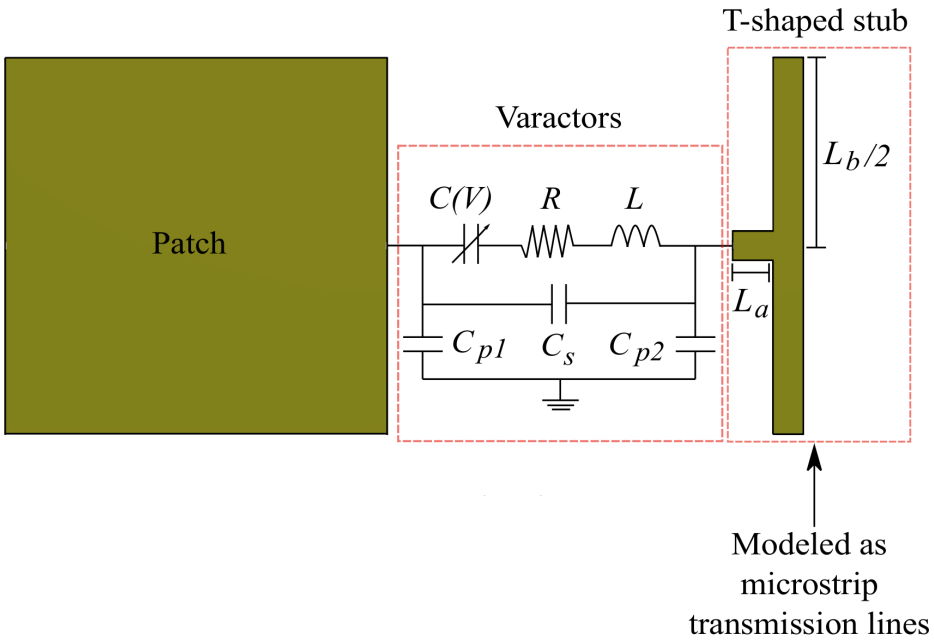

Figure 5.7. Unit cell equivalent circuit. Equivalent circuit for the reconfigurable reflectarray unit cell.

The characteristic impedance of the T-shaped stub is found using transmission line theory: the two sections of length $L_b/2$ are in a parallel configuration, thus giving a load impedance of $Z_L = -0.5jZ_{mo}\cot[\beta_m(L_b/2 + \Delta l)]$, seen by a transmission line section of length L_a. Due to the emergence of the fringing fields at the end of the vertical line stubs, a small Δl is taken into account as equivalent additional stub length, while Z_{m0} and β_m are the characteristic impedance and phase constant of the stub.

5.4.2 Optimisation

To investigate the characteristics and the tunable frequency agility of the unit cell, the varactor capacitance is varied for several fixed vertical line stub length L_b while keeping stub width W_a and the length L_a fixed. The selected of the W_a and L_a are according to standard parameters to simplify the antenna structure and facilitates soldering process. These parameters are not that critical to the antenna design. In Fig. 5.8, the curves illustrate the tuning range of resonance frequency as a function of the capacitance values for the lengths L_b = 0, 7, 12 and 19 mm. When the capacitance equals zero, the resonance frequency of the unit cell is independent on the stub length, and it corresponds to the resonant frequency of the base patch without any stub. Increasing now the varactor capacitance, the resonance frequency values become dependent on the stub length as shown in the figure. The value at infinite capacitance asymptotically converges to a resonance frequency corresponding to a patch directly connected to the open stubs.

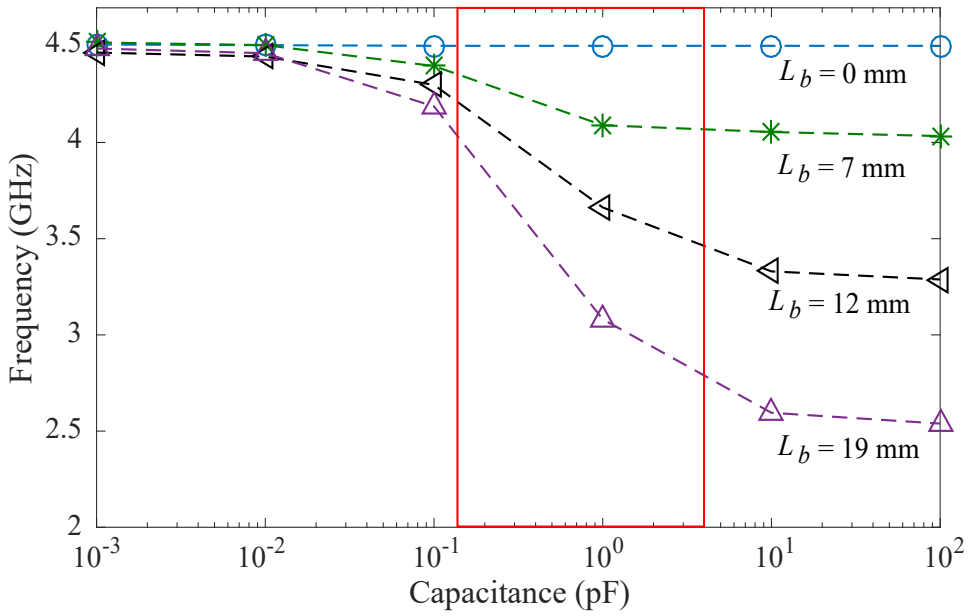

Figure 5.8. Resonance frequency as a function of the varactor capacitance values. Resonance frequency as a function of the varactor capacitance values, for different lengths of the T-shaped stubs.

One observation from Fig. 5.8 is that when there is no stub loading applied to the unit cell, the varactor acts as open circuit and the resonance frequency remains unchanged with varying capacitance values. In contrast, when the length of the stub is increased,

L_p	W_p	W_s	L_a	L_b	W_a
19 mm	19 mm	30 mm	2 mm	19 mm	1.5 mm

Table 5.2. Final design parameters for the unit-cell geometry of Fig. 5.6.

the variation of the resonance frequency becomes increasingly pronounced as a function of capacitance, leading to the desired reconfigurability of the unit cell. The figure indicates that longer stubs provide a wider tuning range, but it is noted that this only holds for stub lengths shorter than half-guided wavelength, i.e. before a band gap in the tuning range appears, as described in (Nguyen-Trong *et al.*, 2015c).

To achieve a given target frequency tuning range, the dimension of the unit cell must be optimised together with the length of the stubs taking into account the capacitance range provided by a practically available varactor. To illustrate this, Fig. 5.8 also highlights (with a red rectangle) the tuning range of the resonance frequency achievable within the capacitance range values offered by the mentioned varactor type (0.149 pF to 1.304 pF).

5.5 Scattering characteristic response

Based on the consideration above, a fixed length of L_b = 19 mm is selected to fulfill the requirement of the unit cell design. The other dimensions of the design are given in Tab. 5.2, and the results of the unit cell simulations are given below. The reflection coefficient response of the unit cell in an infinite array for the capacitance range of 0.149 pF to 1.304 pF is presented in Fig. 5.9 (phase) and Fig. 5.10 (amplitude). The phase response in Fig. 5.11 shows that a tuning of near 300° is achievable between 3.44 GHz and 3.67 GHz, i.e. a phase range which is sufficient for most reflectarray applications. The efficiency of the reflection is illustrated in the amplitude graphs (Fig. 5.10), which shows a magnitude response better than −2.75 dB over the full range of capacitance, and better than −1.4 dB in the quoted frequency range of operation.

To further illustrate the principle, a periodically repeated linear sub-array antenna consisting of 6 radiating elements is designed. This arrangement allows testing the operation of the reflectarray for the case of nonuniform biasing of the varactors. The reflectarray is illuminated with plane wave at normal incidence angle with respect to the array's surface (i.e. at an angle $\theta = 0°$). A selected six points of a progressive phase on

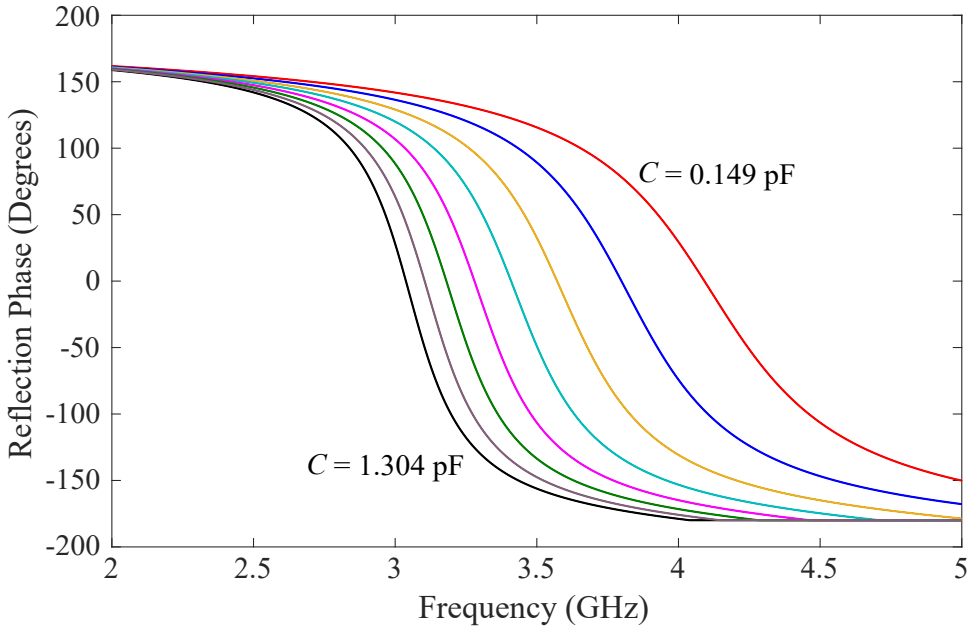

Figure 5.9. Phase of the reflection coefficients. Phase of the deembedded reflection coefficients for various values of capacitances in the range of practical values for the chosen varactor.

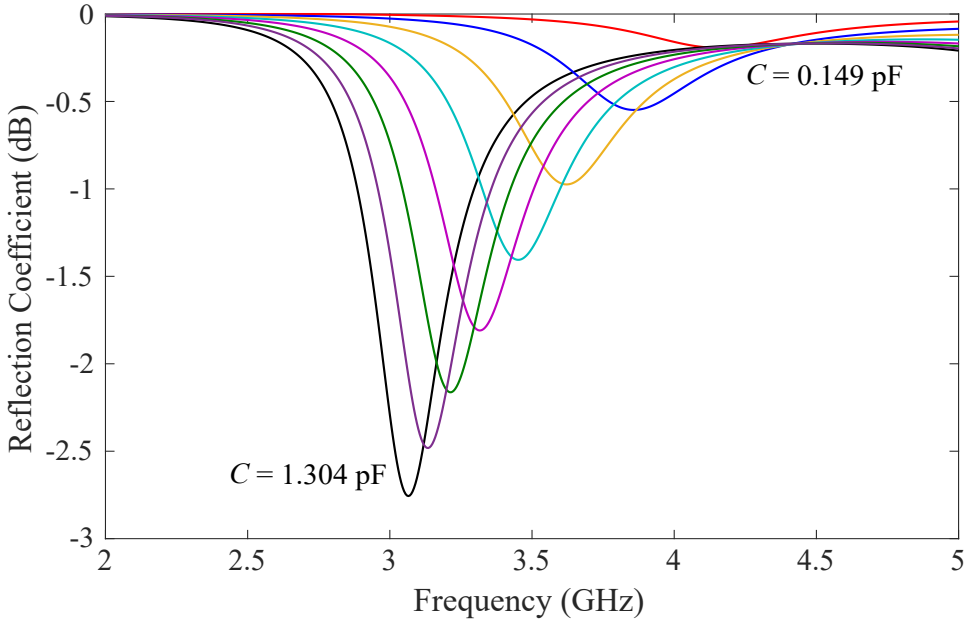

Figure 5.10. Magnitude of the reflection coefficients. Magnitude of the reflection coefficients for various values of capacitances in the range of practical values for the chosen varactor.

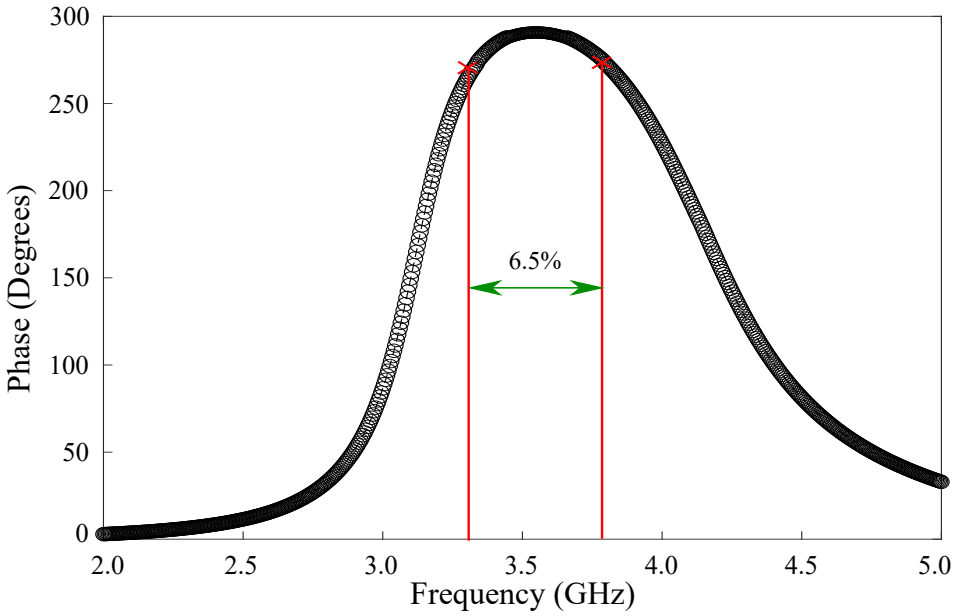

Figure 5.11. Resonance frequency as a function of the varactor capacitance values. Resonance frequency as a function of the varactor capacitance values, for different lengths of the T-shaped stubs.

the phase curve (in Fig. 5.12) is applied to define a full cycle phase change in the antenna. The instantaneous field distribution of a scattered wave at an operating frequency of 3.5 GHz is shown in Fig. 5.13. The simulated results show that the reflected plane wave is steered towards an angle of 23° when the different varactor capacitance values are adjusted in the radiating elements. This demonstrates the reflectarray's functionality in the presence of inhomogeneous mutual coupling when operating with nonuniform biasing of the varactors.

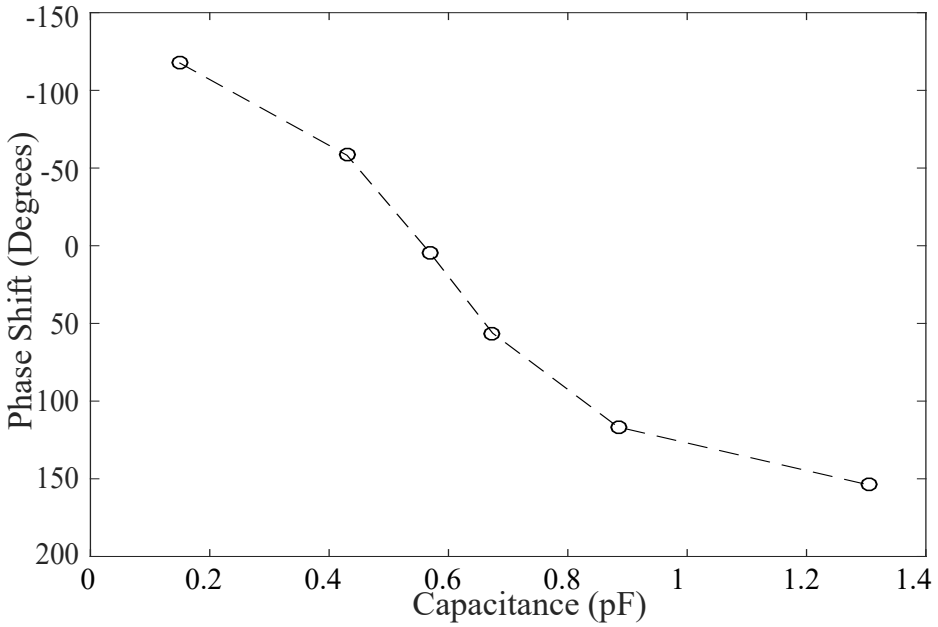

Figure 5.12. Progressive phase response. Progressive phase response at 3.5 GHz as a function of the varactor capacitances.

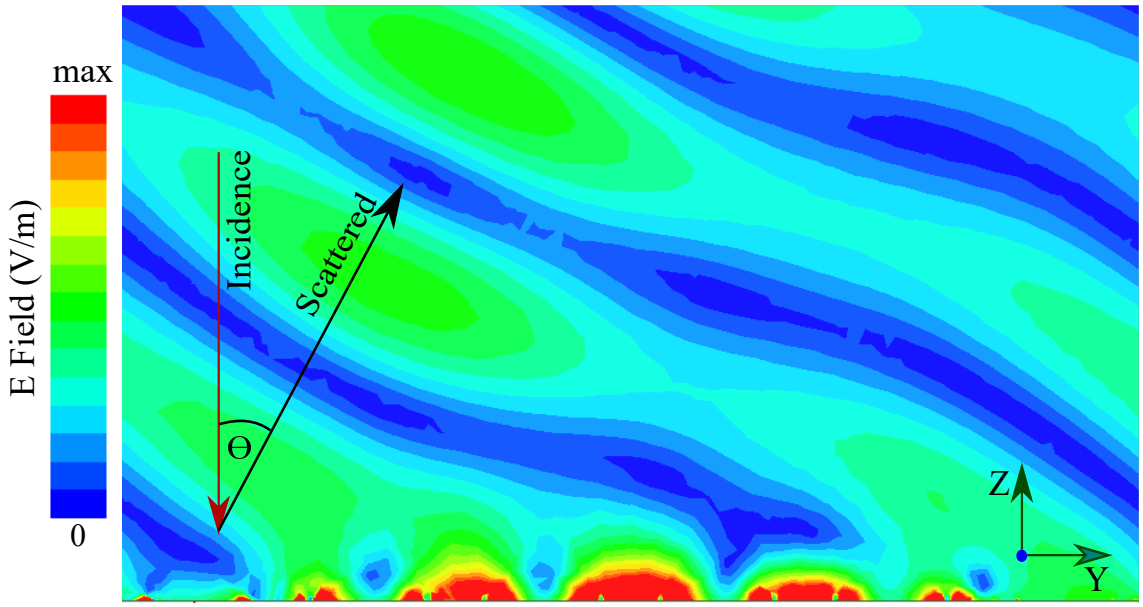

Figure 5.13. Instantaneous scattered field distribution. Instantaneous scattered field distribution for a linear sub-array with progressive phase adjusted through biasing of the varactors.

5.6 Conclusion

In this chapter, a concept of reconfigurable reflectarray unit cell based on a patch controlled by a T-shaped stub-loaded varactor configuration has been proposed. The T-shape allows to accommodate the required length of open stub as determined through an optimisation process motivated by a transmission line model of the stub. The simulation results for the actual range of variable capacitance from a practical varactor indicates a tuning range of near 300° over a range of frequencies from 3.44 GHz to 3.67 GHz (corresponding to 6.5%), with efficiency better than −1.4 dB. The numerical analysis of a linear sub-array of 6 element with progressive phase (adjusted by the varactors bias) show that the antenna can efficiently steer the reflected wave at the expected angle. Next chapter will present a practical way of realising the design with enhanced performance, in particular towards increased phase coverage over a wider frequency tuning range.

Chapter 6

A Reconfigurable Reflectarray Antenna Unit Cell

THIS chapter focuses on the application of a tunable square microstrip unit cell to the design of a wideband reconfigurable reflectarray antenna. The detailed design of this new concept of reflectarray unit cell based on varactor-loaded stubs is presented. A parametric study on the unit cell is performed, including the effect of incidence angle of the incoming wave. On that basis, the unit cell characteristics for the parametrically optimised design are demonstrated in term of phase and amplitude of its reflection coefficient. Towards practical demonstration, a linear sub-array of the reconfigurable reflectarray antenna is designed and simulated in Ansys HFFS. This linear arrangement allows to investigate the reconfigurability of the antenna system for both normal incidence and oblique incidence configurations. To verify the viability of the concept, a prototype of the proposed linear sub-array antenna is fabricated for experimental validation in parallel-plate 2D settings. The results obtained from the measurements of the reflectarray antenna illustrate a good qualitative agreement with predicted results, as demonstrated through experimental determination of the phase tuning range and measurement of the steerability of the radiation pattern in progressive phase settings.

6.1 Introduction

High gain antennas are indispensable for long-distance wireless probing and communication systems such as remote sensing, imaging, radar and space applications. Among antenna types, reflectarray antennas may appear to meet all of these applications requirements with their high gain allowing high resolution. The typical configuration of a reflectarray antenna is developed by patterning an array of printed microstrip reflecting surface elements with varying properties, allowing to control the localised phase on reflection. This structure leads to a low profile planar antenna, with small mass and low cost manufacturing. Since the antennas have the combined advantages of traditional parabolic reflectors and microstrip array technology (as mentioned in Chapter 5), the antennas are capable of achieving excellent efficiency for large aperture devices without the need of a feeding network, which is the main limitation for the efficiency of conventional phased arrays. In addition, reflectarray antennas can also obtain a total re-radiated coherent field along a desired direction with a large inclination angle from their broadside direction. Based on the operation principle described in Chapter 5, many different ideas have been proposed in the literature for synthesising the reflection phase of the reflectarray elements. The approaches can be categorised into 4 groups. There are variable size patches (Lee *et al.*, 2017; Guo *et al.*, 2019), patches with variable attached stubs (Qin *et al.*, 2016; Su *et al.*, 2019), rotated elements (Yang *et al.*, 2017; Gao *et al.*, 2018) and electronically tunable elements (Yang *et al.*, 2016; Tayebi *et al.*, 2015; Zhang *et al.*, 2016). All these techniques allow to obtain a proper phase adjustment in the reflection characteristics of the antenna, leading to accurate reflected beam shaping.

However, reflectarray antennas are facing a challenge associated with their intrinsic narrow bandwidth, which can be explained by several factors. The first factor is the limited bandwidth of the elements used to build the reflecting surface geometry. The element bandwidth usually has an inverse relationship with the relative substrate permitivity, and this problem is usually mitigated by increasing the thickness of the substrate. The second factor is the limited bandwidth caused by the differential spatial phase delay due to the frequency-dependent electrical distance between the phase center of the feed and the element position on the array. Practically, this factor is the source of a frequency-dependent phase error since the compensation phase of each element is usually determined at a fixed frequency. The effect of this phase error is larger for systems with a smaller focal length to diameter (f/D) ratio due to larger electrical path difference from the feed to the elements between the center and edge of the array.

Therefore, the effect can be reduced by increasing the f/D ratio in order to have a more uniform illumination signal on the the array.

Nowadays, reconfigurable antennas receive great attention among researchers because of their unique features. For example, some reconfigurable antennas can realise beam steering by integrating electronically tunable components (such as varactor diodes, PIN diodes or RF-MEMS switches as described in Chapter 2) into their aperture. In the rest of this section, the literature on reconfigurable reflectarray antennas based on varactor diodes as a tunable lumped element is briefly surveyed. In the context of reconfigurable reflectarrays, the switches or diodes can generally provide reconfigurability in operating frequency range, as well as a continuous phase adjustment within the reflectarray antenna elements (Nayeri *et al.*, 2015; Costanzo *et al.*, 2016). Theoretically, a continuous reflection phase tuning range covering nearly 360° is required to satisfy requirements for full phase control over the surface of the reflectarray. For example in (Costanzo *et al.*, 2015a), a novel phasing line for an aperture-coupled reconfigurable reflectarray antenna with 5×5 elements was presented. The unit cell of the antenna consisted of a multi-layer structure composed of a rectangular microstrip patch antenna face (printed on the top substrate) coupled through slots with radial stubs (printed on the bottom substrate). The reconfigurability of the unit cell was obtained by integrating a varactor at one end of the stubs. The antenna was shown to achieve a phase variation range in between 290° to 320° within 3% of frequency tuning range. The proposed geometry also proposed a biasing network circuit to drive the varactor. To improve the performance of the reconfigurable reflectarray antenna for beam-steering over a broader operating frequency tuning range, the same authors proposed a dual-layer active reflectarray configuration in (Costanzo *et al.*, 2018). The antenna achieved a 318° phase variation within a good frequency reconfigurability characteristics attaining about 14.6%. Another example was also reported in (Trampler and Gong, 2019) which demonstrated a higher range of phase reconfigurability attaining about 375° at the average reflection loss of -3.09 dB. These realisations of reconfigurable reflectarray antennas have all offered appreciable performance in terms of phase and frequency tuning range obtained by varying the varactor capacitances in the antenna elements.

In this chapter, a novel frequency- and pattern-reconfigurable reflectarray antenna is proposed to compete with the state-of-the-art reconfigurability performance. The proposed design is also demonstrated in 2D settings for experimental characterisation in realistic reflectarray operation conditions.

6.2 Antenna structure and operation principle

Figure 6.1 illustrates the proposed design of reconfigurable reflectarray unit cell. The design consists of three metallic layers developed with two substrates separated by a metallic ground plane. The substrates have different thicknesses and are bonded together. A square microstrip patch numerically tested to resonate at an operating frequency of 5.00 GHz is printed on the top substrate. Two groups of three varactors are placed symmetrically at two opposite sides of the patch to provide reconfigurability of the unit cell. In order to obtain a wide tuning range of operation, an open-circuited loading stub printed on the bottom substrate is connected to each varactor through a via. All the vias provide connection to their respective stubs through the multi-layer substrates and the ground plane. This arrangement is an improvement of the the previous unit cell design introduced in Section 5.3, where a large area of the substrate was required to accommodate the varactor-loaded T-shape stub together with the patch on the same substrate side. This previous configuration also lead to challenging biasing network connections to provide a DC bias voltage for varactor control. Therefore, in the new proposed configuration, the varactor-loaded stubs are effectively folded, which introduces a compact and an efficient reconfigurable unit cell. To drive the groups of varactors simultaneously, a reverse DC bias network consisting of large resistors, R = 1 MΩ and a choke inductor, L = 100 nH are placed at the end of each open stubs on the bottom layer of the array, i.e. below the ground plane. The resistance values are chosen large enough in order to block RF current from flowing into the bias circuit. In this configuration, the effect of the biasing circuit on the radiation characteristics is minimal.

Practically, the geometrical of the unit cell starts with the primary parameters of the square patch $L_p = W_p$ = 16.3 mm determined based on microstrip antenna standard design procedure described in Chapter 2 (Section 2.1.1). Two different thicknesses, h_1 = 3.175 mm and h_2 = 0.787 mm of Roger Duroid 5888 substrates with a relative permittivity ε_r = 2.22, are chosen to create the multi-layer structure. The thickness h_1 is used to create the top patch and is therefore slightly thicker in order to increase the bandwidth of the unit cell. In contrast, it is advantageous to use a lower thickness for the bottom substrate, as it accommodates the stubs which are non-radiating structures. Varactors with model number MA46H120 from MACOM Technical Solutions (MACOM, 2015) are considered as electronically tunable components. According to their data sheet, the varactors provide a tunable variable junction capacitance in the range of 0.149 pF to 1.304 pF for a reverse bias voltage varying from 18 V to 0 V. A via with diameter of

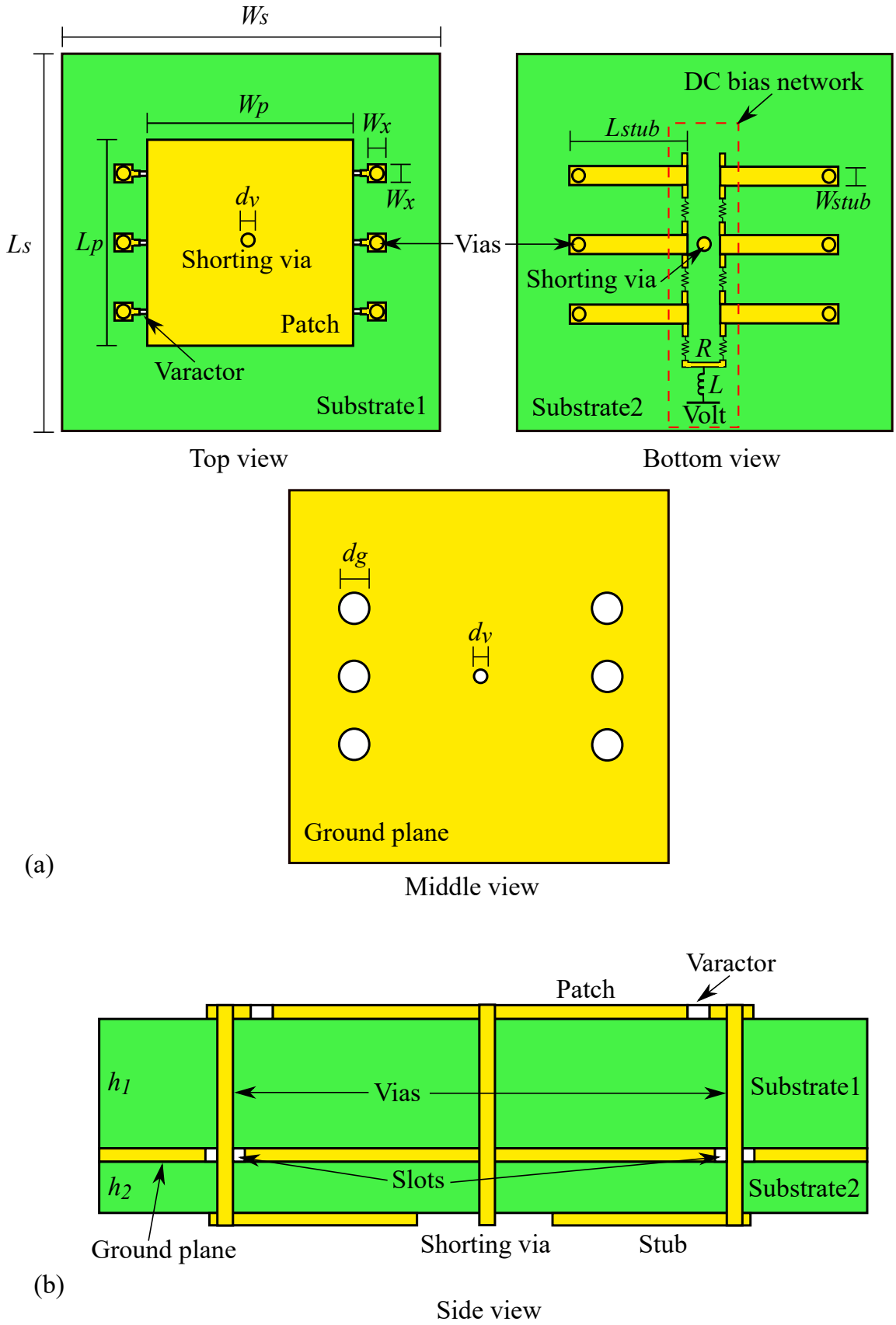

Figure 6.1. Unit cell configuration. Reconfigurable reflectarray unit cell configuration. (a) Geometry of the multi-layer structure and (b) side view of the unit cell.

d_v = 1 mm is used as the intermediate vertical connection between every varactor and its loading stub in this design. A small metallic soldering patch with dimensions $W_x \times W_x$ is printed on the top and the bottom of every via to provide additional contact as well as to facilitate substrate perforation process. In order to have the vias going through the ground plane without shorting them, circular slots with diameter of d_g = 2 mm are cut on the ground plane to create clearance around the vias. A shorting via is also added in the center of the patch to set the patch itself at the DC ground of the unit cell. Similarly as described in Chapter 5 for patch antennas, the stubs loaded with the varactors offer additional impedance manipulation which allow to maximise the tuning range achieved when varying the capacitance of the varactors. In the present case, the optimisation of the stubs lengths aims at achieving the best performance of the unit cell in terms of tunable operating frequency range, as well as in terms of reflection phase range, while maintaining the efficiency of the device as high as possible. In this study, a stub length L_{stub} = 8 mm and the stub width W_{stub} = 1.5 mm are selected based on a parametric optimisation.

6.3 Infinite periodic structure analysis

To realise a dynamic radiation pattern, the reflection phase of the reconfigurable reflectarray unit cells needs to be tuned with an appropriate distribution corresponding to the intended beam-steering direction. This section describes a study of the proposed unit cell behaviour in an infinite periodic environment. The study is performed using Ansys HFFS applied in unit cell periodic settings under both normal and an oblique incident plane waves.

6.3.1 Normal incidence

In this sub-section, the actual geometry of the unit cell together with its bias network circuitry is analysed using full-wave simulations. The simulation setup (shown in Fig. 6.2) includes periodic boundary conditions around the unit cell supported by a Floquet harmonics approach. A first Floquet port is required in order to define a plane wave incident from the top surface of the unit cell and measure the wave reflection on that surface. Since the ground plane is not continuous, a second Floquet port is needed to check that the transmission through the structure is negligible, with this second port located on the bottom surface. The periodic boundary conditions of the unit cell are

implemented through the phase-shift walls of master and slave couples (Incorporation, 2016). The behaviour of the reconfigurable reflectarray unit cell is firstly investigated by applying a normal incident plane wave on it. As the varactors include an internal series resistance, this parameter is taken into account in the examination since it affects the reflection loss of the unit cell. Figure 6.3 shows the reflection coefficient of the unit cell obtained when varying the value of the series resistance of the varactors. It can be observed, as can be expected, that the amplitude of the total reflection loss increases when the varactor resistance increases. These losses can be reduced by selecting a varactor with a lower value of the series resistance. In this particular case, the proposed varactors for the reconfigurable reflectarray unit cell has an estimated series resistance of $R = 2\ \Omega$ (Nguyen-Trong *et al.*, 2015d).

The scattering characteristics responses of the unit cell with parameters summarised in Tab. 6.1 are presented in the following. All results are deembedded to the top surface of the reflectarray. Figures 6.4 and 6.5 illustrate both the phase and the amplitude of reflection coefficient at frequencies in the intended operating range. In these figures, the reflection phase and the amplitude are examined for reverse bias voltages from 18 V to 0 V and the results show that this variation of the bias voltage introduces a 44% resonance frequency tuning range at an amplitude better than -4 dB. In addition, as shown in Fig. 6.6, a tuning phase shift between 300° to 320° (i.e. nearly one cycle) is achievable between 2.60 GHz to 3.34 GHz (which corresponds to a 25% tunable range) with magnitude response better than -3 dB (Fig. 6.5).

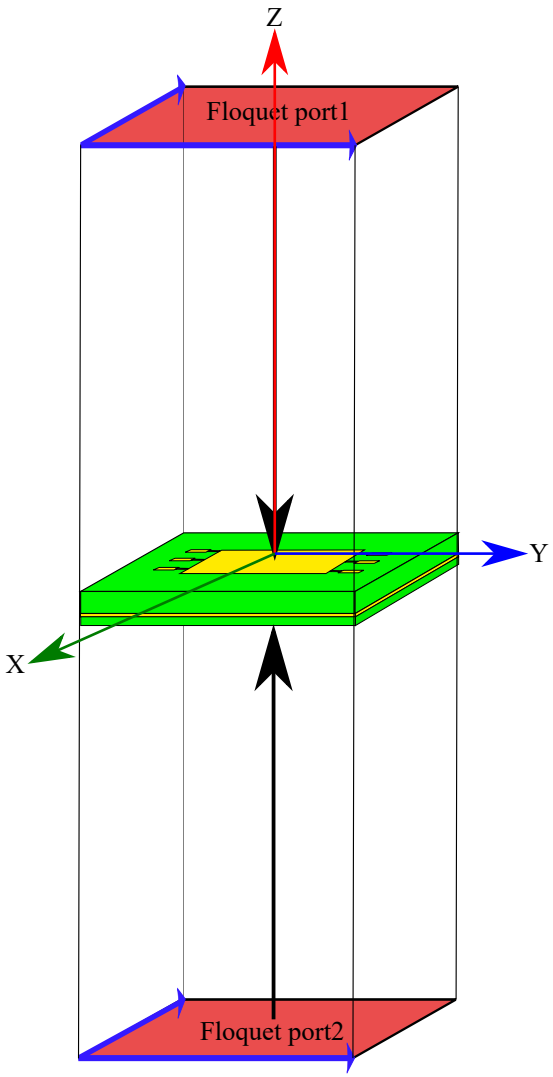

Figure 6.2. The periodic boundary simulation. The periodic boundary simulation in Ansys HFFS allows to compute the reflection characteristics of the proposed reconfigurable reflectarray unit cell in an infinite periodic array.

Length and width of patch (L_p and W_p)	16.3 mm
Length and width of unit cell (L_s and W_s)	30 mm
Thickness of top substrate (h_1)	3.175 mm
Thickness of bottom substrate (h_2)	0.787 mm
Diameter of via (d_v)	1 mm
Diameter of slot (d_g)	2 mm
Length of stub (L_{stub})	8 mm
Width of stub (W_{stub})	1.5 mm

Table 6.1. Unit cell design parameters

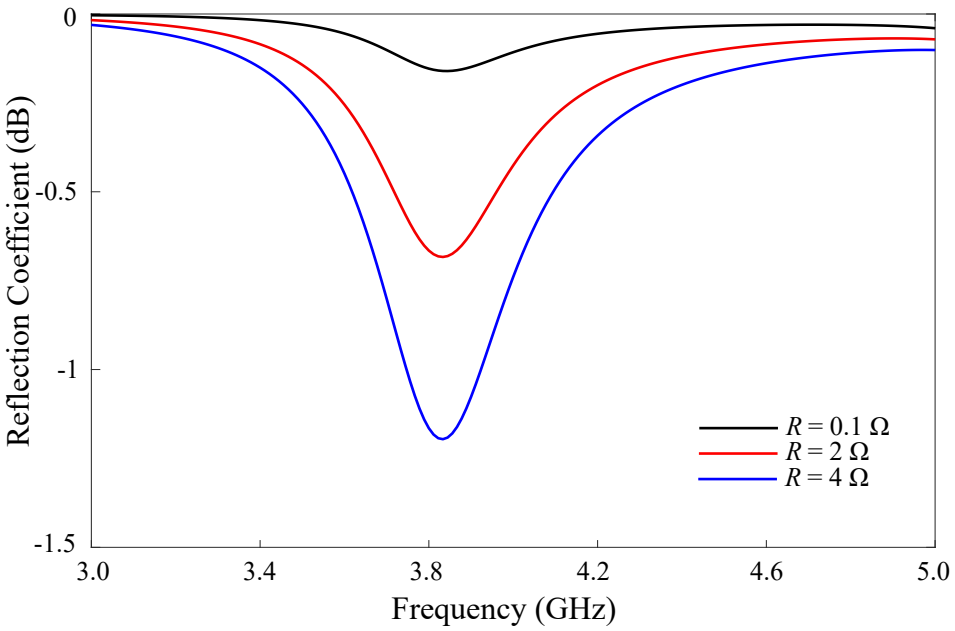

Figure 6.3. Diode losses. Amplitude of reflection coefficient computed for different values of the varactor series resistance.

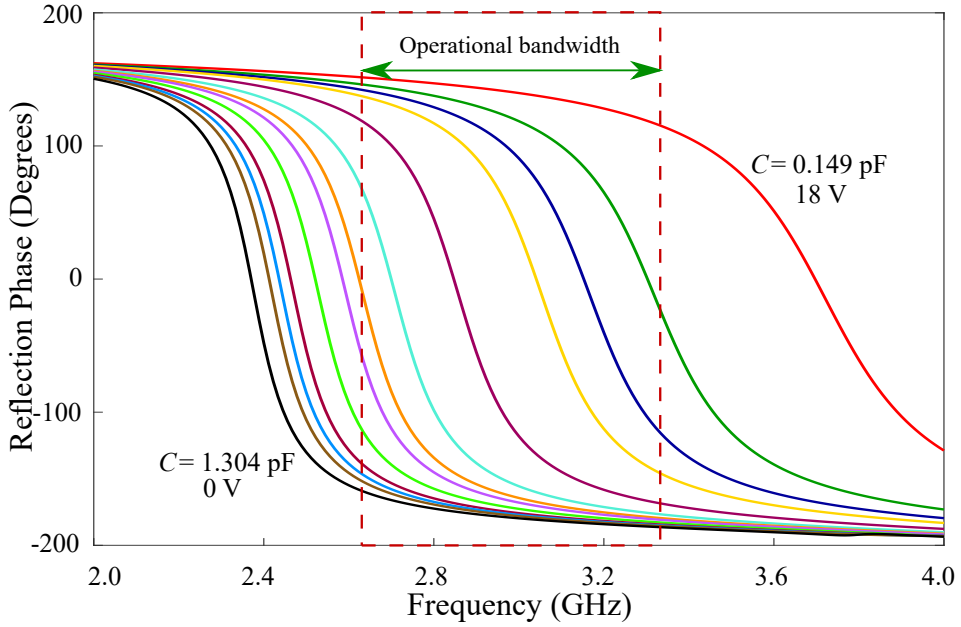

Figure 6.4. Phase of the reflection coefficients for normal incidence case. Phase of the deembedded reflection coefficients for various values of capacitances in the range of practical values for the chosen varactor.

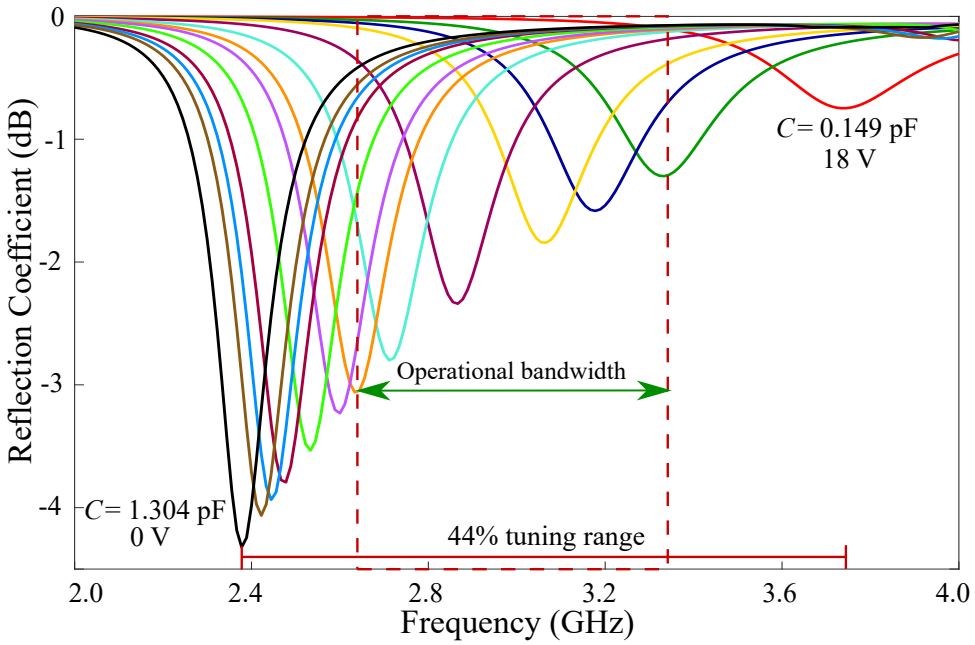

Figure 6.5. Magnitude of the reflection coefficients for normal incidence case. Magnitude of the reflection coefficients for various values of capacitances in the range of practical values for the chosen varactor.

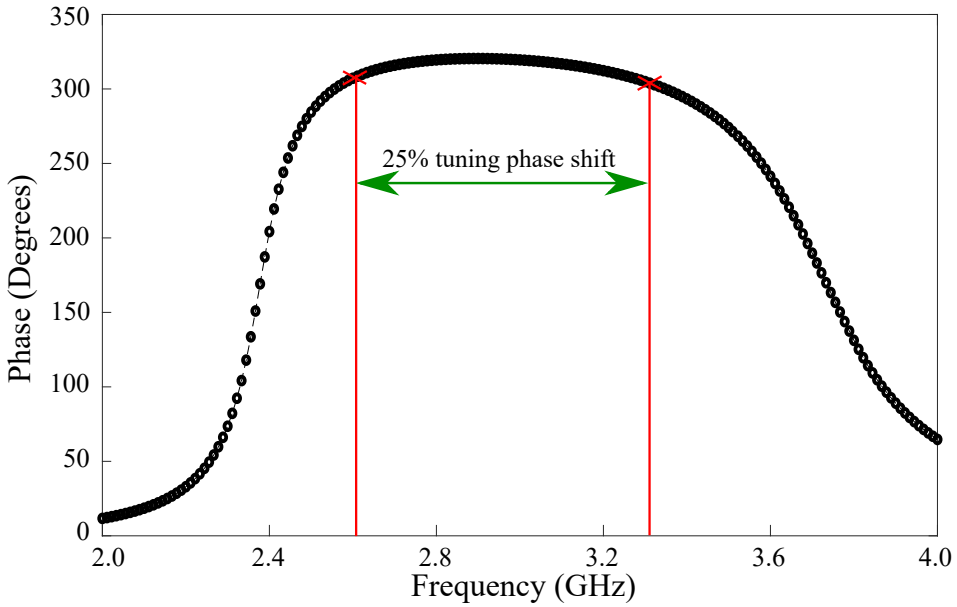

Figure 6.6. Reflection phase difference for normal incidence case. Maximum reflection phase difference of the unit cell.

6.3.2 Oblique incidence

As the angle of the incident wave plays an important role in determining the aperture efficiency for a reflectarray system, the performance of the unit cell at oblique incidence needs to be investigated and compared to normal incidence. To this end, the response of the unit cell to a wave with an incident angle of 30° is investigated here. This particular incidence angle is chosen as it corresponds to a typical configuration of reflectarray feeding, and is similar to the reconfigurable reflectarray antenna prototype configuration that will be developed for experimental validation, as explained in detail in Section 6.5. Figures 6.7 and 6.8 illustrate the phase and the amplitude of the reflection coefficient of the unit cell at an angle of incidence of 30°, obtained varying the varactor variable junction capacitance. From the Fig. 6.8, it can be seen that the minimum amplitude of the reflected wave is slightly decreased to −5 dB while the frequency tuning range still remains unchanged at 44%, namely from 2.37 GHz to 3.70 GHz. Furthermore, a tuning phase shift of more than 300° (in Fig. 6.9) is achieved over a operational relative bandwidth of 21% (from 2.74 GHz to 3.37 GHz) with a magnitude response of more than −3 dB as illustrated in Figs. 6.7 and 6.8. According to this analysis at an oblique incidence of 30°, the total phase range remains nearly unchanged compared to the normal incident plane case.

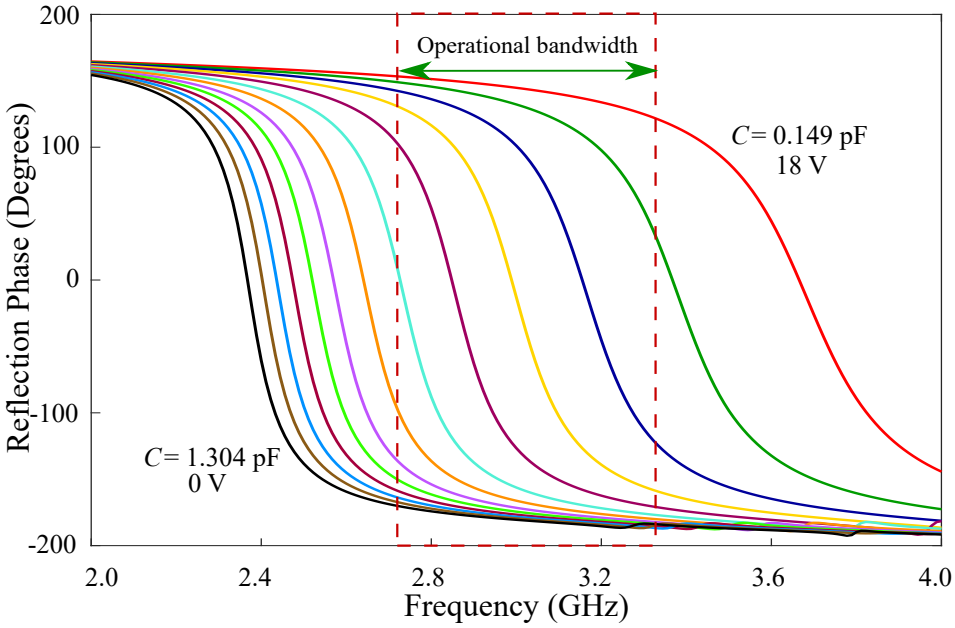

Figure 6.7. Phase of the reflection coefficients for oblique incidence case. Phase of the deembedded reflection coefficients for various values of capacitances in the range of practical values for the chosen varactor.

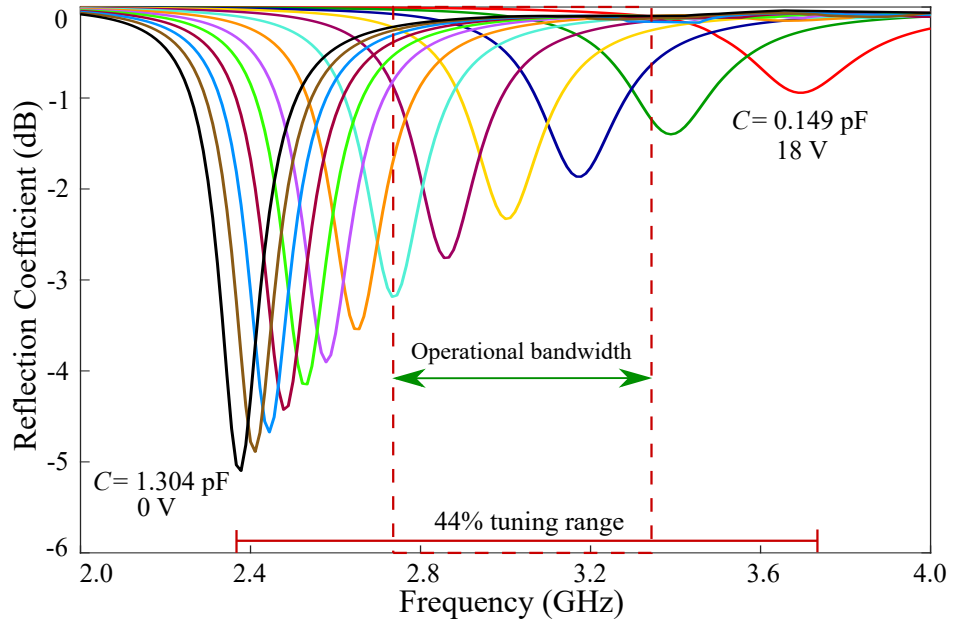

Figure 6.8. Magnitude of the reflection coefficients for oblique incidence case. Magnitude of the reflection coefficients for various values of capacitances in the range of practical values for the chosen varactor.

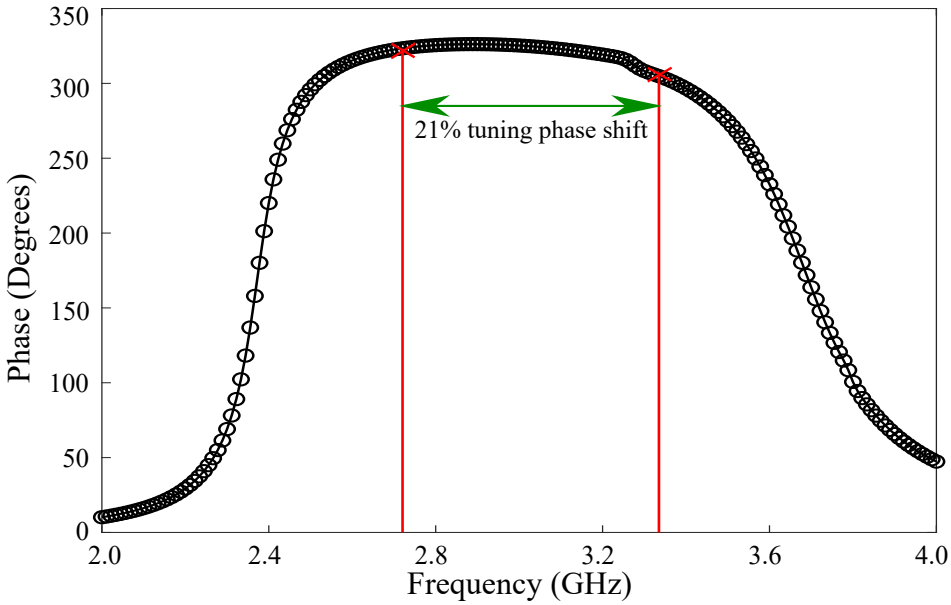

Figure 6.9. Reflection phase difference for oblique incidence case. Maximum reflection phase difference of the unit cell.

6.4 Periodic analysis of a linear sub-array

To validate the relationship between the reflection phase and the varactor bias-controlled junction capacitance in practical settings, a periodically repeated linear sub-array consisting of 1×12 reconfigurable reflectarray cells is considered for testing. The sub-array arrangement allows to have the biasing status of the neighboring elements varying in one direction, and it is simulated in the Finite Array Environment (FAE) of Ansys HFSS. A normally incident plane wave (corresponding to theta = 0°) illuminates the surface of the antenna array. In order to cover a full cycle of phase (i.e. 360°) with the 12 elements in a sub-array, the progressive phase change between the radiating elements is fixed at 30°. The selected 12 points corresponding to the 30° progressive phase for the proposed reconfigurable sub-array are shown on the unit cell phase curve in Fig. 6.10. As the results of this progressive phase, Fig. 6.11 illustrates three cases of instantaneous field distribution of a wave scattered by the array at the center operating frequency of 3.00 GHz. Three different main directions of the antenna scattered field distributions are demonstrated, including broadside and scanning angles for progressive phase of $\pm30°$. For broadside operation, the scattered plane wave is simply reflected towards an angle of 0° when the varactor capacitance values of all array elements are the same (corresponding to uniform phase distribution). By adjusting the varactor capacitance

based on the phase response characteristics to achieve a positive or negative 30° progressive phase, the reflectarray can steer the reflected beam between right and left directions towards an angle of ±23°. This non-uniform progressive phase distribution corresponds to the phases decreasing from 138° to −179° in 30° increments, as shown in Fig. 6.10. The radiation patterns of the array for the three cases are shown in Fig. 6.12. We note that the broadside main lobe beam has a maximum amplitude slightly lower than the scanned beams, due to the fact that all radiating elements are choosen on resonance, thereby giving the worst-case loss of power in the antenna. In contrast, the maximum steering beam provide higher main lobe levels as the power loss in the antenna is minimal.

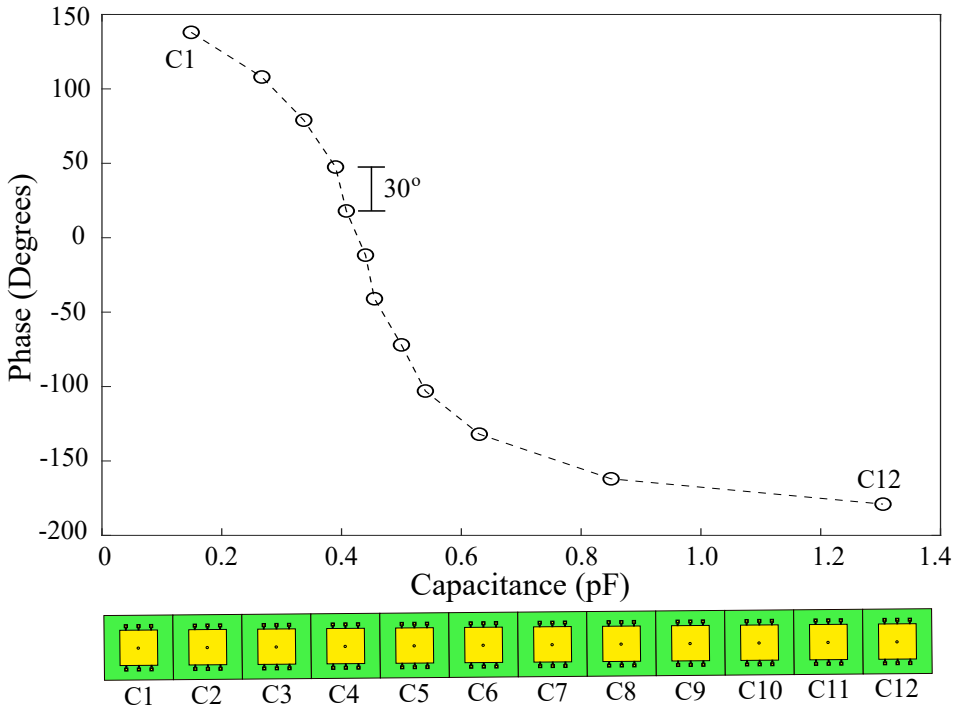

Figure 6.10. Progressive phase response. Progressive phase response at 3.00 GHz as a function of the varactor capacitances in the 1×12 periodically repeated sub-array..

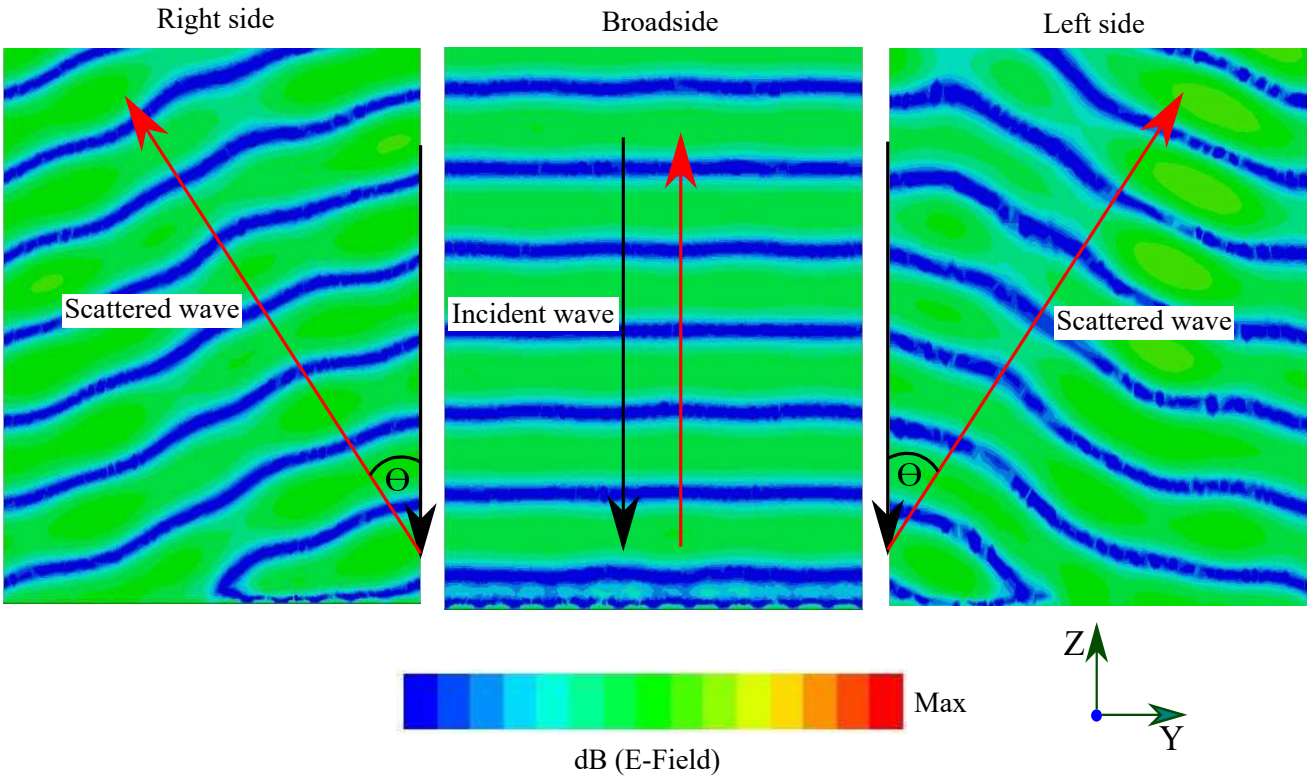

Figure 6.11. Instantaneous scattered field distribution. Instantaneous scattered field distribution for a linear sub-array of 12 element with progressive phase adjusted through biasing of the varactors.

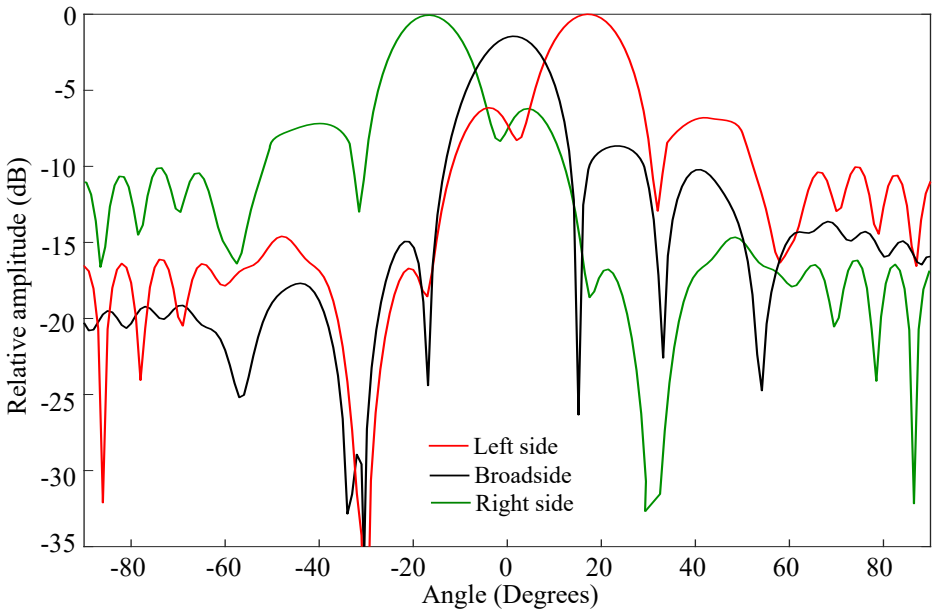

Figure 6.12. Reconfigurable radiation pattern. Reconfigurable radiation pattern for a linear sub-array with progressive phase adjusted through biasing of the varactors.

6.5 Design and simulation of offset-fed reconfigurable reflectarray antenna configuration

In this section, the characteristics of the reconfigurable reflectarray antenna in offset-fed configuration is analysed. Technically, the field incident at each element of a reflectarray antenna is determined by the position and radiation pattern of its feed antenna. To define an appropriate reflectarray feed configuration, the position of the feed needs to be carefully considered in order to optimise the performance and prevent undesirable effects such as significant spillover loss and high side lobe levels, as well as reduction in the antenna gain due to shadowing from the feed physical volume. A common solution to mitigate this shadowing problem is to offset the position of the feed, so that it is not in the way of the main radiation direction. In practice, it would be desirable to demonstrate the far-field radiation pattern of a reflectarray antenna in three-dimensional (3D) measurement such as performed in (Chen *et al.*, 2015; Almajali and McNamara, 2016; Samaiyar *et al.*, 2019). However, practical considerations make such a full 3D validation challenging in a university environment. Firstly, the field distance (based on far-field standard calculation (Balanis, 2015)) becomes very large for a reflectarray of sufficiently large aperture, and therefore, the 3D measurement becomes not feasible in the university anechoic chamber. Secondly, the fabrication of a multi-layer reconfigurable reflectarray of large size is very expensive since it needs to be outsourced to external specialised external manufacturers. Therefore, for a proof-of-concept, a solution based on a two-dimensional (2D) measurement in a parallel plate configuration combined with a near-field to far-field transformation is applied here. The detailed design and analysis of the proposed offset-fed reconfigurable reflectarray antenna in 2D settings is demonstrated in the following.

6.5.1 Analysis of offset-fed configuration for the 2D reflectarray antenna

Prior to the actual design, there are several important characteristics of the reflectarray antenna that have to be well understood, including phase element tuning range, bandwidth, ratio of feed focal length to reflectarray antenna diameter (f/D), feed radiation pattern, position and orientation. As the geometrical characteristics of the reflectarray antenna have been given previously, the design parameters of the f/D ratio and the minimum side lobe level (which causes unwanted radiation in undesired directions)

of the reflectarray antenna need careful consideration in order to achieve an optimum aperture efficiency. One of the important aspects in the configuration is to use a high directivity feed illuminating the reflectarray surface with acceptable amplitude tapering, aperture phase and side lobe level. A selected horn antenna should be placed at a reasonable distance from the reflectarray antenna to maximise the obtained aperture efficiency.

Figure 6.13 shows the overall schematic of the reconfigurable reflectarray antenna in offset-fed configuration. The system is a two-dimensional (2D) parallel plate arrangement which provides a convenient framework for experimental validation. Two parallel half-circle metal plates define a 2D transverse electric setup. In order to eliminate any interference effects, an absorber with a thickness of 30 mm is used to bound the measurement domain. The discussed linear 1×12 sub-array of the designed reflectarray antenna is illuminated by a 2D horn antenna (elaborated in Section 6.5.2) placed at a distance determined from an appropriate f/D ratio of 1, which is typical for reflectarrays. An offset angle of 30° is selected so that the feed does not block the reflected beam, and the feed is placed so that it points to the geometrical center of the reflectarray aperture. Typically, the optimum position of the feed and the angular offset angle are chosen based on the illumination taper from the feed that balances the conflicting characteristics of minimum spillover loss and maximum aperture efficiency. In this context, to minimise spillover of power, the edges of the reflectarray antenna will receive less energy from the feed compared to the reflectarray center (Nayeri *et al.*, 2018). Therefore, a feed irradiation pattern with strong amplitude taper will illuminate the reflectarray aperture. A large offset angle of the feed will cause the reflectarray elements to be excited at very oblique angles, which will degrade the performance of the reflectarray. Therefore, it would be desirable to keep the offset angle to a minimum. However, the feed position needs to be defined as a trade-off with the feed blockage, since when the offset angle becomes small, the reflected beam of the reflectarray is blocked due to the feed absorption, which weakens the reflected power.

Finally, a Digital-to-Analog DC converter (DAC) with an advanced multi-channel output is connected to the DC-bias network of the linear 1×12 reflectarray to drive the bias of the antenna varactors, allowing independent control of the bias voltage for each reflectarray element. The converter is placed outside of the metal plates to avoid disturbance of the experimental system. By varying the individual bias voltages on the antenna elements, the characteristic of the antenna radiation pattern can be modified.

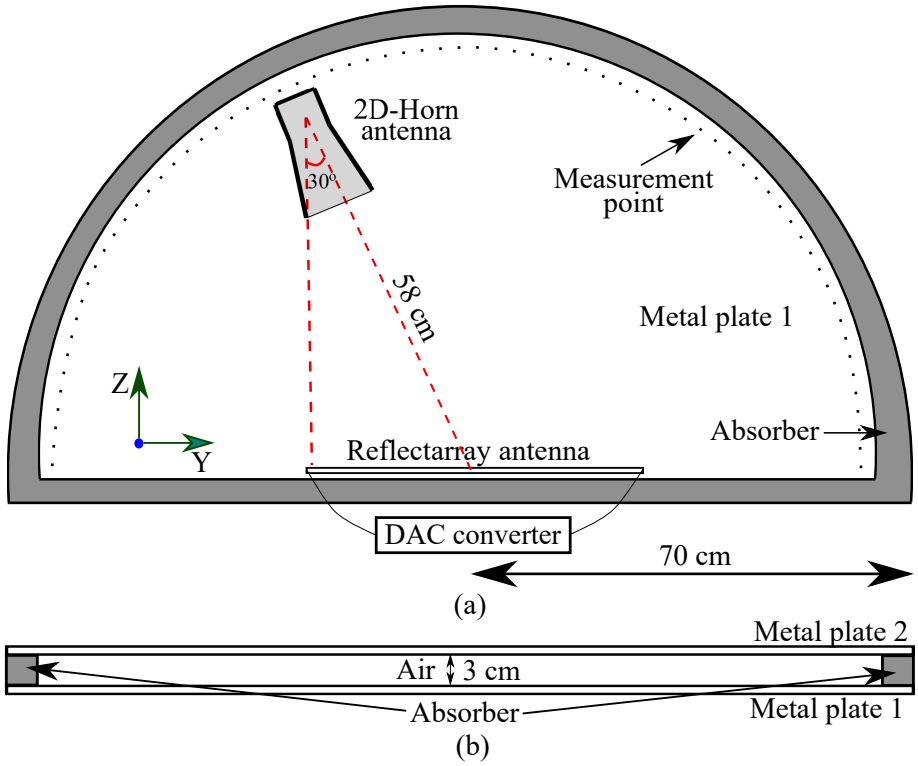

Figure 6.13. Reflectarray antenna measurement system architecture. Entire experimental setup of the designed reconfigurable reflectarray antenna for 2D experimental validation. (a) Top view and (b) side view.

6.5.2 Feed model

A key factor in the reflectarray design procedure is to predict and maximise the reflectarray directivity and also to obtain a reasonable aperture efficiency. An optimised performance can be attained by appropriate feed placement and design of the feed radiation pattern. More specifically, the feed defines the performance of the reflectarray since the aperture efficiency depends on the spillover loss and the field tapering values. Therefore, the antenna's feed need to be carefully designed in order to improve the reflectarray system performance.

A horn antenna is commonly used as a feeding device in most reflectarray configurations. In the 2D settings, the horn becomes a H-plane sectoral horn and consists in a flat tapered metal waveguide that shapes a wave in a beam directed towards the reflectarray. The advantages of horn antennas are low voltage standing wave ratio, wide bandwidth, simple construction and simple adjustment. The role of the horn antenna is to improve the impedance matching between the feeding waveguide and free space. In this study,

a rectangular two-dimensional horn antenna is designed. The design procedure is straightforward based on the basic parameters that determine the performance of the antenna. The length, the flare angle and the dimensions of the horn are optimised. The optimisation of these parameters will provide the desired characteristics such as impedance matching over a frequency bandwidth covering the desired tuning range and directive radiation pattern as required for efficient operation of the reconfigurable reflectarray system.

Figure 6.14 shows the structure of the proposed rectangular two-dimensional horn antenna. The antenna is divided into two parts where the initial segment is a straight waveguide part and the second part is the tapered horn body. The initial waveguide part provides a transition from a coaxial feed to maximise the energy flows through the horn part. A plexiglass dielectric disk with relative permitivity of 3.4 is required around the feeding coaxial probe to widen the impedance bandwidth and thus meet the requirement of the reconfigurable reflectarray antenna frequency tuning range. The horn antenna dimensions are given in Fig. 6.14. As the result, the reflection coefficient of the horn antenna shown in Fig. 6.15 covers a bandwidth that broadly includes the tuning frequency range of the reflectarray antenna from 2.70 GHz to 3.47 GHz. A good agreement between simulated and measured results can be observed. However, the measured results of the reflection coefficient in the frequency range from 3.40 GHz to 3.47 GHz does not strictly meet the criteria of the impedance bandwidth, with a reflection coefficient breaching the limit of -10 dB at some frequencies due to the fabrication error. The breach frequencies are however at the margins of the reflectarray antenna tuning range, so that they can be neglected.

6.6 Validation of the reconfigurable reflectarray: numerical and experimental results

To verify the reconfigurability of the proposed reflectarray, a prototype of the linear subarray has been fabricated, as shown in Fig. 6.16. The parallel plate experimental system (described in previous section) for measuring the reconfigurable linear reflectarray antenna allows to compute the antenna radiation pattern in 2D settings. According to the antenna operation principle, the reconfigurability of the antenna system can be demonstrated by varying the varactor biasing voltages to create a specific pattern of element excitation phases. This, in turn will result in radiation patterns of the

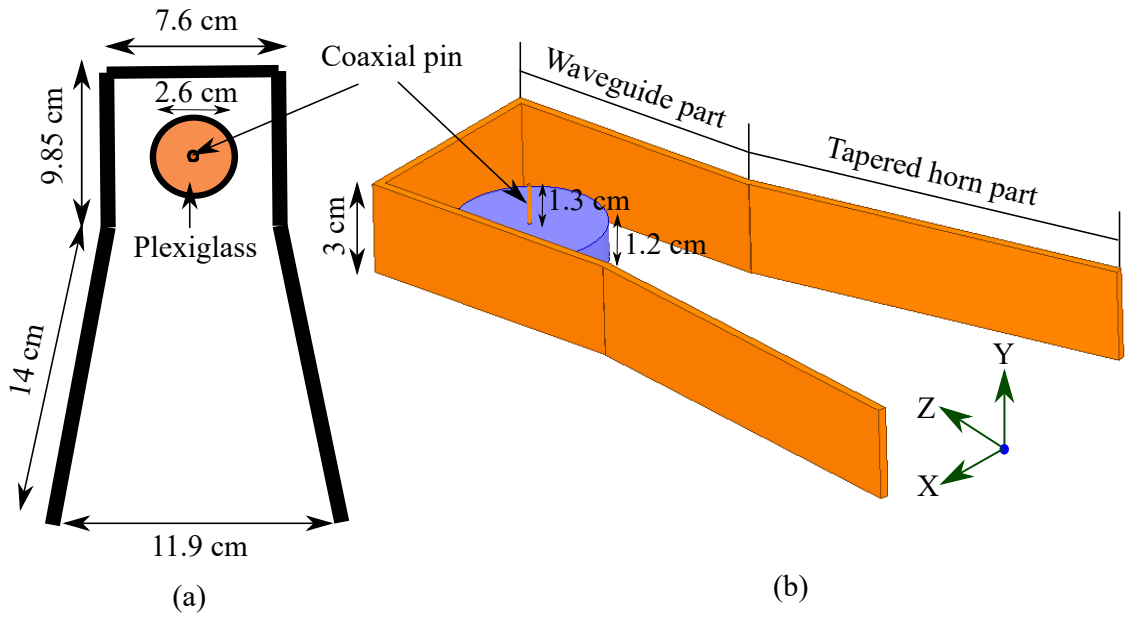

Figure 6.14. H-plane sectoral horn antenna structure. The dimensions of the rectangular two-dimensional horn antenna. (a) Top view and (b) side view.

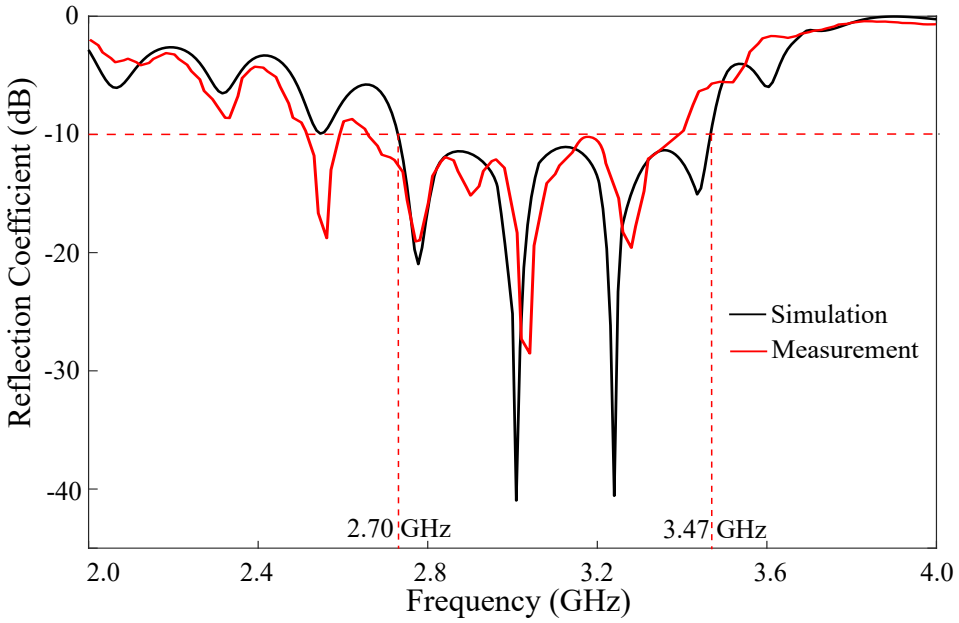

Figure 6.15. The horn antenna reflection coefficient. Measured and simulated reflection coefficient of the 2D sectoral horn antenna.

reflectarray antenna that can be measured in the 2D experiment. Figure 6.17 shows a photograph of the complete experimental testing of the reflectarray antenna as given in Fig. 6.13.

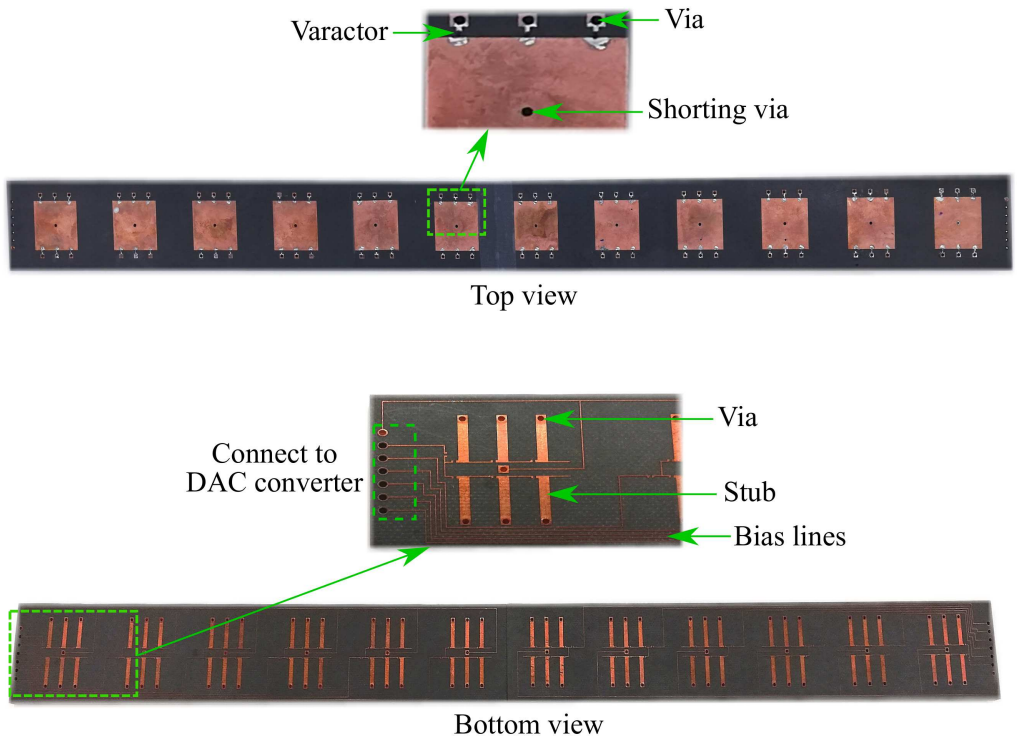

Figure 6.16. Prototype of the reflectarray antenna. Photograph of 1×12 reconfigurable reflectarray antenna, including top and bottom views with zooms providing views on details.

6.6.1 Measurement with uniform phase

In order to test the operation of the reflectarray unit cell, the 12-element linear array is first measured with uniform phase. A computer is used to set-up DAC multi-channel output voltages that are properly connected to the DC-bias network of the linear reflectarray, thus providing a defined bias signal to the varactors. Since the converter has a high internal resistance, the DAC output voltages are very sensitive to the tuning of each radiating element. This aspect can introduce a relative high phase error into the radiating elements which may affect the quality of the radiation pattern. To address

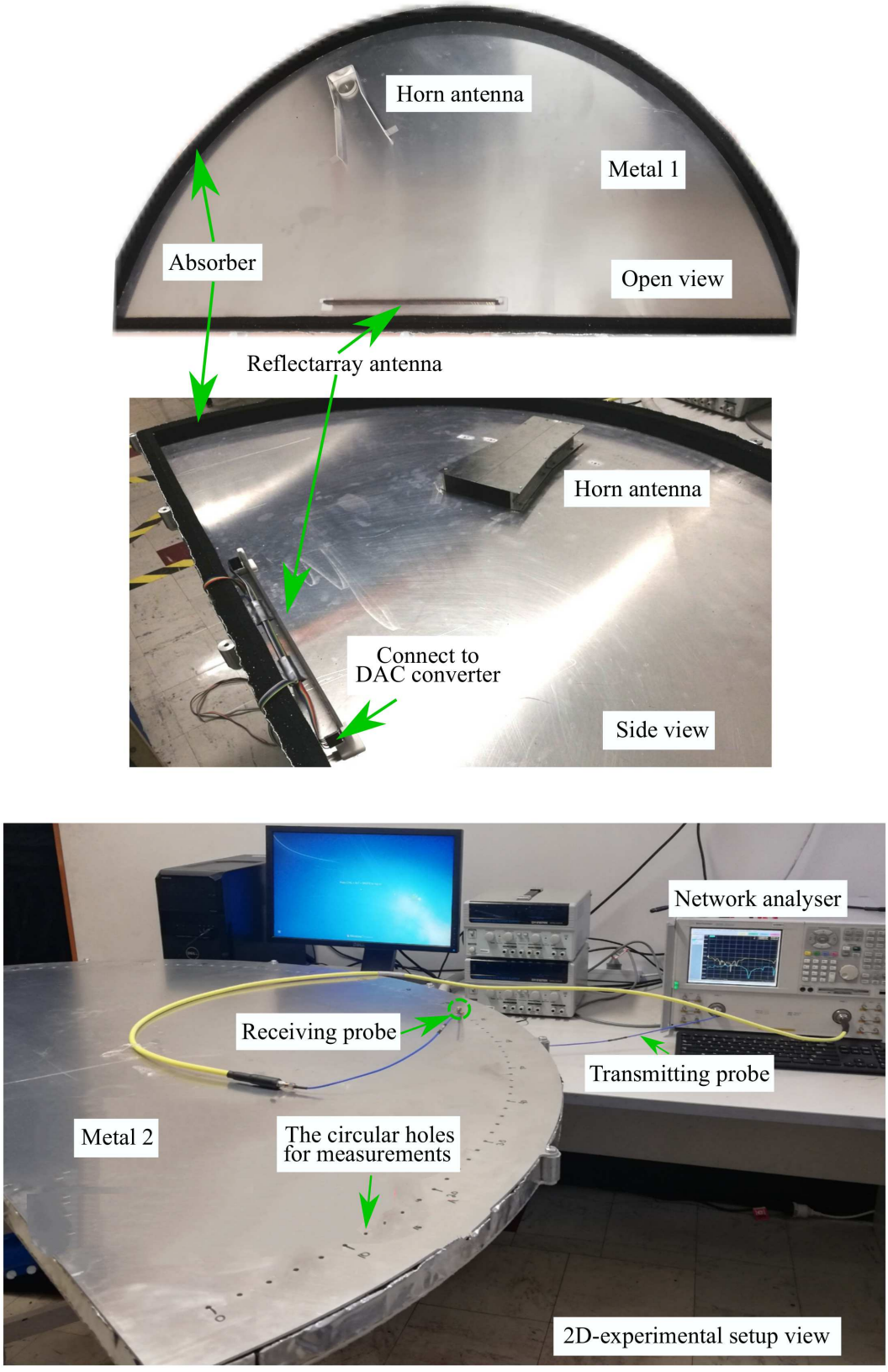

Figure 6.17. Experimental setup. Photograph of the 2D experimental setup illustrating the measurement procedure, where a coaxial probe is moved on a circular pattern around the reflectarray.

the problem, every DAC output voltages used will be carefully tested to insure that the correct voltages is applied to the reflectarray elements. As visible in Fig. 6.17, the measurement system include the transmitting and the receiving probes which are both connected to a network analyser. The transmitting probe is used to feed the horn antenna. Meanwhile, the receiving probe is used to detect the amplitude and phase of the electric field components radiated by the reflectarray antenna over a preselected circular line at every 2° angle through small holes perforated in the half-circle metal plate. In this context, the scattered field components are recorded in the near-field to synthesise the array factor for an uniform circular array (Ioannides and Balanis, 2005). The analytical far-field radiation pattern of the reflectarray can then be expressed by using far-field transformation (computational Fast Fourier Transform (FFT)). The standard procedure to determine the far-field from the near-field measurement is elaborated in Chapter 17 of (Balanis, 2015).

Figures 6.18 and 6.19 show the simulated and measured reflection phase (in offset-fed configuration) for different values of uniform varactors voltages over the tuning frequency band. The shaded region in the figures determines the operational bandwidth of the reflectarray antenna. This frequency range is defined as the range where it is possible to tune the phase range over more than 300°. Due to the fabrication imperfection of the antenna prototype, the measured curves (in Fig. 6.19) are shifted to a highest frequency band by about 9%. In addition, the phase characteristics within the lowest frequency band are observed slightly reduced by 60°. In this case, the reason of this phase reduction is still being investigated but a preliminary conclusion is that this may be caused by the fabrication imperfections as well.

Figure 6.20 illustrates the reflection phase obtained by varying the biasing voltages at three different operation frequencies along the antenna tuning frequency band. The curves are demonstrated based on the maximum phase tuning range obtained from the measured reflection phase results (shaded region) in Fig. 6.19. Due to the shifted frequency in the measurement, the simulated results for the phase tuning range of these frequencies are shifted to lower frequencies, which is especially visible at 3.30 GHz and 3.38 GHz. Based on observation of Fig. 6.19, a phase tuning range of more than 300° can be achieved within an operating frequency range from 2.82 GHz to 3.38 GHz, corresponding to 18% tuning range. The highest phase range of 320° is achieved at a frequency of 3.30 GHz as illustrated in Fig. 6.21. At this stage, the reconfigurable beam

steering of the reflectarray can be achieved along the tuning band.

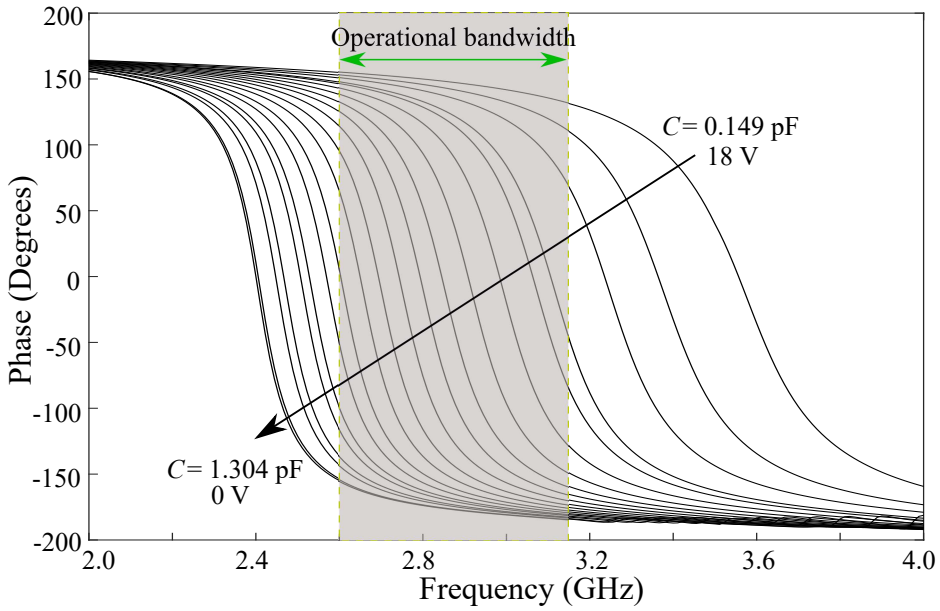

Figure 6.18. Simulated reflection phase along the tuning frequency band. Simulated result of the reflection phase (in offset-fed configuration) along the antenna tuning frequency band for different values of capacitance when all cells of the reflectarray are under the same bias voltage.

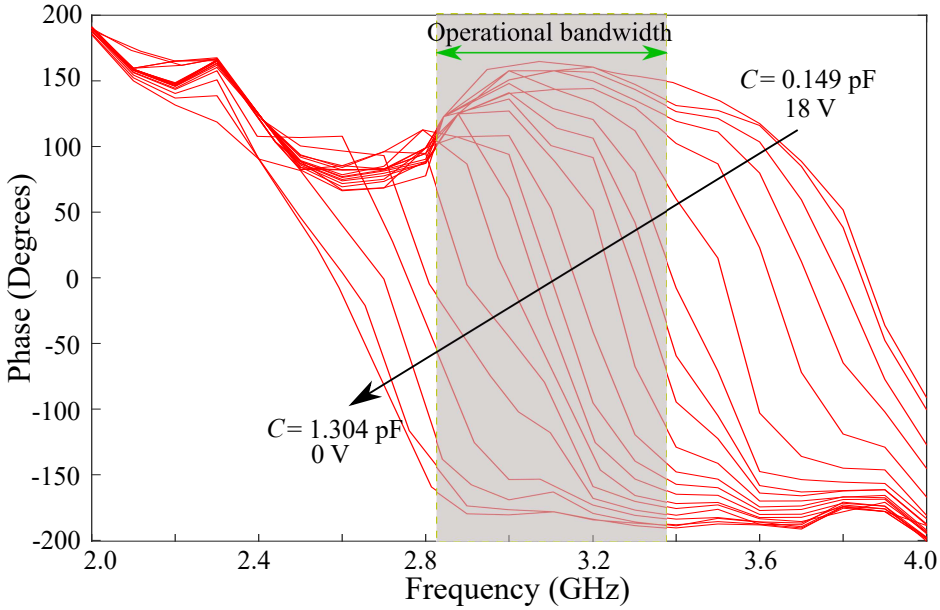

Figure 6.19. Measured reflection phase along the tuning frequency band. Measured result of the reflection phase (in offset-fed configuration) along the antenna tuning frequency band for different values of capacitance when all cells of the reflectarray are under the same bias voltage.

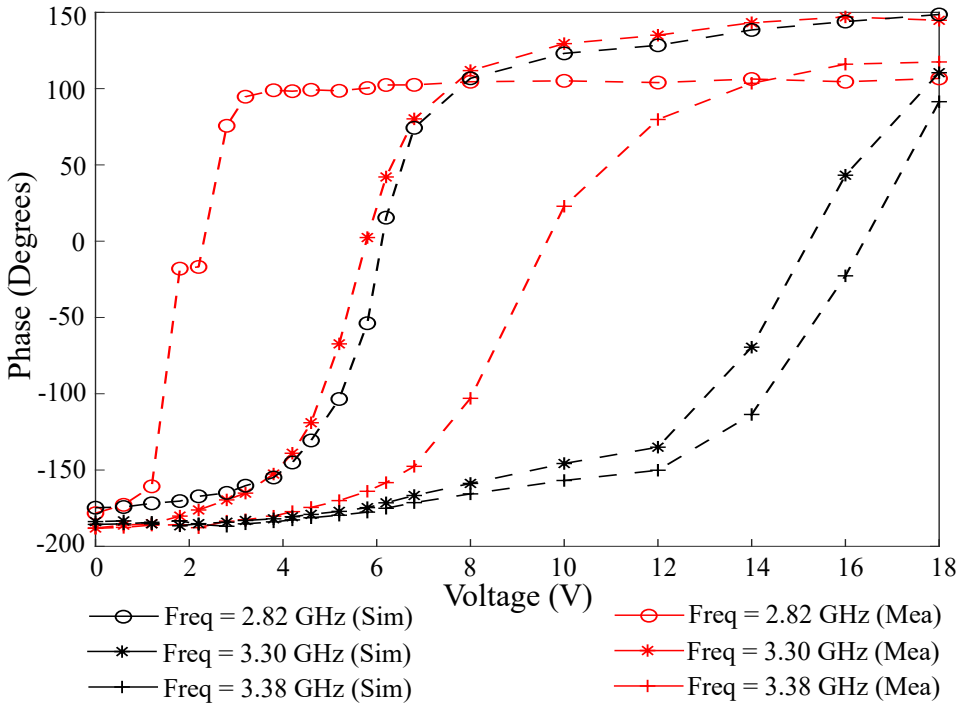

Figure 6.20. Reflection phase through biasing of the varactors. Simulated and measured result of the reflection phase adjusted through biasing of the varactors.

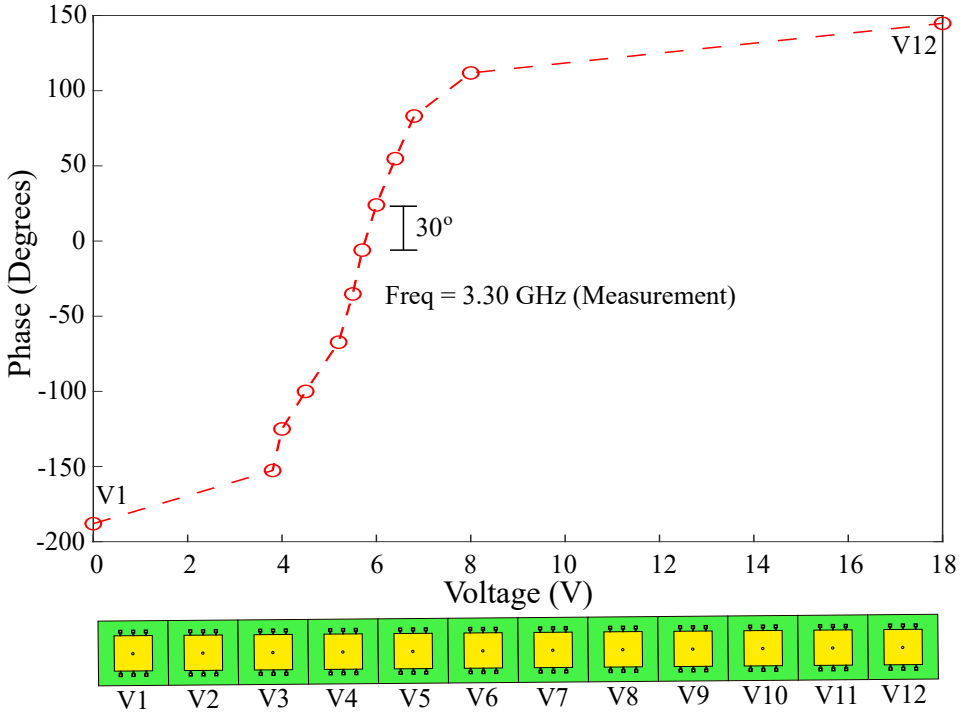

Figure 6.21. Reflection phase at the frequency of 3.30 GHz. Measured result of the reflection phase at the frequency of 3.30 GHz.

6.6.2 Radiation pattern

For verification of the antenna radiation characteristics, a uniform biasing voltage is firstly applied onto the reflectarray antenna elements at the frequency of 3.30 GHz. Since all the reflectarray elements produce the same phase change on reflection, this condition allows to verify that the scattered beam for illumination from 30° will result in reflection at the same angle. In other words, the reflectarray with uniform phasing can be considered as a reflecting mirror, with a phase on reflection that can be controlled through the bias voltage applied to the varactors. Figure 6.22 shows the simulated instantaneous scattered field distribution of the reflectarray antenna with the uniform phase change in the 2D setting. A good agreement between simulated and measured results of the far-field radiation pattern of the antenna is observed in Fig. 6.23.

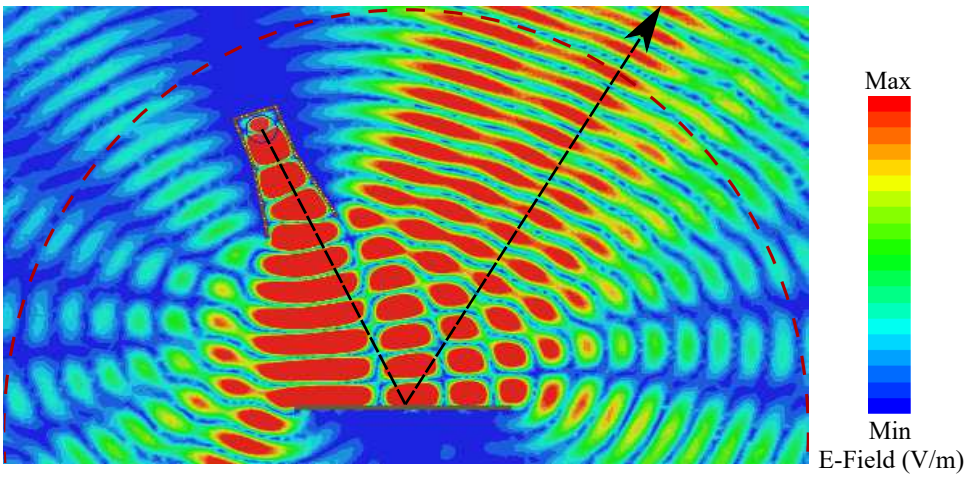

Figure 6.22. Field Distribution for a uniform varactors. Instantaneous E-field distribution for a uniform varactors bias voltages reflectarray configuration at frequency of 3.30 GHz.

In order to verify the reconfigurability of the prototype, the biasing voltages of the varactors are then varied based on the 30° progressive phase between adjacent elements at the frequency of 3.30 GHz. Figure 6.24 demonstrates the simulated instantaneous scattered field distribution of the reflectarray antenna where the steering of the beam in non-specular direction is observed. The radiation pattern of the beam steering towards the expected angle of 53° is shown in Fig. 6.25. The results present a good agreement between simulation and measurement. The side lobe level of the measured result seems slightly higher than expected, but is still acceptable as it remains below than −10 dB.

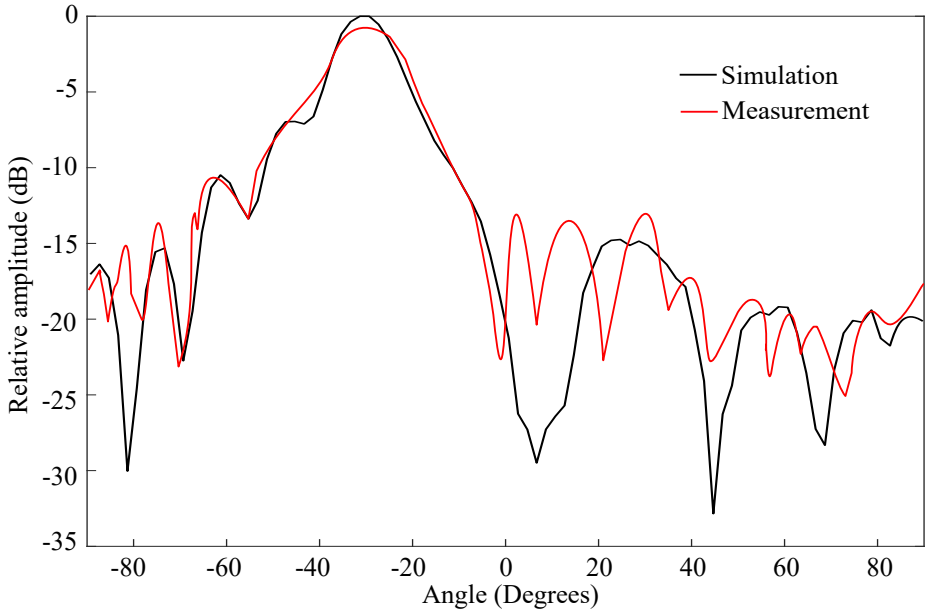

Figure 6.23. Radiation pattern. Radiation pattern for a uniform distribution of varactors bias voltages at frequency of 3.30 GHz.

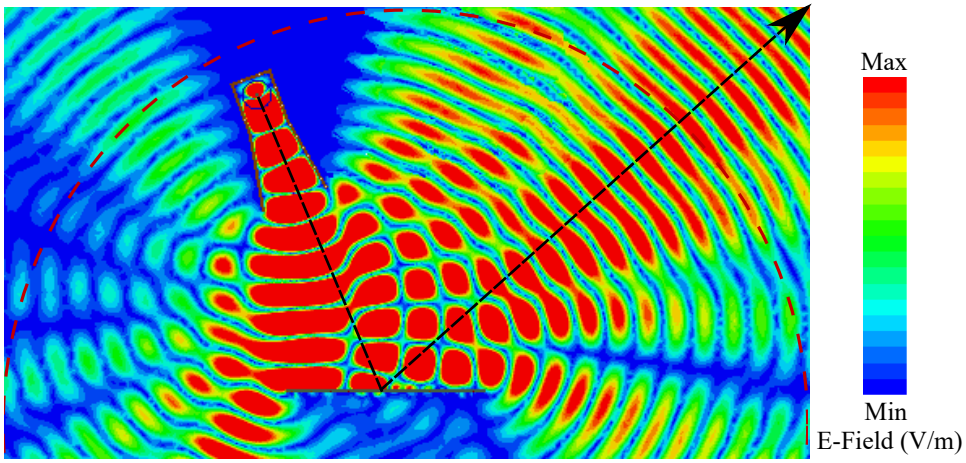

Figure 6.24. Field Distribution for a progressive distribution of varactors. Radiation pattern for a progressive distribution of varactors bias voltages at frequency of 3.30 GHz.

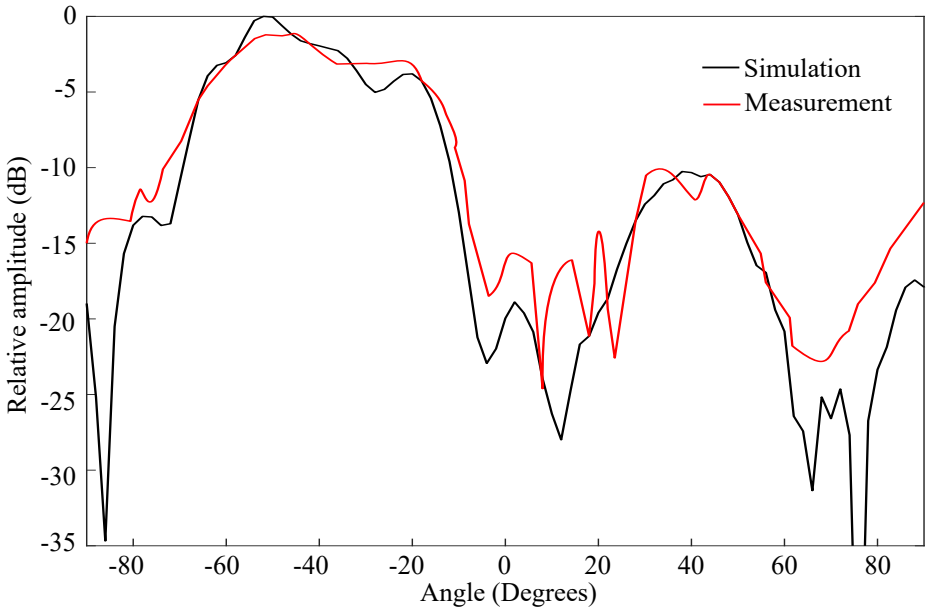

Figure 6.25. Radiation pattern with maximum beam steering. Radiation pattern for maximum beam steering with a variation of varactors bias voltages distribution at frequency of 3.30 GHz.

6.7 Conclusion

A reconfigurable reflectarray unit cell tuned by a group of varactors-loaded stubs has been presented in this chapter. The proposed unit cell has been designed to achieve a nearly full-cycle phase tuning ability within a relatively wide operating frequency band extending from 2.82 GHz to 3.38 GHz. The effects of incidence wave angle onto the characteristics of the antenna unit cell has also been discussed. To validate the reconfigurability of the reflectarray antenna, a linear sub-array of 1×12 elements in periodic boundaries has been simulated, illuminated by a normal incident plane wave. The simulated results have demonstrated that the reflectarray can successfully steer the reflected beam, away from broadside direction. For experimental validation, an offset-fed configuration for the reflectarray antenna system has also been utilised. A prototype of a linear 1×12-cell reflectarray has been manufactured, and measured in a two-dimensional experimental setup, allowing to verify the antenna performance. The experimental results with a uniform varactors bias voltages distribution have successfully demonstrated the effectiveness of the proposed reconfigurable reflectarray antenna concept, however with a frequency shift attributed to fabrication imperfections. It has been also demonstrated that by introducing a progressive phase through nonuniform the varactors bias voltages, the reflectarray antenna is able to scan the beam away from specular direction.

Chapter 7

Summary and Future Work

THIS thesis has been inspired by the concept of stub-loaded varactor control for the study and development of novel reconfigurable antenna designs. Various configurations have been proposed across numerous generic communications applications, with agility of the antennas demonstrated in term of multiple operating frequencies and radiation patterns. This chapter summarises the finding of the presented research that has been organised into two major parts dedicated to reconfigurable antennas and reconfigurable periodic structures, respectively. At the end of each section, possible future work directions based on the current presented results are suggested.

7.1 Thesis contributions

This chapter summarises the original thesis contributions and the results obtained for several novel reconfigurable antennas and periodic structures, and provides suggestions on possible future research work.

7.2 Part1: Reconfigurable antennas

Chapter 3 and Chapter 4 have been identified as the first major contribution parts of this thesis. These chapters focussed on electronically reconfigurable beam steering antennas, able to operate within a tunable frequency band. The operating frequency and phase control have been achieved by using varactors together with additional loading from open circuit stubs. The achievement of continuously beam-steerable radiation patterns has been presented in detail in those chapters.

7.2.1 Summary of original contributions

- For the purpose of beam scanning, a reconfigurable two-element patch array antenna has been presented in Chapter 3. A varactor has been used as a tuning mechanism in order to selectively modify the characteristics of the electrical length or current distribution of each antenna element. In the antenna design procedure, a rectangular single-element patch has been first considered with a varactor placed at the edge of the antenna open aperture to obtain reconfigurability. Since the classical approach does not provide a large tuning range of frequency, an additional impedance manipulation is obtained by loading a properly chosen length of an open-circuit stub together with the varactor. This results in a wide frequency tuning range with enhanced performance achieved through stub parameter optimisation. A bias circuit network that consists of a large resistor and a choke inductor is conveniently connected at the other end of the stub to drive the varactor. As mentioned in Chapter 2, the varactor variable junction capacitance C_0 can be controlled using a bias the voltage ranging from 0 to 18 V which corresponds to capacitance of 1.305 pF to 0.149 pF for the selected varactor model. In the two-element array, individual control of the elements allows to obtain different operation frequencies with impedance bandwidth (defined by $|S11| < -10$ dB) extending over a tuning range of 16%.

- In this reconfigurable design, a relative phase shift which can be exploited for beam scanning also can be determined for each single element when detuned around its resonance. To achieve beam scanning at a given frequency, firstly, an operating frequency f_0 is identified by adjusting the varactor capacitance C_0. Then, by introducing a small additional capacitance $\pm\Delta C_0$ with opposite signs around C_0, both patches are slightly detuned from their resonance. As the result, a phase shift is introduced between the two elements antenna which allow to achieve beam scanning functionality. The two reconfigurable patch elements are placed next to each other in an array configuration with an inter-element distance d_p and they are fed by a T-junction power divider. In this configuration, the optimisation of the mutual coupling effects between the elements and through the feeding line must be taken into account to achieve a maximum beam scanning angle for the antenna. To gain a better understanding of the operation principle, the antenna can be operated in various states at a given frequency f_0. When the two elements share a same value of capacitance value of C_0, they radiate in phase resulting in a broadside radiation pattern. Meanwhile, when the two elements are detuned through respective addition of the $\pm\Delta C_0$, a continuously H-plane beam scanning ranging from -23° to $+23^\circ$ around broadside can be obtained. The antenna thus demonstrates multiple functionalities since it is frequency and pattern reconfigurable.

- Inspired by a similar operation, a new idea of simplified antenna configuration was initiated by considering a single-element with combination of two modes for beam scanning. This lead to a simple design of compact antenna for a similar functionality. The demonstrated device starts from a standard design of a rectangular patch antenna. The antenna is fed by a coaxial probe located at a certain distance from the center of the structure to achieve reasonable impedance matching. In order to form a relative phase difference between the radiating apertures in the single-element structure, a series of vias are placed near the patch center. This metallic wall allows to realise two coupled cavities with nearly independent resonance frequencies. The reconfiguration of the antenna is achieved by connecting a stub-loaded varactor to the edge on one side of the cavity. This allows to tune the electrical length of one of the cavities. This scenario can create a phase difference between the two cavities, thus providing a beam scanning mechanism as mentioned in the previous design. As the excitation of the antenna is realised

through a probe in the first half cavity, the second half cavity is excited by direct coupling to the fed cavity. To compensate the imbalance caused by this feeding probe, the length at second half cavity is made slightly longer. The antenna has been shown to provide a continuous E-plane beam scanning, however limited to one side from boresight direction.

- For this design of single-element antenna, beam scanning can be achieved in two different ways. Firstly, the pattern reconfiguration can be obtained by the variation of the varactor bias voltages at a fixed frequency, where the reconfigurable beam scanning is achieved from 20° to 39°. In addition, the beam scanning also can be achieved as a function of the frequency at a fixed bias voltage. This scanning happens within the impedance bandwidth of 4.6% and provide the beam scanning in a range extending from around 8° to 43°.

7.2.2 Future work

The modification of the electrical length by changing the antenna aperture impedance characteristics provides a promising potential to design antennas with multi-functional or reconfigurability operation in one integrated device. Since these antennas have received a good attention in many applications, the two antennas mentioned above have been designed to focus on achieving a continuous beam scanning angle combined with frequency reconfigurability. One of the main challenges of the design is maintaining satisfactory impedance matching for each element in the array configurations. This is complicated by the mutual coupling effects that significantly change the beam scanning angle. The effect of the coupling is serious when the distance between the antenna elements is small. Although, it can improve the antenna beam scanning angle, it also introduces an increase of side lobes. Therefore, future work will concentrate on an efficient decoupling method as a key challenge to improve the performance of the antenna beam scanning angle. Additionally, the effect of increasing the number of varactors and loading stubs will also be investigated to enhance the efficiency of the antenna. Next, the single antenna should be enhanced to allow scanning in both sides of the boresight direction. Finally, different techniques can be explored to improve the antennas performance.

7.3 Part2: Reconfigurable periodic structure

Reflectarray antennas are used as high-gain antennas for several applications such as remote sensing, microwave imaging system and space applications. As main features, reconfigurable reflectarray antennas present potentially exceptional performance in scanning or tracking velocity, enhanced tolerance to vibration, coverage modification and robustness against interferences. As they can offer beam scanning function with high gain and high resolution, they are an ideal choice for all these applications. In this section, the achievements in the second major part of this thesis covered in Chapters 5 and 6 are summarised.

7.3.1 Summary of original contributions

- A reconfigurable reflectarray antenna is generally designed to steer a reflected wave to a desired direction. To achieve this aim, all array elements should be capable of one near-full cycle of phase change. The antenna operation involves an incident wave which can be of any polarisation and impinges either at normal or oblique incidence. This wave is generated by a primary feed and creates a first phase profile at the surface of the reflectarray antenna. When the elements introduce progressive phase changes, the reflected wave will be subjected to deflection at an angle that can be controlled to produce beam scanning. It is worth to mention that the amplitude at each elements is imposed by the radiation pattern of the primary feed.

- Since the reflection coefficient and full phase range are important parameters to characterise the performance of the reflectarray antenna, the initial configuration of the unit cell is a natural first step in designing the antenna. The reflection coefficient is indicative of the efficiency of the reflectarray, and the phase response characteristics define its agility. Chapter 5 has introduced a rectangular microstrip unit cell antenna configuration with a symmetrical loading condition implemented with two varactor-loaded straight stubs placed at the opposite radiating edges of the patch. The dimension of the resonant patch is determined based on the standard microstrip antenna design procedure. The length of the stubs is optimised to achieve best tuning performance. However, the design in the stub configuration may require a large area of dielectric substrate on each side of the patch, making it no longer suitable for a unit cell design because of the appearance of grating lobes.

To provide a compact structure and more efficient design, a new configuration of T-shaped stub loading has been conceptually proposed.

- The frequency agility of the unit cell proposed in Chapter 5 is determined by the presence of two sections of stub length $L_b/2$ in a parallel configuration. This effectively gives a load impedance seen by a transmission line section of an effective length L_a. This approach has been shown to provide 30% of tuning range, namely from 3 GHz to 4 GHz, with a magnitude response better than -3 dB over the full range of the varactor capacitances. On the other hand, the phase response characteristics of a unit cell presented a phase tuning range of near 300° achievable between 3.44 GHz and 3.67 GHz with better than -1.4 dB reflection coefficient in the quoted frequency range of operation.

- To improve the frequency tuning range and the phase response characteristics, the structure of the reconfigurable reflectarray unit cell antenna has been slightly modified. The number of varactor-loaded straight stubs at the edge of the patch has been increased to three at the open aperture on both sides. An in-depth analysis was performed to demonstrate that this helps improving the unit cell performance and reduce the losses associated with the varactor diode operation. In the new unit cell configuration, two layers of substrates have been used with a ground plane in between them. The varactors are loaded with the square microstrip antenna on the top layer of the substrate. Due to the length of the stubs, they are folded and are printed on the bottom layer of the substrate together with the bias circuit network. Vias are used across the two substrates in order to connect the varactors and the stubs. As the reflectarray have typically a large number of elements, the advantage of the backside stubs and biasing network configuration is that it minimises the size of the reconfigurable reflectarray antenna. This compact unit cell is a requirement for avoiding grating lobes. According to the microstrip antenna theory, the top layer of substrate is slightly thicker compared to the bottom layer to improve the bandwidth of the unit cell. The reconfigurable resonant patch unit cell is then analysed in full-wave simulations and achieves 43% tuning range, covering 2.5 GHz to 3.8 GHz. Meanwhile, the tuning of the phase response is also found to reach nearly 300° to 315° within a fractional frequency range of operation of 18%. In contrast, most reflectarray antenna designs in the literature provide a limited phase range at a fixed operating frequency or within a narrower frequency tuning range.

- To prove the effectiveness of the proposed reconfigurable element, a prototype of 1×12 elements with a standard interspacing of half-wavelength between them have been fabricated for experimental validation in a parallel-plate 2D settings. The array antenna is illuminated by a 2D H-plane sectoral horn antenna which placed at a distance of 47 cm from the reflecting surface. The design is optimised to minimise spillover power losses that reduce the reflectarray antenna overall efficiency. The effect of variations from normal incidence to 30° oblique incidence on the phase curves has been discussed in Chapter 6. The capability of the reconfigurable reflected beam scanning has been successfully verified by obtaining a steerable radiation pattern.

7.3.2 Future work

Since the aim of the reflectarray antenna design was to facilitate arbitrary phased-only beam forming, there are several aspects of the antenna that can be further investigated for a more complete validation and full characterisation of the limits of the concept. In principle, the requirement of the antenna beam scanning can be fulfilled for any direction in space based on the progressive phase arrangement. However, practical considerations will limit the accessible range. Further, the general principle of the antenna can be applied in as a parabolic configuration that can offer advantages for achieving maximal aperture efficiency in various applications. On that basis, the periodic phase ramp configuration also can be further explored and combined with a parabolic profile to achieve maximum beam scanning and gain.

7.4 Concluding statement

Finally, as a general conclusion, this thesis has described two major research parts that correspond to reconfigurable antennas and reconfigurable periodic structures. Both parts were connected in their general concept, since all devices were based on varactor-loaded stubs, thus demonstrating the capability of the approach. The design procedures for frequency- and pattern-reconfigurable antennas and reconfigurable reflectarray antennas were explored with a combination of full-wave commercial electromagnetic simulation software CST Technology and Ansys HFSS, and validated experimentally with good agreement. The variety of reconfigurables antennas demonstrated in this thesis exhibits unique agile characteristics and radiation performance. The presented

achievements have illustrated that the technology of reconfigurable electronics and advanced antennas can help explore prospective solutions to meet the present and the future antenna design challenges.

Bibliography

ALMAJALI-E. R., AND MCNAMARA-D. A. (2016). Angle of incidence effects in reflectarray antenna design: making gain increases possible by including incidence angle effects., *IEEE Antennas and Propagation Magazine*, **58**(5), pp. 52–64.

ATCODI CO.-L. (n.d.). Array antenna (microstrip patch array antenna).

BABAKHANI-B., AND SHARMA-S. (2015). Wideband frequency tunable concentric circular microstrip patch antenna with simultaneous polarization reconfiguration, *IEEE Antennas and Propagation Magazine*, **57**(2), pp. 203–216.

BALANIS-C. A. (2015). *Antenna Theory: Analysis and Design*, Hoboken: John Wiley and Sons, Incorporated.

BANSAL-M., SARKAR-D., AND SRIVASTAVA-K. V. (2018). Frequency reconfigurable compact multi-band printed monopole antenna using capacitively loaded loops, *in 2018 5th IEEE Uttar Pradesh Section International Conference on Electrical, Electronics and Computer Engineering (UPCON)*, pp. 1–6.

BERNHARD-J. T. (2007a). *Reconfigurable Antennas*, Morgan and Claypool Publisher, University of Illinois at Urbana.

BERNHARD-J. T. (2007b). Reconfigurable antennas, *Synthesis lectures on antennas*, **2**(1), pp. 1 – 66.

BESOLI-A. G., AND FLAVIIS-F. D. (2011). A multifunctional reconfigurable pixeled antenna using MEMS technology on printed circuit board, *IEEE Transactions on Antennas and Propagation*, **59**(12), pp. 4413–4424.

BORHANI-M., REZAEI-P., AND VALIZADE-A. (2016). Design of a reconfigurable miniaturized microstrip antenna for switchable multiband systems, *IEEE Antennas and Wireless Propagation Letters*, **15**, pp. 822 – 825.

CARRASCO-E., BARBA-M., AND ENCINAR-J. A. (2010). Electronically switchable-beam reflectarray antenna, *Proceedings of the Fourth European Conference on Antennas and Propagation*, pp. 1–5.

CARRASCO-E., ENCINAR-J. A., AND RAHMAT-SAMII-Y. (2016). Reflectarray antennas: A review, *Forum for Electromagnetic Research Methods and Application Technologies (FERMAT)*.

CHEN-S.-H., ROW-J.-S., AND WONG-K.-L. (2007). Reconfigurable square-ring patch antenna with pattern diversity, *IEEE Transactions on Antennas and Propagation*, **55**(2), pp. 472 – 475.

CHEN-S.-L., QIN-P.-Y., DING-C., AND GUO-Y. J. (2017a). Cavity-backed proximity-coupled reconfigurable microstrip antenna with agile polarizations and steerable beams, *IEEE Transactions on Antennas and Propagation*, **65**(10), pp. 5553–5558.

CHEN-S.-L., QIN-P.-Y., LIN-W., AND GUO-Y. J. (2018a). Pattern-reconfigurable antenna with five switchable beams in elevation plane, *IEEE Antennas and Wireless Propagation Letters*, **17**(3), pp. 454–457.

CHEN-S.-L., QIN-P.-Y., LIN-W., AND GUO-Y. J. (2018b). Pattern-reconfigurable antenna with five switchable beams in elevation plane, *IEEE Antennas and Wireless Propagation Letters*, **17**(3), pp. 454–457.

CHEN-S.-L., WEI-F., QIN-P.-Y., GUO-Y. J., AND CHEN-X. (2017b). A multi-linear polarization reconfigurable unidirectional patch antenna, *IEEE Transactions on Antennas and Propagation*, **65**(8), pp. 4299–4304.

CHEN-Y.-Y., GE-Y., AND BIRD-T. S. (2015). An offset reflectarray antenna for multipolarization applications., *IEEE Antennas and Wireless Propagation Letters*, **15**, pp. 1353–1356.

CHRISTODOULOU-C. G., TAWK-Y., LANE-S. A., AND ERWIN-S. R. (2012). Reconfigurable antennas for wireless and space applications, *Proceedings of the IEEE*, **100**(7), pp. 2250 – 2261.

COJOCARU-V. I., AND BRAZIL-T. J. (1992). A large-signal equivalent circuit model for hyperabrupt p-n junction varactor diodes, *1992 22nd European Microwave Conference*, **2**, pp. 1115–1121.

COLLIN-R. (2007). Foundations for microwave engineering.

COSTANTINE-J., TAWK-Y., AND CHRISTODOULOU-C. G. (2013). Design of reconfigurable antennas using graph models, *Synthesis Lectures on Antennas*, **5**(1), pp. 1–148.

COSTANZO-S., VENNERI-F., RAFFO-A., AND MASSA-G. D. (2018). Dual-layer single-varactor driven reflectarray cell for broad-band beam-steering and frequency tunable applications, *IEEE Access*, **6**, pp. 71793 – 71800.

COSTANZO-S., VENNERI-F., RAFFO-A., MASSA-G. D., AND COORSONELLA-P. (2015a). Novel varactor-loaded phasing line for reflectarray unit cell with large reconfigurability frequency range, *Advances in Intelligent Systems and Computing*, **354**, pp. 3 – 9.

COSTANZO-S., VENNERI-F., RAFFO-A., MASSA-G. D., AND CORSONELLO-P. (2015b). Novel varactor-loaded phasing line for reflectarray unit cell with large reconfigurability frequency range, *Advances in Intelligent Systems and Computing*, **354**, pp. 3–9.

COSTANZO-S., VENNERI-F., RAFFO-A., MASSA-G. D., AND CORSONELLO-P. (2016). Radial-shaped single varactor-tuned phasing line for active reflectarrays, *IEEE Transactions on Antennas and Propagation*, **64**(7), pp. 3254 – 3259.

(CST)-C. S. T. (2019). Cst studio suite electromagnetic field simulation software, *available in https://www.3ds.com/products-services/simulia/products/cst-studio-suite/*.

DE LA TORRE-P. P., AND SIERRA-CASTANER-M. (2007). Design and prototype of a 12ghz transmitarray, *2007 IEEE Antennas and Propagation Society International Symposium*, **49**(12), pp. 3020–3026.

DENG-W.-Q., YANG-X.-S., SHEN-C.-S., ZHAO-J., AND WANG-B.-Z. (2017). A dual-polarized pattern reconfigurable yagi patch antenna for microbase stations, *IEEE Transactions on Antennas and Propagation*, **65**(10), pp. 5095–5102.

DENG-Z., GUO-X., WEI-H., GAN-J., AND WANG-Y. (2016). Design, analysis, and verification of K-B and pattern reconfigurable patch antenna using RF MEMS switches, *Micromachine Article*, **7**(8), p. 144.

DOHERTY-B., AND WATERTOWN-M. (2015). Micronote series 701 PIN diode fundamentals, *available in https://www.microsemi.com/document-portal/doc_download/134814-micronote-701-pin-diode-fundamentals*.

ELSHERBINY-M., FATHY-A. E., ROSEN-A., AYERS-G., AND PERLOW-S. M. (2004). Holographic antenna concept, analysis, and parameters, *IEEE Transactions on Antennas and Propagation*, **52**(3), pp. 830–839.

ERDIL-E., TOPALLI-K., UNLU-M., CIVI-O. A., AND AKIN-T. (2007). Frequency tunable microstrip patch antenna using RF MEMS technology, *IEEE Transactions on Antennas and Propagation*, **55**(4), pp. 1193–1196.

FARZAMI-F., KHALEDIAN-S., SMIDA-B., AND ERRICOLO-D. (2017). Pattern-reconfigurable printed dipole antenna using loaded parasitic elements, *IEEE Antennas and Wireless Propagation Letters*, **16**, pp. 1151–1154.

GAO-Q., WANG-J., LI-Y., AND LI-Z. (2018). A multiresonant element for bandwidth enhancement of circularly polarized reflectarray antennas, *IEEE Antennas and Wireless Propagation Letters*, pp. 727–730.

GE-L., LI-M., WANG-J., AND GU-H. (2017). Unidirectional dual-band stacked patch antenna with independent frequency reconfiguration, *IEEE Antennas and Wireless Propagation Letters*, **16**, pp. 113 – 116.

GENOVESI-S., CANDIA-A. D., AND MONORCHIO-A. (2014). Compact and low profile frequency agile antenna for multistandard wireless communication systems, *IEEE Transactions on Antennas and Propagation*, **62**(3), pp. 1019–1026.

GIANVITTORIO-J. P., AND RAHMAT-SAMII-Y. (2006a). Reconfigurable patch antennas for steerable reflectarray applications, *IEEE Transactions on Antennas and Propagation*, **54**(5), pp. 1388–1392.

GIANVITTORIO-J. P., AND RAHMAT-SAMII-Y. (2006b). Reconfigurable patch antennas for steerable reflectarray applications, *IEEE Transactions on Antennas and Propagation*, **54**(5), pp. 1388–1392.

GU-H., WANG-J., GE-L., AND SIM-C.-Y.-D. (2016). A new quadri-polarization reconfigurable circular patch antenna, *IEEE Access*, **4**, pp. 4646–4651.

GUO-L., YU-H., CHE-W., AND YANG-W. (2019). A broadband reflectarray antenna using single-layer rectangular patches embedded with inverted L-shaped slots, *IEEE Transactions on Antennas and Propagation*, **67**(5), pp. 3132–3139.

HAN-L., WANG-C., CHEN-X., AND ZHANG-W. (2016). Compact frequency-reconfigurable slot antenna for wireless applications, *IEEE Antennas and Wireless Propagation Letters*, **15**, pp. 1795 – 1798.

HAO-Z.-C., FAN-K.-K., AND WANG-H. (2017). A planar polarisation-reconfigurable antenna, *IEEE Transactions on Antennas and Propagation*, **65**(4), pp. 1624–1632.

HAUPT-R. L., AND LANAGAN-M. T. (2013). Reconfigurable antennas, *IEEE Antennas and Propagation Magazine*, **55**(1), pp. 49–61.

HO-K. M.-J., AND REBEIZ-G. M. (2014). A 0.91.5 ghz microstrip antenna with full polarization diversity and frequency agility, *IEEE Transactions on Antennas and Propagation*, **62**(5), pp. 2398–2406.

HUANG-C., PAN-W., MA-X., AND LUO-X. (2016). A frequency reconfigurable directive antenna with wideband low-RCS property, *IEEE Transactions on Antennas and Propagation*, **64**(3), pp. 1173 – 1178.

HUFF-G., FENG-J., ZHANG-S., AND BERNHARD-J. (2003). A novel radiation pattern and frequency reconfigurable single turn square spiral microstrip antenna, *IEEE Microwave and Wireless Letters*, **13**(2), pp. 57–59.

HUM-S. V., AND PERRUISSEAU-CARRIER-J. (2014). Reconfigurable reflectarrays and array lenses for dynamic antenna beam control: A review, *IEEE Transactions on Antennas and Propagation*, **62**(1), pp. 183–198.

HUM-S. V., OKONIEWSKI-M., AND DAVIES-R. J. (2005a). An evolvable antenna platform based on reconfigurable reflectarrays, *NASA/DoD Conference on Evolvable Hardware 2005*, pp. 139–146.

HUM-S. V., OKONIEWSKI-M., AND DAVIES-R. J. (2005b). Realizing an electronically tunable reflectarray using varactor diode-tuned elements, *IEEE Microwave and Wireless Components Letters*, **15**(6), pp. 422–424.

INCORPORATION-A. (2016). Getting started with HFSS: Floquet ports, *available in http://www.1cae.com/articleAccessory/2017/04/16/HFSS%20Floquet%20Ports.pdf*.

IOANNIDES-P., AND BALANIS-C. (2005). Uniform circular arrays for smart antennas, *IEEE Antennas and Propagation Magazine*, **47**(4), pp. 192–206.

JEFORS-E., CHENG-S., FROM-K., SKARIN-I., HALLBJRNER-P., AND RYDBERG-A. (2007). Electrically steerable single-layer microstrip traveling wave antenna with varactor diode based phase shifters, *IEEE Transactions on Antennas and Propagation*, **55**(9), p. 2451(10).

JIANG-X., ZHANG-Z., LI-Y., AND FENG-Z. (2014). A novel null scanning antenna using even and odd modes of a shorted patch, *IEEE Transactions on Antennas and Propagation*, **62**(4), pp. 1903–1909.

JIN-G., LI-M., LIU-D., AND ZENG-G. (2018). A simple four-beam reconfigurable antenna based on monopole, *IEEE Access*, **6**, pp. 30309–30316.

JOHANSSON-F. S. (1990). A new planar grating-reflector antenna, *IEEE Transactions on Antennas and Propagation*, **38**(9), pp. 1491–1495.

JOHNSON-R. C. (1992). *Antenna Engineering Handbook*, McGraw-Hill, Inc.

JUSOH-M., ABOUFOUL-T., SABAPATHY-T., ALOMAINY-A., AND KAMARUDIN-M. R. (2014a). Pattern-reconfigurable microstrip patch antenna with multidirectional beam for WIMAX application, *IEEE Antennas and Wireless Propagation Letters*, **13**, pp. 860–863.

JUSOH-M., SABAPATHY-T., JAMLOS-M. F., AND KAMARUDIN-M. R. (2014b). Reconfigurable four-parasitic-elements patch antenna for high-gain beam switching application, *IEEE Antennas and Wireless Propagation Letters*, **13**, pp. 79–82.

KAMODA-H., IWASAKI-T., TSUMOCHI-J., AND KUKI-T. (2009). 60-ghz electrically reconfigurable reflectarray using p-i-n diode, *2009 IEEE MTT-S International Microwave Symposium Digest*, pp. 1177–1180.

KANSHENG-Y., XIULONG-B., PATRICK-M., AND J.-A. M. (2016). Pattern reconfigurable back-to-back microstrip patch antenna, *IET Microwaves, Antennas and Propagation*, **10**(13), pp. 1390–1394.

KHIDRE-A., YANG-F., AND ELSHERBENI-A. Z. (2015a). Circularly polarized beam-scanning microstrip antenna using a reconfigurable parasitic patch of tunable electrical size, *IEEE Transactions on Antennas and Propagation*, **63**(7), pp. 2858–2866.

KHIDRE-A., YANG-F., AND ELSHERBENI-A. Z. (2015b). A patch antenna with a varactor-loaded slot for reconfigurable dual-band operation, *IEEE Transactions on Antennas and Propagation*, **63**(2), pp. 755 – 760.

KIRSCHNING-M., JANSEN-R., AND KOSTER-N. (1983). Measurement and computer-aided modeling of microstrip discontinuities by an improved resonator method, *1983 IEEE MTT-S International Microwave Symposium Digest*, pp. 495–497.

KOVITZ-J. M., RAJAGOPALAN-H., AND RAHMAT-SAMII-Y. (2015). Design and implementation of broadband MEMS RHCP/LHCP reconfigurable arrays using rotated E-shaped patch elements, *IEEE Transactions on Antennas and Propagation*, **63**(6), pp. 2497–2507.

LEE-S., LIM-E., LO-F., AND NG-W. (2017). Circularly polarized elliptical microstrip patch reflectarray, *IEEE Transactions on Antennas and Propagation*, **65**(8), pp. 4322–4327.

LEE-S. W., AND SUNG-Y. J. (2014). Reconfigurable rhombus-shaped patch antenna with Y-shaped feed for polarization diversity, *IEEE Antennas and Wireless Propagation Letters*, **14**, pp. 163–166.

LEGAY-H., CAILLOCE-Y., VENDIER-O., CAILLE-G., PERRUISSEAU-CARRIER-J., LATHI-M., POLIZZI-J. P., OESTERMANN-U., PONS-P., AND RAVEU-N. (2007). Satellite antennas based on mems tunable reflectarrays, *The Second European Conference on Antennas and Propagation, EuCAP 2007*, pp. 1–6.

LEGAY-H., PINTE-B., CHARRIER-M., ZIAEI-A., GIRARD-E., AND GILLARD-R. (2003). A steerable reflectarray antenna with mems controls, *IEEE International Symposium on Phased Array Systems and Technology 2003*, pp. 494–499.

LIANG-B., SANZ-IZQUIERDO-B., PARKER-E. A., AND BATCHELOR-J. C. (2015). A frequency and polarization reconfigurable circularly polarized antenna using active EBGstructure for satellite navigation, *IEEE Transactions on Antennas and Propagation*, **63**(1), pp. 33 – 40.

LIN-W., AND WONG-H. (2015a). Polarization reconfigurable wheel-shaped antenna with conical-beam radiation pattern, *IEEE Transactions on Antennas and Propagation*, **63**(2), pp. 491–499.

LIN-W., AND WONG-H. (2015b). Wideband circular polarisation reconfigurable antenna, *IEEE Transactions on Antennas and Propagation*, **63**(12), pp. 5938–5944.

LIN-W., AND WONG-H. (2017). Wideband circular-polarization reconfigurable antenna with L-shaped feeding probes, *IEEE Antennas and Wireless Propagation Letters*, **16**, pp. 2114–2117.

LIN-W., WONG-H., AND ZIOLKOWSKI-R. W. (2017a). Wideband pattern-reconfigurable antenna with switchable broadside and conical beams, *IEEE Antennas and Wireless Propagation Letters*, **16**, pp. 2638–2641.

LIN-W., WONG-H., ZIOLKOWSKI., AND W.-R. (2017b). Wideband pattern-reconfigurable antenna with switchable broadside and conical beams, *IEEE Antennas and Wireless Propagation Letters*, **16**, pp. 2638–2641.

LIU-L., AND LANGLEY-R. J. (2008). Liquid crystal tunable microstrip patch antenna, *Electronic Letters*, **55**(4), pp. 1179–1180.

MACOM-T. S. (2015). MA46H120 varactor datasheet, *available in https://cdn.macom.com/datasheets/MA46H120%20Series.pdf*.

MAILLOUX-R., MCILVENNA-J., AND KERNWEIS-N. (1981). Microstrip array technology, *IEEE Transactions on Antennas and Propagation*, **29**(1), pp. 25–37.

MAJID-H. A., RAHIM-M. K. A., HAMID-M. R., AND ISMAIL-M. F. (2014). Frequency and pattern reconfigurable slot antenna, *IEEE Transactions on Antennas and Propagation*, **62**(10), pp. 5339–5343.

MAJID-H. A., RAHIM-M. K. A., HAMID-M. R., MURAD-N. A., AND ISMAIL-M. F. (2013). Frequency-reconfigurable microstrip patch-slot antenna, *IEEE Antennas and Wireless Propagation Letters*, **12**, pp. 218–220.

MAJUMDAR-B., AND ESSELLE-K. (2016). A single band beam scanning active phased array antenna, *2016 International Conference on Electromagnetics in Advanced Applications (ICEAA)*, pp. 832–835.

MAK-K. M., LAI-H. W., LUK-K. M., AND HO-K. L. (2017). Polarization reconfigurable circular patch antenna with a C-shaped, *IEEE Transactions on Antennas and Propagation*, **65**(3), pp. 1388–1392.

NAYERI-P., YANG-F., AND ELSHERBENI-A. Z. (2012). Design and experiment of a single-feed quad-beam reflectarray antenna, *IEEE Transactions on Antennas and Propagation*, **60**(2), pp. 1166–1171.

NAYERI-P., YANG-F., AND ELSHERBENI-A. Z. (2015). Beam-scanning reflectarray antennas: a technical overview and state of the art., *IEEE Antennas and Propagation Magazine*, **57**(4), pp. 32 – 47.

NAYERI-P., YANG-F., AND ELSHERBENI-A. Z. (2018). *Reflectarray Antennas: Theory, Designs and Applications*, John Wiley and Sons, Incorporated.

NEMATI-M. H., KAZEMI-R., AND TEKIN-I. (2014). Pattern reconfigurable patch array for 2.4 ghz wlan systems, *Microwave and Optical Technology Letters*, **56**(10), pp. 2377–2381.

NGUYEN-TRONG-N., AND FUMEAUX-C. (2018). Tuning range and efficiency optimization of a frequency-reconfigurable patch antenna, *IEEE Antennas and Wireless Propagation Letters*, **17**(1), pp. 150 – 154.

NGUYEN-TRONG-N., HALL-L., AND FUMEAUX-C. (2015a). A frequency- and polarization-reconfigurable stub-loaded microstrip patch antenna, *IEEE Transactions on Antennas and Propagation*, **63**(11), pp. 5235–5240.

NGUYEN-TRONG-N., HALL-L., AND FUMEAUX-C. (2015b). A frequency-and polarization-reconfigurable stub-loaded microstrip patch antenna, *IEEE Transactions on Antennas and Propagation*, **63**(11), pp. 5235–5240.

NGUYEN-TRONG-N., HALL-L., AND FUMEAUX-C. (2016a). A frequency- and pattern-reconfiguration center-shorted microstrip antenna, *IEEE Antennas and Wireless Propagation Letters*, **15**, pp. 1955–1958.

NGUYEN-TRONG-N., HALL-L., AND FUMEAUX-C. (2016b). A frequency-and pattern-reconfigurable center-shorted microstrip antenna, *IEEE Antennas and Wireless Propagation Letters*, **15**, pp. 1955–1958.

NGUYEN-TRONG-N., HALL-L., AND FUMEAUX-C. (2016c). Impedance matching of a frequency-and pattern-reconfigurable antenna, *2016 17th International Symposium on Antenna Technology and Applied Electromagnetics (ANTEM)*, pp. 1–2.

NGUYEN-TRONG-N., HALL-L., AND FUMEAUX-C. (2016d). A reconfigurable quarter-wave patch antenna employing a folded loading stub, *2016 IEEE International Symposium on Antennas and Propagation (APSURSI)*, pp. 831–832.

NGUYEN-TRONG-N., KAUFMANN-T., HALL-L., AND FUMEAUX-C. (2015c). Analysis and design of a reconfigurable antenna based on half-mode substrate-integrated cavity, *IEEE Transactions on Antennas and Propagation*, **63**(8), pp. 3345–3353.

NGUYEN-TRONG-N., KAUFMANN-T., HALL-L., AND FUMEAUX-C. (2015d). Analysis and design of a reconfigurable antenna based on half-mode substrate-integrated cavity, *IEEE Transactions on Antennas and Propagation*, **63**(8), pp. 3345–3353.

NGUYEN-TRONG-N., PIOTROWSKI-A., AND FUMEAUX-C. (2017a). A frequency-reconfigurable dual-band low-profile monopolar antenna, *IEEE Transactions on Antennas and Propagation*, **65**(7), pp. 3336 – 3343.

NGUYEN-TRONG-N., PIOTROWSKI-A., HALL-L., AND FUMEAUX-C. (2017b). A frequency- and polarization-reconfigurable circular cavity antenna, *IEEE Antennas and Wireless Propagation Letters*, **16**, pp. 999 – 1002.

NIU-T., WITHAYACHUMNANKUL-W., UNG-B. S.-Y., MENEKSE-H., BHASKARAN-M., SRIRAM-S., AND FUMEAUX-C. (2013). Experimental demonstration of reflectarray antennas at terahertz frequencies, *Optics Express*, **21**(3), pp. 2875–2889.

OUYANG-J., PAN-Y. M., AND ZHENG-S. Y. (2018). Center-fed unilateral and pattern reconfigurable planar antennas with slotted ground plane, *IEEE Transactions on Antennas and Propagation*, **66**(10), pp. 5139–5149.

PANAGAMUWA-C., CHAURAYA-A., AND VARDAXOGLOU-J. (2006a). Frequency and beam reconfigurable antenna using photoconducting switches, *IEEE Transactions on Antennas and Propagation*, **54**(2), pp. 449–454.

PANAGAMUWA-C. J., CHAURAYA-A., AND VARDAXOGLOU-J. C. (2006b). Frequency and beam reconfigurable antenna using photoconducting switches, *IEEE Transactions on Antennas and Propagation*, **54**(2), pp. 449–454.

PAN-W., HUANG-C., CHEN-P., PU-M., MA-X., AND LUO-X. (2013). A beam steering horn antenna using active frequency selective surface, *IEEE Transactions on Antennas and Propagation*, **61**(12), pp. 6218–6223.

PATEL-S. K., ARGYROPOULOS-C., AND KOSTA-Y. P. (2018). Pattern controlled and frequency tunable microstrip antenna loaded with multiple split ring resonators, *IET Microwaves, Antennas and Propagation*, **12**(3), pp. 390–394.

PAZIN-L., AND LEVIATAN-Y. (2013). Reconfigurable slot antenna for switchable multi-band operation in a wide frequency range, *IEEE Antennas and Wireless Propagation Letters*, **12**, pp. 329–332.

POZAR-D. M. (1998). *Microwave Engineering*, John Wiley and Sons, New York.

POZAR-D. M., TARGONSKI-S. D., AND POKULS-R. (1999). A shaped-beam microstrip patch reflectarray, *IEEE Transactions on Antennas and Propagation*, **47**(7), pp. 1167–1173.

QIN-P.-Y., GUO-Y. J., AND WEILY-A. R. (2016). Broadband reflectarray antenna using subwavelength elements based on double square meander-line rings, *IEEE Transactions on Antennas and Propagation*, **64**(1), pp. 378–383.

QIN-P.-Y., GUO-Y. J., WEILY-A. R., AND LIANG-C.-H. (2012). A pattern reconfigurable u-slot antenna and its applications in mimo systems, *IEEE Transactions on Antennas and Propagation*, **60**(2), pp. 516–528.

REBEIZ-G., TAN-G.-L., AND HAYDEN-J. (2002). RF MEMS phase shifters: design and applications, *IEEE Microwave Magazine*, **3**(2), pp. 72–81.

RODRIGO-D., CETINER-B. A., AND JOFRE-L. (2014a). Frequency, radiation pattern and polarisation reconfigurable antenna using a parasitic pixel layer, *IEEE Transactions on Antennas and Propagation*, **62**(6), pp. 3422–3427.

RODRIGO-D., CETINER-B. A., AND JOFRE-L. (2014b). Frequency, radiation pattern and polarization reconfigurable antenna using a parasitic pixel layer, *IEEE Transactions on Antennas and Propagation*, **62**(6), pp. 3422–3427.

ROW-J.-S., AND WU-Y.-H. (2018). Pattern reconfigurable slotted-patch array, *IEEE Transactions on Antennas and Propagation*, **66**(3), pp. 1580–1583.

ROW-J.-S., LIU-W.-L., AND CHEN-T.-R. (2012). Circular polarisation and polarisation reconfigurable designs for annular slot antennas, *IEEE Transactions on Antennas and Propagation*, **60**(12), pp. 5998–6002.

SAMAIYAR-A., ABDELRAHMAN-A. H., BOSKOVIC-L. B., AND FILIPOVIC-D. S. (2019). Extreme offset-fed reflectarray antenna for xompact deployable platforms, *IEEE Antennas and Wireless Propagation Letters*, **18**(6), pp. 1139–1143.

SARSHAR-A., AND TABARI-A. E. (2013). Design of a stacked stub-loaded patch element for x-band reflectarray antenna with true time delay, *7th European Conference on Antennas and Propagation (EuCAP)*, pp. 3343–3346.

SELVAM-Y. P., ELUMALAI-L., ALSATH-M. G. N., KANAGASABAI-M., SUBBARAJ-S., AND KINGSLY-S. (2017). Novel frequency- and pattern-reconfigurable rhombic patch antenna with switchable polarization, *IEEE Antennas and Wireless Propagation Letters*, **16**, pp. 1639–1642.

SHI-Y., CAI-Y., YANG-J., AND LI-L. (2019). A magnetoelectric dipole antenna with beamwidth reconfiguration, *IEEE Antennas and Wireless Propagation Letters*, **18**(4), pp. 621–625.

SIEVENPIPER-D. F., SCHAFFNER-J. H., SONG-H. J., LOO-R. Y., AND TANGONAN-G. (2003). Two-dimensional beam steering using an electrically tunable impedance surface, *IEEE Transactions on Antennas and Propagation*, **51**(10), pp. 2713–2722.

SUN-H., AND SUN-S. (2016). A novel reconfigurable feeding network for quad-polarization-agile antenna design, *IEEE Transactions on Antennas and Propagation*, **64**(1), pp. 311–316.

SU-T., YI-X., AND BIANWU. (2019). X/Ku dual-band single-layer reflectarray antenna, *IEEE Antennas and Wireless Propagation Letters*, **18**(2), pp. 338–342.

TAYEBI-A., TANG-J., PALADHI-P. R., UDPA-L., UDPA-S. S., AND ROTHWELL-E. J. (2015). Dynamic beam shaping using a dual-band electronically tunable reflectarray antenna, *IEEE Transactions on Antennas and Propagation*, **63**(10), pp. 4534–4539.

TIAN-H., DHWAJ-K., JIANG-L. J., AND ITOH-T. (2018a). Beam scanning realized by coupled modes in a single-patch antenna, *IEEE Antennas and Wireless Propagation Letters*, **17**(2), pp. 1077–1080.

TIAN-H., DHWAJ-K., JIANG-L. J., AND ITOH-T. (2018b). Beam scanning realized by coupled modes in a single-patch antenna, *IEEE Antennas and Wireless Propagation Letters*, **17**(6), pp. 1077–1080.

TIAN-H., JIANG-L., AND ITOH-T. (2019). A compact single-element pattern reconfigurable antenna with wide-angle scanning tuned by a single varactor, *Progress In Electromagnetics Research*, **92**, pp. 137–150.

TOPALLI-K., ZLEM AYDIN CIVI., DEMIR-S., KOC-S., AND AKIN-T. (2008). A monolithic phased array using 3-bit distributed RF MEMS phase shifters, *IEEE Transactions on Microwave Theory and Techniques*, **56**(2), pp. 270–277.

TRAMPLER-M. E., AND GONG-X. (2019). Phase-agile dual-resonance single linearly polarized antenna element for reconfigurable reflectarray applications, *IEEE Transactions on Antennas and Propagation*, **67**(6), pp. 3752 – 3761.

UNIVERSITY-C. (n.d.). Galaxies across the universe.

UNLU-M., DEMIR-S., AND AKIN-T. (2013). A 1540-ghz frequency reconfigurable rf mems phase shifter, *IEEE Transactions on Microwave Theory and Techniques*, **61**(8), pp. 2865–2877.

VAUGHAN-R. (2004). Model and results for single mode pifa antenna, *IEEE Antennas and Propagation Society Symposium*, **4**, pp. 4028–4031.

VENNERI-F., BOCCIA-L., ANGIULLI-G., AMENDOLA-G., AND MASSA-G. D. (2003). Analysis and design of passive and active microstrip reflectarrays, *International Journal of RF and Microwave Computer-Aided Engineering*, **13**(5), pp. 370–377.

VENNERI-F., COSTANZO-S., MASSA-D., BORGIA-A., CORSONELLO-P., AND SALZANO-M. (2012). Design of a reconfigurable reflectarray based on a varactor tuned element, *2012 6th European Conference on Antennas and Propagation*, pp. 2628–2631.

WINCZA-K., AND GRUSZCZYNSKI-S. (2010). Miniaturized quasi-lumped coupled-line single section and multisection directional couplers, *IEEE Transactions on Microwave Theory and Techniques*, **48**(11), pp. 2924–2931.

WRIGHT-M. D., BARON-W., MILLER-J., TUSS-J., ZEPPETTELLA-D., AND ALI-M. (2018). MEMS reconfigurable broadband patch antenna for conformal applications, *IEEE Transactions on Antennas and Propagation*, **66**(6), pp. 2770 – 2778.

XIAO-S., ZHENG-C., LI-M., XIONG-J., AND WANG-B.-Z. (2015a). Varactor-loaded pattern reconfigurable array for wide-angle scanning with low gain fluctuation, *IEEE Transactions on Antennas and Propagation*, **11**(5), pp. 2364–2369.

XIAO-S., ZHENG-C., LI-M., XIONG-J., AND WANG-B.-Z. (2015b). Varactor-loaded pattern reconfigurable array for wide-angle scanning with low gain fluctuation, *IEEE Transactions on Antennas and Propagation*, **63**(5), pp. 2364–2369.

YANG-G., LI-J., WEI-D., GANG ZHOU-S., AND XU-R. (2019). Pattern reconfigurable microstrip antenna with multidirectional beam for wireless communication, *IEEE Transactions on Antennas and Propagation*, **67**(3), pp. 1910–1915.

YANG-H., YANG-F., XU-S., MAO-Y., LI-M., CAO-X., AND GAO-J. (2016). A 1-bit 10×10 reconfigurable reflectarray antenna: design, optimization, and experiment, *IEEE Transactions on Antennas and Propagation*, **64**(6), pp. 2246–2254.

YANG-S.-L., AND LUK-K.-M. (2006). Design of a wide-band L-probe patch antenna for pattern reconfiguration or diversity applications, *IEEE Transactions on Antennas and Propagation*, **54**(2), pp. 433–438.

YANG-S., ZHANG-C., PAN-H. K., FATHY-A. E., AND NAIR-V. K. (2009). Frequency-reconfigurable antennas for multiradio wireless platforms, *IEEE Microwave Magazine*, **10**(1), pp. 66–83.

YANG-X., LIN-H., GU-H., GE-L., AND ZENG-X. (2018). Broadband pattern diversity patch antenna with switchable feeding network, *IEEE Access*, **6**, pp. 69612–69619.

YANG-X.-S., WANG-B.-Z., AND LIU-H.-L. (2006). Reconfigurable yagi patch array by utilizing odd-even-mode method, *Journal of Electromagnetic Waves and Applications*, **20**(13), pp. 1725–738.

YANG-X.-S., WANG-B.-Z., WU-W., AND XIAO-S. (2007). Yagi patch antenna with dual-band and pattern reconfigurable characteristics, *IEEE Antennas and Wireless Propagation Letters*, **6**, pp. 168–171.

YANG-X., XU-S., YANG-F., LI-M., HOU-Y., JIANG-S., AND LIU-L. (2017). A broadband high-efficiency reconfigurable reflectarray antenna using mechanically rotational elements, *IEEE Transactions on Antennas and Propagation*, **65**(8), pp. 3959–3966.

YONG-S., AND BERNHARD-J. T. (2009). Investigation into the relationship between microstrip patch width and efficiency, *IEEE Antennas and Wireless Propagation Letters*, **8**, pp. 1171–1174.

ZADEHPARIZI-F., AND JAM-S. (2018). Increasing reliability of frequency-reconfigurable antennas, *IEEE Antennas and Wireless Propagation Letters*, **17**(5), pp. 920 – 923.

ZAINARRY-S. N. M., NGUYEN-TRONG-N., AND FUMEAUX-C. (2018). A frequency and pattern-reconfigurable two-element array antenna, *IEEE Antennas and Wireless Propagation Letters*, **17**(4), pp. 617–620.

ZHANG-M.-T., GAO-S., JIAO-Y.-C., WAN-J.-X., TIAN-B.-N., WU-C.-B., AND FARRALL-A.-J. (2016). Design of novel reconfigurable reflectarrays with single-bit phase resolution for Ku-band satellite antenna applications, *IEEE Transactions on Antennas and Propagation*, **64**(5), pp. 1634–1641.

ZHOU-M., SRENSEN-S. B., JRGENSEN-E., MEINCKE-P., KIM-O. S., AND BREINBJERG-O. (2011). Analysis of printed reflectarrays using extended local periodicity, *Proceedings of the 5th European Conference on Antennas and Propagation (EUCAP)*, pp. 1408–1412.

ZOHUR-A., MOPIDEVI-H., RODRIGO-D., UNLU-M., JOFRE-L., AND CETINER-B. A. (2013). RF MEMS reconfigurable two-band antenna, *IEEE Antennas and Wireless Propagation Letters*, **12**, pp. 72–75.

Biography

Siti Nailah Mastura Zainarry was born in Kedah, Malaysia. She received her bachelor's degree (Microelectronic Engineering) from the School of Microelectronic Engineering, University of Malaysia Perlis in 2009, and her master's degree (Electronic Systems Design Engineering) from the School of Electrical and Electronic, University of Science, Malaysia in 2010. In 2014, she came to Australia to pursue her PhD research in the School of Electrical and Electronic Engineering at the University of Adelaide. She is studying in the field of microwave and millimeter-wave under the supervision of Prof. Christophe Fumeaux and Prof. Cheng-Chew Lim.

During her candidature, she has focused her research on applied electromagnetics, more specifically on the analysis and optimisation of printed microwave and millimeter-wave components. Her research involves the design of electronically tunable structures such as reconfigurable antennas and reconfigurable reflectarray antennas for wireless communications and remote sensing applications. She also interested in reconfigurable artificial magnetic conductor arrays.

In 2018, she was the recipient of the University of Adelaide Completion Scholarship and also received a best paper award at the IEEE Radio and Antenna Days of The Indian Ocean conference in Mauritius in 2018. Siti Nailah Mastura Zainarry is a student member of the Institute of Electrical and Electronics Engineers (IEEE) and IEEE Antennas and Propagation Society.

Siti Nailah Mastura Zainarry
sitinailahmastura.zainarry@adelaide.edu.au